Cerebellar stimulations prevent Levodopa-induced dyskinesia in mice and normalize brain activity

Bérénice Coutant[1], Jimena Laura Frontera[1,3], Elodie Perrin[2,3], Adèle Combes[1,3], Thibault Tarpin[1], Fabien Menardy[1], Caroline Mailhes-Hamon[1], Sylvie Perez[2], Bertrand Degos[2], Laurent Venance[2], Clément Léna[1], Daniela Popa[1]

[1] Neurophysiology of Brain Circuits Team, Institut de biologie de l'Ecole normale supérieure (IBENS), Ecole normale supérieure, CNRS, INSERM, PSL Research University, 75005 Paris, France

[2] Dynamics and Pathophysiology of Neuronal Networks Team, Center for Interdisciplinary Research in Biology (CIRB), College de France, CNRS, INSERM, Université PSL, Paris, France

[3] These authors contributed equally to the study

Correspondence should be addressed to D.P. (daniela.popa@bio.ens.psl.eu) or to C.L. (clement.lena@bio.ens.psl.eu).

SUMMARY

Chronic Levodopa therapy, the gold-standard treatment of Parkinson's Disease (PD), leads to the emergence of involuntary movements, called levodopa-induced dyskinesia (LID). Cerebellar stimulations have been shown to decrease LID severity in PD patients. Here, in order to determine how cerebellar stimulations induce LID alleviation, we performed daily short trains of optogenetic stimulations of Purkinje cells (PC) in freely moving mice. We demonstrated that these stimulations are sufficient to suppress LID or even prevent their development. This symptomatic relief is accompanied by the normalization of aberrant neuronal discharge in the cerebellar nuclei, the motor cortex and the parafascicular thalamus. Inhibition of the cerebello-parafascicular pathway counteracted the beneficial effect of cerebellar stimulations. Moreover, cerebellar stimulations reversed plasticity in D1 striatal neurons and normalized the overexpression of FosB, a transcription factor causally linked to LID. These findings demonstrate LID alleviation and prevention by daily PC stimulations, which restore the function of a wide brain motor network, and may be valuable for LID treatment.

INTRODUCTION

Motor symptoms of Parkinson's disease (PD) are caused by a progressive loss of dopaminergic neurons in the substantia nigra *pars compacta*, and of their dense projections to the striatum. The gold-standard symptomatic therapy for PD patients is Levodopa (L-DOPA). However, with disease progression and chronic exposure to L-DOPA, 50-80% of patients experience a range of motor levodopa-induced complications within 5 years of treatment [1] including debilitating abnormal involuntary movements, called levodopa-induced dyskinesia (LID) [2]. So far, very few therapeutic options are available to circumvent the advent of LID in the course of L-DOPA treatment. A better understanding of the brain networks controlling LID generation and expression is critical to the development of appropriate treatments.

LID-associated abnormalities have been consistently observed in the basal ganglia, the thalamus and the motor cortex in humans [3, 4, 5, 6], primates [7, 8, 9, 10] and rodents [11, 12, 13, 14, 15]. In line with these observations, interactions in this inter-connected motor network contribute to LID pathopysiology [16]. More recently, alleviation of LID in humans have been observed following stimulations of the cerebellum [5, 17, 18, 19, 20]. While a single short (1-2 minutes) session of repetitive transcranial magnetic (rTMS) continuous theta burst (cTBS) stimulation over the cerebellum only transiently reduced LID, the repetition of stimulation sessions over 2 weeks yielded a reduction of peak-dose LID over weeks after the sessions [18, 19]. This showed that cerebellar stimulations could reduce the expression of LID. The impact of these stimulations was observed in the cerebellar nuclei [17], suggesting that their effect is mediated by the output cells of the cerebellar cortex, the Purkinje cells (PC) and propagated to downstream structures.

A first possibility is that cerebellar stimulations correct motor cortex dysfunction observed in dyskinesia. Indeed, dyskinetic patients present an increase in cerebral blood flow in the primary motor cortex [21], as well as abnormal synaptic plasticity [22]. Similarly, dyskinetic rats exhibit changes in gene expression [23] and an increased activity in about half of the neurons of the motor cortex [24]. In addition, subthalamic deep brain stimulation, which reduce PD symptoms and thus prevent the need of high L-DOPA dosage producing LID, have been proposed to act via an effect on the motor cortex [25, 26]. Likewise, cerebellar cTBS has been shown to exert a control on motor cortex plasticity [27]. Moreover, anodal direct current stimulation over the cerebellum, which is thought to increase the cerebello-cortical coupling [28], also led to a decrease in LID [29]. Therefore, the motor cortex could be the relay of cerebellar stimulations in the treatment of LID.

LID is also directly linked to abnormal molecular events taking place in striatal neurons [30, 31]. Most notably, LID has been causally linked to changes in the expression of FosB, a transcription factor, and its truncated splice variant ΔFosB. Dyskinetic patients [32], primates [33, 34] and rodents [35, 36, 37, 38, 39] show an overexpression of FosB/ΔFosB that strongly correlates with the severity of dyskinesia [38]. The upregulation of FosB/ΔFosB in striatal neurons of experimental animals is sufficient to trigger LID in response to acute administration of levodopa [7, 40], and reciprocally the inactivation of striatal FosB/ΔFosB reduces LID [34, 41] establishing the causal contribution of this transcription factor to LID. LID is associated with strong changes in striatal synaptic plasticity [14, 42]. These aberrant corticostriatal plasticity's are indeed a feature shared with a number of other hyperkinetic movement disorders, suggesting that they participate to the pathological state [43, 44]. Besides its cortical inputs, the striatum receives massive inputs from the thalamus [45]. The thalamo-

striatal pathway could also relay therapeutic activities as demonstrated by the reduction of LID following deep brain stimulation of the intralaminar thalamo-striatal CM-PF complex in PD patients [46] and dyskinetic rats [47]. The cerebellum indeed projects to the basal ganglia by way of the intralaminar thalamus [48, 49, 50, 51] and may control the cortico-striatal plasticity [49]. Cerebellar stimulations could therefore directly restore striatal function in LID.

To investigate the mechanisms underlying the alleviation of LID by cerebellar stimulations, we studied the effect of optogenetic PC stimulations on these abnormal involuntary movements using L7-ChR2-YFP mice [52] in combination with a well-known mouse model of LID [53]. We performed daily brief sessions of theta-rhythm optogenetic stimulations of PC in Crus II, the region associated with orolingual sensorimotor function of the cerebellum [54, 55]. These stimulations did specifically suppress, or even prevent, if administered early enough, severe orolingual LID. These behavioral findings were paralleled with a normalization of the aberrant neuronal activity in the deep cerebellar nuclei, especially the interposed nucleus, in the oral primary motor cortex and in the parafascicular thalamus, indicating a wide-scale action of cerebellar stimulations on the motor system. The chemogenetic inactivation of the cerebello-parafascicular pathway counteracted the beneficial effects of cerebellar stimulations, suggesting that they are mediated via the cerebello-thalamo-striatal pathway. Indeed, cerebellar stimulations reversed the sign of corticostriatal plasticity by promoting long-term depression in D1-expressing neurons and normalized the striatal expression of FosB/ΔFosB indicating that cerebellar stimulations act on the core of LID genesis.

RESULTS

Optogenetic Purkinje cell stimulations in the orolingual region of the cerebellar hemisphere specifically suppress or prevent orolingual dyskinesia

To study the effect of repeated sessions of optogenetic stimulations of PC on dyskinesia, we used a classical mouse model of LID. LID were produced by repeated systemic injections of levodopa in mice that underwent dopaminergic depletion following 6-OHDA injection in the median forebrain bundle, which project mainly to the dorsal striatum (**Figure 1a-c**). 6-OHDA-lesioned animals chronically treated with levodopa alone (condition “LID”, N=19) indeed exhibited severe oral, axial and limb dyskinesia, compared to non-lesioned levodopa-treated sham mice (condition “SHAM”, N=17) (**Figure 1d-g**). The dyskinesia score peaked around 30-40 minutes after levodopa injection (**Figures S1b, S2b, S3b**) as described in previous studies [56, 57], consistent with LID severity following plasmatic levels of levodopa [53, 58], hence referred to as peak-dose dyskinesia. These effects were observed during the 6 weeks of daily levodopa administration.

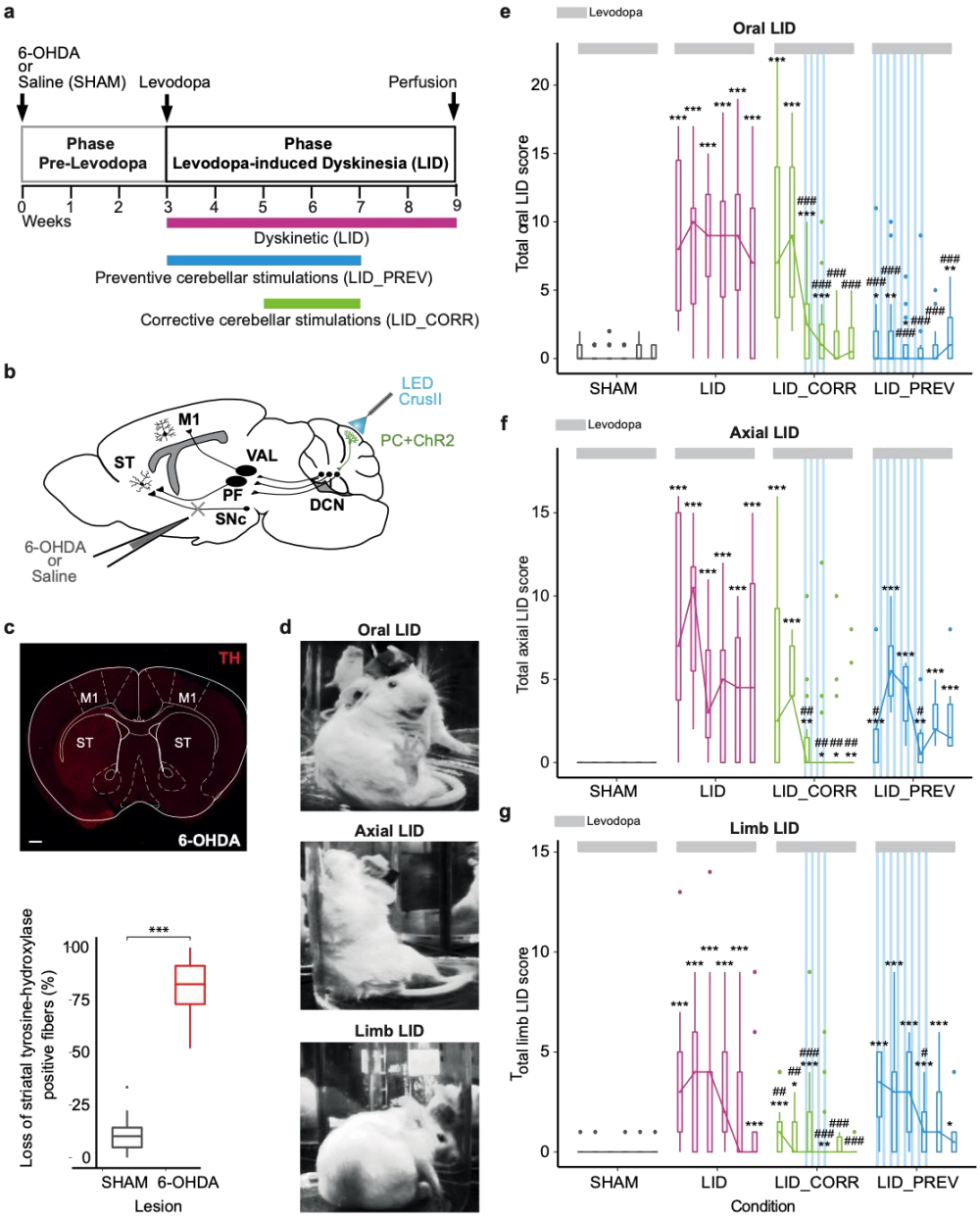

Fig. 1 Optogenetic stimulations of Crus II Purkinje cells both reduce and prevent severe oral peak-dose dyskinesia.

a Experimental timeline. Dyskinetic mice (LID, magenta): 6 weeks of levodopa treatment. Preventive mice (LID_PREV, blue): 6 weeks of levodopa treatment + 4 weeks of cerebellar stimulations. Corrective mice (LID_CORR, green): 6 weeks of levodopa treatment + 2 weeks of cerebellar stimulations. **b** Sagittal schematic of a mouse brain showing cerebello-thalamo-cortical and -striatal pathways, ChR2-YFP in Purkinje cells (PC+ChR2, green), and injection site of 6-OHDA or saline. M1: Primary motor cortex, ST: striatum, VAL: Ventroanterior-ventrolateral complex of the thalamus, PF: Parafascicular nucleus of the thalamus, SNc: Substantia nigra *pars compacta*, DCN: deep cerebellar nuclei, CrusII: Crus2 of the ansiform lobule. **c** *Upper panel*: Coronal section from a mouse unilaterally-lesioned with 6-OHDA stained with anti-tyrosine hydroxylase (TH). Scale bar: 0.5 mm. M1: Primary motor cortex, ST: Striatum. *Bottom panel*: Loss of striatal TH-positive fibers (%) between the lesioned and the intact striatum in control mice (grey, N=17) and parkinsonian animals (red, N=40). **d** Examples of orolingual (top), axial (middle), and limb (bottom) levodopa-induced dyskinesia in dyskinetic mice. **e** Boxplot showing the sum of oral LID scores across the 6 weeks of levodopa treatment (light grey bar) for SHAM (grey, N=18), LID (magenta, N=19); LID_CORR (green, N=17); LID_PREV (bleu, N=24). Stripped blue lines: weeks of theta-burst PC stimulations. **f** Boxplot showing the sum of axial LID across the 6 weeks of levodopa treatment (light grey bar) for SHAM (grey, N=12), LID (magenta, N=8), LID_CORR (green, N=14), LID_PREV (bleu, N=6). Stripped blue lines: weeks of theta-burst PC stimulations. **g** Boxplot showing the sum of limb LID scores across the 6 weeks of levodopa treatment (light grey bar) for SHAM (grey, N=14), LID (magenta, N=9), LID_CORR (green, N=15), LID_PREV (bleu, N=9). Stripped blue lines: weeks of theta-burst PC stimulations.

Boxplots represents the lower and the upper quartiles as well as the median of LID score. Kruskal-Wallis test with pairwise Wilcoxon test and Benjamini & Hochberg correction. ***p < 0.001; **p < 0.01; *p < 0.05; * compared to SHAM; # compared to LID. See also Table S1.

Sham-lesioned mice exposed to chronic levodopa treatment received either corrective or preventive optogenetic cerebellar stimulations, or none. They did not exhibit any kind of severe dyskinesia, neither before nor during cerebellar stimulations (**Figure S4**), and were therefore pooled together for behavioral analysis.

To examine whether PC stimulations efficiently reversed or prevented LID, brief trains of optogenetic stimulations at theta frequency [19, 59] were delivered daily in mice expressing ChR2 specifically in PC [52, 60] (**Figure 2b,c**). Stimulations either started 2 weeks after ("corrective stimulations"), or preceded ("preventive stimulations"), LID onset (**Figure 1a**).

In 6-OHDA-lesioned mice exhibiting severe dyskinesia upon repeated levodopa injections, 2 weeks of daily corrective PC stimulations on the cerebellar orolingual region Crus II significantly reduced oral dyskinesia (condition "LID_CORR", N=24, **Figures 1e, S1b, Table S1**). This effect persisted at least for 2 weeks after the end of cerebellar stimulations (weeks 8 and 9, **Figures 1e, S1b, Table S1**) and the dyskinesia scores were then similar to those of the control group (**Table S1**). Furthermore, after corrective PC stimulations over orolingual CrusII, the reduction in oral LID was more pronounced than in axial and limb dyskinesia (**Figures 1f-g, S2b, S3b**).

Another group of 6-OHDA-lesioned mice received daily cerebellar stimulations starting from the first day of levodopa administration (3mg/kg) i.e before the development of dyskinesia (condition "LID_PREV", N=18). Remarkably, this group exhibited only few to none orolingual dyskinesia, contrarily to LID animals (**Figures 1e, S1b, Table S1**). In conclusion, 2 weeks of daily cerebellar stimulations led to a dramatic decrease of LID expression that outlasted the stimulations for at least 2

weeks, while stimulations starting concomitantly with levodopa administration prevented LID development. Therefore, these results indicate a strong suppressive effect of peak-dose dyskinesia by cerebellar PC stimulations.

Previous studies in animals models of LID addressed exclusively "peak-dose" dyskinesia [61]. Yet, mild dyskinesia also occurred outside the 2 hours following the injection time as in PD patients at the trough of blood levodopa concentration ("off-period" dyskinesia) or during the rising and falling phase of blood levodopa concentrations (diphasic dyskinesia) review in [62]. Therefore, analysis of dyskinesia observed 20 minutes before levodopa injection revealed that chronic PC stimulations on CrusII also suppressed or prevented oral "off-period" dyskinesia depending on the protocol used (**Figure S1c, Table S1)**.

In conclusion, daily sessions of opto-stimulations of PC in CrusII, which corresponds to the orolingual region of the cerebellar cortex, is sufficient to obtain a significant decrease of oral LID. These results bear resemblance with those obtained in PD patients in whom rTMS targeting posterior cerebellum improved LID scores [18, 19] but show a stronger effect than in humans were the severity of dyskinesia was only reduced at the peak effect of levodopa.

Purkinje cell stimulations over CrusII modulate aberrant activity of the cerebellar nuclei

To test whether and how systemic levodopa treatment results in changes of activity in the cerebellum, we chronically recorded neurons in the three deep cerebellar nuclei (DCN): the interposed nucleus (IN), the dentate nucleus (DN), and the fastigial nucleus (FN) (**Figures 2b, S5b**). Neuronal activity was recorded both before and

after levodopa administration in freely moving 6-OHDA-lesioned and control mice, for a total of 9 weeks (**Figures 2a,b, S5a-c**). Recordings in three mice from DCN neurons during the stimulation protocol revealed that cells in the three DCN, strongly inhibited by the stimulation (hence likely receiving inputs from the stimulated area), exhibited an alternation of cessation of firing and increased firing relative to the baseline activity along the protocol (**Figure 2c**). We observed that levodopa decreased the global activity of IN and DN, but not FN, in LID animals (**Figures 2d**, **S5d-f, Tables S2, S3**). We verified that this did not reflect changes in motor activity (**Supp. Text, Figure S6**). Altogether, these results constitute the first evidence of a

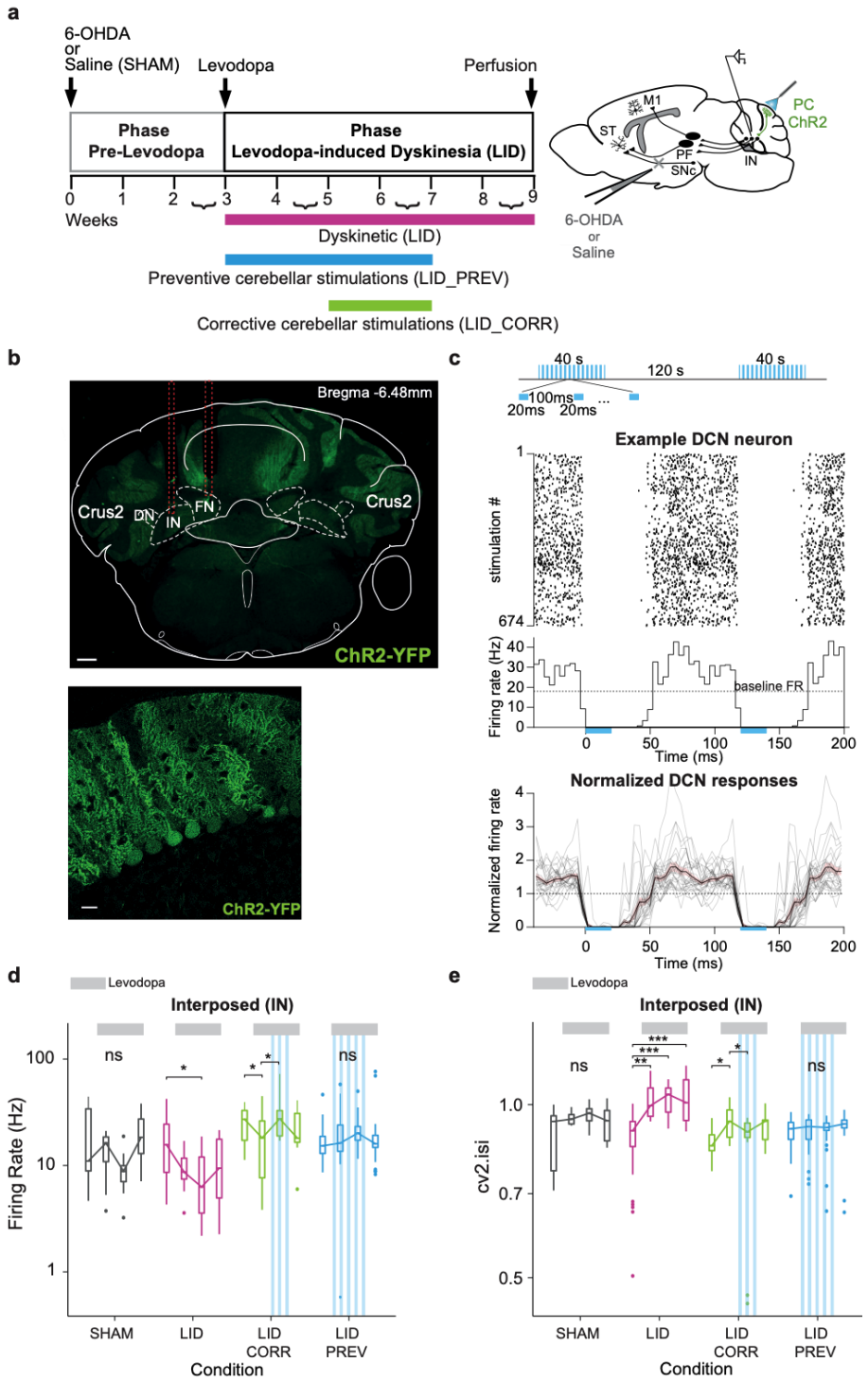

Fig. 2 Purkinje cell stimulations normalize firing rate and regularize pattern of activity in the interposed nucleus. a *Left*: Experimental timeline. *Right*: Schematic of electrode implantation in the interposed nucleus (IN), ChR2-YFP expression in Purkinje cells (PC+ChR2, green) and injection site of 6-OHDA or saline. ST: Striatum; SNc: substantia nigra *pars compacta*; M1: Primary motor cortex; PF: Parafascicular nucleus of the thalamus. **b** *Top*: Coronal section from L7-ChR2-YFP mouse. Red lines: electrode's trajectory. Dotted white lines: IN and fastigial (FN) nuclei. Scale bar: 0.5 mm. Crus2: Crus2 of the ansiform lobule, DN: Dentate cerebellar nucleus. *Bottom*: PC expressing YFP. Scale bar: 20µm. **c** *Top*: Theta-burst protocol. *Middle*: Raster plot of a deep cerebellar nuclei (DCN) neuron for each stimulation. Dotted line: Basal firing rate (FR) before the onset of stimulations. Blue box: Time of optogenetic stimulation. *Bottom*: Summary of DCN firing profiles (n=27; N=3) exhibiting a strong inhibition (>90%) during PC stimulations. The firing rate of each unit was normalized to its baseline. Shaded lines: mean +/- std. **d** Firing rate (Hz) across 9 weeks in the IN. Boxplots show the median rate (horizontal bars) over 4 categories of weeks. First boxplot: 2nd and 3rd weeks; second boxplot: 4th and 5th weeks when levodopa begins; third boxplot: 6th and 7th weeks; last boxplot: 8th and 9th weeks when stimulations stopped. Grey = SHAM (N=5); Magenta = LID (N=3); Green = LID_CORR (N=4); Blue = LID_PREV (N=3). Light grey lines: 6 weeks of levodopa treatment (3 boxplots). Stripped blue lines: weeks of theta-burst stimulations. **e** Coefficient of variation 2 (cv2.isi) across 9 weeks in the IN. Same order of boxplot as panel **d**. Grey = SHAM (N=5); Magenta = LID (N=3); Green = LID_CORR (N=4); Blue = LID_PREV (N=3). Light grey lines: 6 weeks of levodopa treatment (3 boxplots). Stripped blue lines: weeks of theta-burst stimulations. Boxplots represents the lower and the upper quartiles. Welch Anova with Games Howell post-hoc test and one-way Anova's with Tukey post-hoc test based on Levene test. ***p < 0.001; **p < 0.01; *p < 0.05; ns: p > 0.5. See also Tables S2, S3, and S4.

188

dysregulated activity of the output nuclei of the cerebellum by levodopa in LID.

Purkinje cell stimulations over CrusII prevent the decrease of activity in the interposed nucleus

For animals receiving 2 weeks of PC stimulations (LID_CORR), we found that the depressed activity in IN induced by levodopa treatment was restored during the period of cerebellar stimulations, but this effect did not last after the end of the stimulations (**Figures 2d, Tables S2, S3**). The effect was stronger in animals receiving 4 weeks of preventive PC stimulations (LID_PREV). The most striking effect was observed in IN where PC stimulations prevented the global decrease of firing rate (**Figure 2d**, **Tables S2, S3**). The effects of PC stimulations were less clear in DN and FN (**Figure S5d-f, Tables S2, S3**). Taken together, these data show that repeated sessions of cerebellar stimulations affected the aberrant activities observed under levodopa treatment in the three DCN. However, only IN exhibited a consistent normalization, which suggests a prominent role of this structure in the normalization of the dyskinesia.

Levodopa treatment causes DCN neurons to develop a more erratic activity in dyskinetic mice

The irregularity of neural discharge in the cerebellum is detrimental to motor control [63] and has been observed in rapid-onset dystonia-Parkinsonism [64, 65] and tremor [66]. The average normalized difference of successive interspike intervals (cv2.isi) is a measure of irregularity of directly adjacent interspike intervals, and therefore higher cv2.isi value indicates a more irregular cell activity [67]. Interestingly, LID mice exhibited a higher cv2.isi in IN, DN and FN during the entire period of levodopa

treatment (**Figures 2e**, **S5e-g, Tables S2, S4**). The higher values of cv2.isi did not simply reflect increased bursting (**Supp. Text, Figure S8a**). Therefore, these results showed a more erratic and irregular pattern in DCN neurons in LID mice, mostly during periods of activity, during levodopa treatment.

Purkinje cells stimulations in CrusII prevent changes in pattern of activity in the interposed nucleus

In mice receiving 2 weeks of PC stimulations (LID_CORR), the cv2.isi significantly increased the first 2 weeks of levodopa treatment in IN and was normalized during PC stimulations (**Figure 2e**, **Tables S2, S4**). In contrast, cv2.isi values remained significantly elevated in DN and FN (**Figure S5e-g, Tables S2, S4**).

In mice receiving 4 weeks of PC stimulations (LID_PREV), we found that the increased cv2.isi in IN was prevented by PC stimulations (**Figure 2e**, **Tables S2, S4**). However, increased cv2.isi was still present in DN and FN (**Figure S5e-g, Tables S2, S4).** Moreover, as in LID animals, locomotor activity did not change the cv2.isi values neither in LID_CORR nor in LID_PREV mice.

Overall, these electrophysiological data suggest that dyskinesia-related abnormal activity is conveyed to the DCN, especially to IN, leading to aberrant firing rate and firing patterns, which are reversed by chronic PC stimulations. Finally, these experiments suggest a tighter association between the changes in IN activity and the alleviation of the pathological phenotype.

Chronic levodopa treatment increases the activity of the oral motor cortex and decreases the firing rate in the parafascicular thalamic nucleus of dyskinetic mice

Since LID strongly involve the forebrain motor circuits [16], and cerebellar nuclei have multiple ascending projections toward these circuits [68, 69], we next investigated the impact of cerebellar stimulations in the thalamus and motor cortex. Changes in motor cortex activity, intralaminar nuclei of the thalamus, including the parafascicular nucleus (PF), and the ventroanterior-ventrolateral (VAL) complex of the thalamus have been observed in dyskinetic patients [21, 22, 46] and animals [23, 24, 47]. Moreover, cerebello-cortical loops [70, 71] and parafascicular projections to the striatum and to the cerebral cortex [72] are topographically organized. Therefore, to examine the impact of cerebellar stimulations on the thalamus and motor cortex, we chronically recorded neurons in the oral region of M1, and in the thalamic PF and VAL, during 5 weeks of chronic levodopa treatment (**Figures 3a,b, S9a,b**).

The activity in M1 and PF varied slightly over the course of levodopa treatment in SHAM animals, whereas LID mice exhibited a significant increase of the firing rate in M1 (**Figure 3c, Tables S5, S6**) and a significant decrease in the firing rate in PF after levodopa administration (**Figure 3d**, **Tables S5, S6**). The effects were more inconsistent in VAL (**Figure S9d, Tables S5, S6)**. Altogether, these results confirm the presence of functional alterations in PF and oral M1 in dyskinesia.

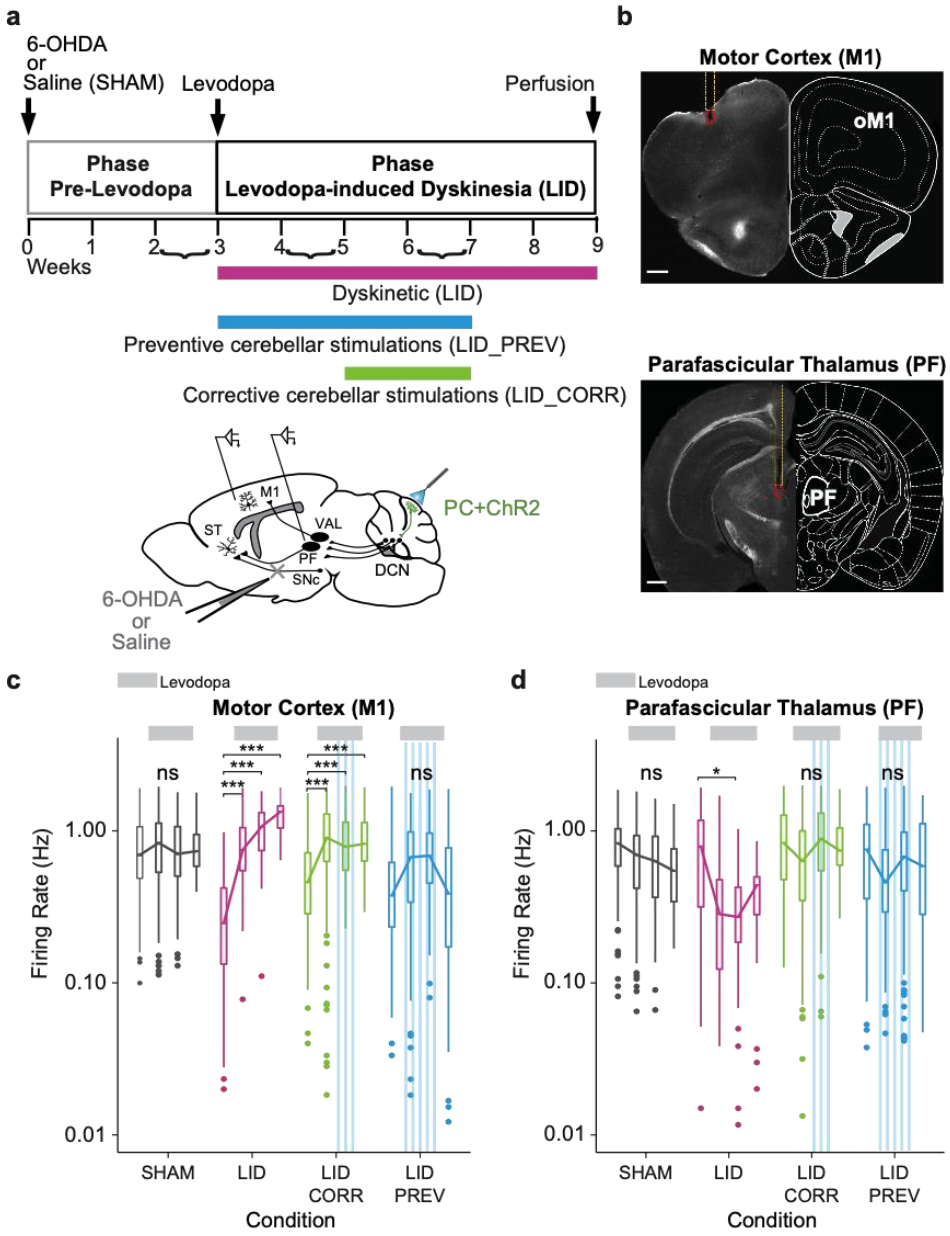

Fig. 3 Aberrant activity in the motor cortex and the parafascicular nucleus of the thalamus in dyskinesia is restored by Purkinje cell stimulations.

a *Top*: Experimental timeline. *Bottom*: Schematic of electrode implantation in the primary motor cortex (M1) and the parafascicular nucleus of the thalamus (PF), ChR2-YFP expression in the Purkinje cells (PC+ChR2, green), and injection site of 6-OHDA or saline. ST: Striatum; SNc: substantia nigra *pars compacta*; DCN: deep cerebellar nuclei: VAL: Ventroanterior-ventrolateral complex of the thalamus. **b** *Top*: Coronal section from L7-ChR2-YFP mouse showing the electrode's trajectory (dotted yellow line) and the lesion site (red circle) in layer 5 of the oral M1 (oM1). Scale bar: 0.5 mm. *Bottom*: Coronal section from L7-ChR2-YFP mouse showing the electrode's trajectory (dotted yellow line) and the lesion site (red circle) in the parafascicular nucleus of the thalamus (PF). Scale bar: 0.5 mm. **c** Firing rate (Hz) across 9 weeks in M1. Boxplots show the median rate (horizontal bars), over 4 categories of weeks. First boxplot: 2nd and 3rd week of the protocol, second boxplot: 4th and 5th weeks when levodopa begins, third boxplot: 6th and 7th weeks, last boxplot: 8th of the protocol when stimulations stopped. Grey = SHAM (N=5); Magenta = LID (N=4); Green = LID_CORR (N=6); Blue = LID_PREV (N=8). Light grey lines: 6 weeks of levodopa treatment (3 boxplots). Stripped blue lines: weeks of theta-burst PC stimulations. **d** Firing rate (Hz) across 9 weeks in the parafascicular nucleus of the thalamus (PF). Same order of boxplot as panel **c**. Grey = SHAM (N=5); Magenta = LID (N=4); Green = LID_CORR (N=6); Blue = LID_PREV (N=8). Light grey lines: 6 weeks of levodopa treatment (3 boxplots). Stripped blue lines: weeks of theta-burst PC stimulations.

Boxplots represents the lower and the upper quartiles. One-way Anova with Tukey HSD post-hoc test. ***p < 0.001; **p < 0.01; *p < 0.05; ns: p > 0.5. See also Tables S5 and S6.

257

Purkinje cell stimulations over CrusII prevent both the abnormal increase of activity in M1 and the decrease in PF in dyskinetic mice

We then investigated whether the abnormal activities observed in M1 and PF could also be normalized by chronic PC stimulations. Chronic extracellular recordings in dyskinetic mice receiving 2 weeks of PC stimulations (LID_CORR) showed that the global firing rate of oral M1 significantly increased the first 2 weeks of levodopa treatment (**Figure 3c,** 2nd boxplot), as observed in LID animals (**Figure 3c**, **Tables S5, S6**). However, contrarily to these animals, no further increase was found after the stimulations started (**Figure 3c,** 3rd boxplot). In PF, the decrease observed in dyskinetic mice was not observed during cerebellar stimulations (**Figure 3d, Tables S5, S6**).

In animals receiving 4 weeks of preventive cerebellar stimulations (LID_PREV), both the increased activity in oral M1 observed in LID (**Figure 3c, Tables S5, S6**) and the decreased activity in PF in LID were prevented (**Figure 3d, Tables S5, S6**), and remained normal even after the end of the stimulations. As for LID mice, the effects observed in the motor thalamus VAL were more variable in the corrective and the preventive conditions, suggesting that both levodopa and repeated sessions of cerebellar stimulations have less impact on this structure (**Figure S9d, Tables S5, S6**)**.**

Taken together, these results suggest that the effects induced by cerebellar stimulations restore activities of both oral M1 and PF, by being able to reverse the changes in firing rate associated with dyskinesia.

The cerebellum is connected to the parafascicular nucleus of the thalamus

Because both DCN and PF showed a similar modulation of their firing rate, we examined how IN, DN, and FN project to PF. For this purpose, we used retrograde viral tracing that allowed us to determine the distribution of DCN neurons projecting to PF (**Figure 4a**). Quantification of retrograde labeled neurons from PF showed 42.1 ± 9.0 % of projecting neurons in IN, 41.4 ± 2.6 % of neurons in DN, and 16.5 ± 1.7 % of neurons in FN (N=6, **Figure 4b-d**), suggesting that IN and DN might have an important contribution in the cerebellar control of PF activity. Moreover, PF-projecting DCN neurons were localized along the entire antero-posterior axis in the three nuclei (**Figure 4b,c,e**).

To confirm the presence of DCN synaptic terminals in PF neurons, we localized the synaptic terminals of DCN neurons projecting to PF using Cre-dependent viral expression of the presynaptic marker synaptophysin (SynP)-GFP in combination with the expression of Cre-recombinase obtained by retrograde viral injections in PF (**Figure 4f**). Large amount of DCN terminals expressing SynP-GFP were found in PF (**Figure 4g,h**), and much less in other thalamic nuclei as VAL (**Figure 4i,j**). Overall, these results confirm the presence of cerebellar projections to PF and demonstrate that they originate from a population distinct from the one projecting to VAL.

301

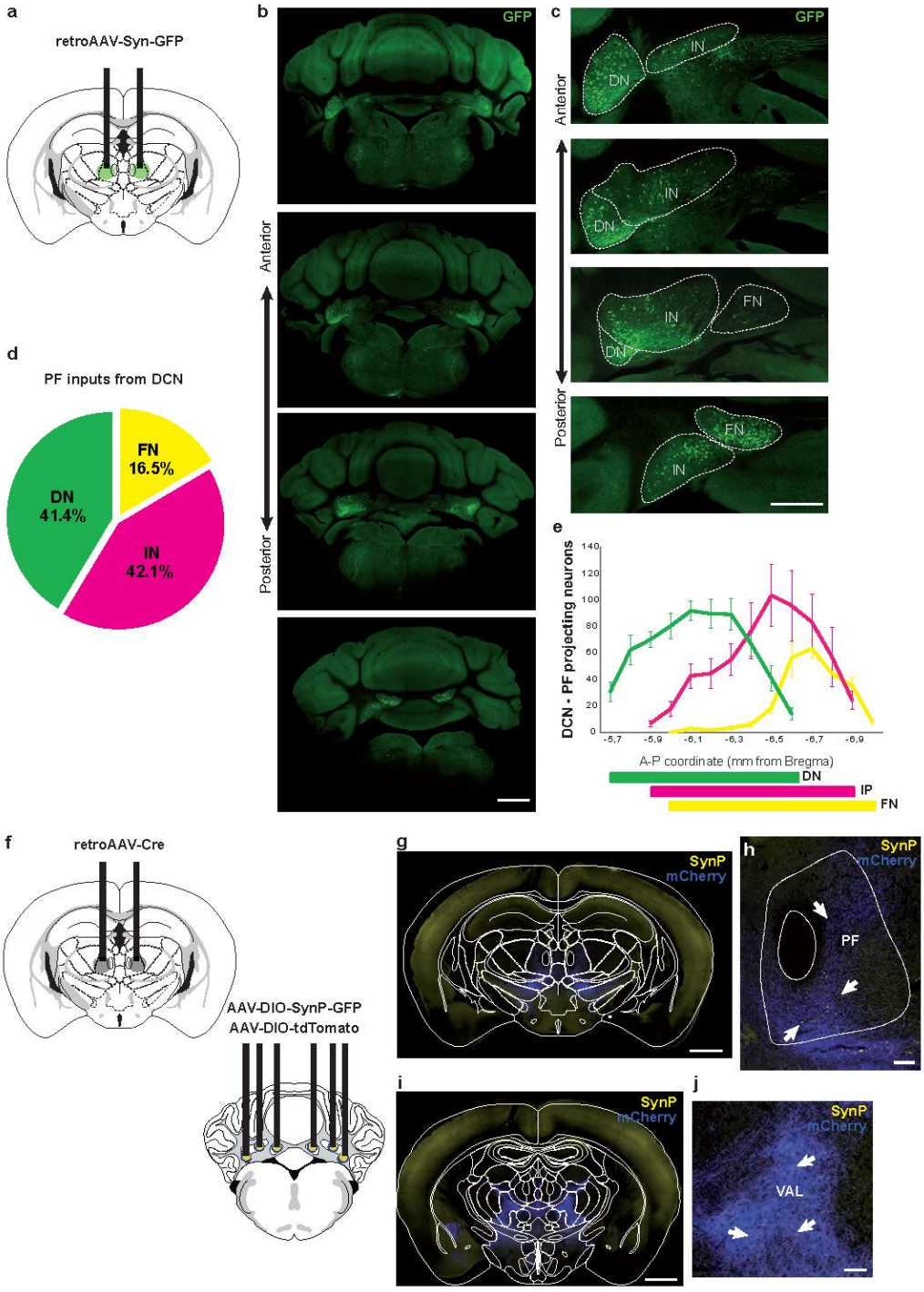

Fig. 4 DCN monosynaptic inputs to PF and collaterals.
a Retrograde labeling strategy by viral injection of retrograde AAV-syn-GFP in the parafascicular nucleus of the thalamus (PF). **b** Anterior to posterior cerebellar sections showing retrograde labeled neurons in the three deep cerebellar nuclei (DCN): dentate (DN), interposed (IN), and fastigial (FN). Scale bar: 1 mm. **c** High-magnification on DCN from **b**. Scale bar: 0.5 mm. **d** Quantification of the cell fraction (%) of retrograde labeled DN, IN and FN neurons projecting to PF. **e** Distribution of retrograde labeled DCN neurons projecting to PF in each nucleus. **f** Tracing of axon collaterals from DCN-PF projecting neurons by expression of retrograde AAV-Cre in PF, AAV-DIO-SynP-GFP and AAV-DIO-tdTomato in IN, FN, and DN. **g** Posterior thalamic section showing DCN neurons projecting to PF expressing Cre-dependent Synaptophysin (SynP)-GFP and tdTomato. Scale bar: 1mm. **h** Zoom-in of PF section exhibiting synaptic boutons (arrows) in DCN inputs Scale bar: 100 µm. **i-j** Anterior thalamic section showing axon collaterals within the thalamus. Scale bar: 1mm. **j** Zoom-in from **i** of VAL section exhibiting some synaptic boutons (arrows) from DCN-PF axon collaterals. Scale bar: 1mm.

DCN-PF pathway inhibition counteracts the effects of Purkinje cell stimulations on oral dyskinesia in preventive mice

Since DCN may entrain PF, and since PF stimulations have been used to avoid LID [46, 47], we examined the involvement of the DCN-PF pathway in the effect of cerebellar stimulations in LID. We therefore examined the effect of transiently inactivating the specific projections from DCN to PF during the repeated sessions of PC opto-stimulations. For this purpose, we expressed inhibitory hM4Di DREADD receptors in DCN neurons that target PF, by injecting retrograde CAV2-Cre-GFP in PF in complementation with a Cre-dependent AAV-DIO-hM4Di-mCherry in DCN (**Figure 5a-d**) in mice receiving 4 weeks of PC stimulations.

As oral LID peaked around 30 minutes after levodopa injection, we scored oral LID severity in preventive mice at this time point, and after chronic cerebellar stimulations were applied, to highlight the difference of effects between chemogenetic inhibition and optogenetic activation. Mice injected with inhibitory DREADDs, stimulated for 4 weeks and receiving daily CNO injections before the stimulations, presented significantly more severe oral dyskinesia than control mice also injected with inhibitory DREADDs, stimulated for 4 weeks but receiving only daily saline injections ($p<0.001$; **Figure 5e**). These results indicate that DCN to PF inputs are involved in the preventive effect of PC stimulations.

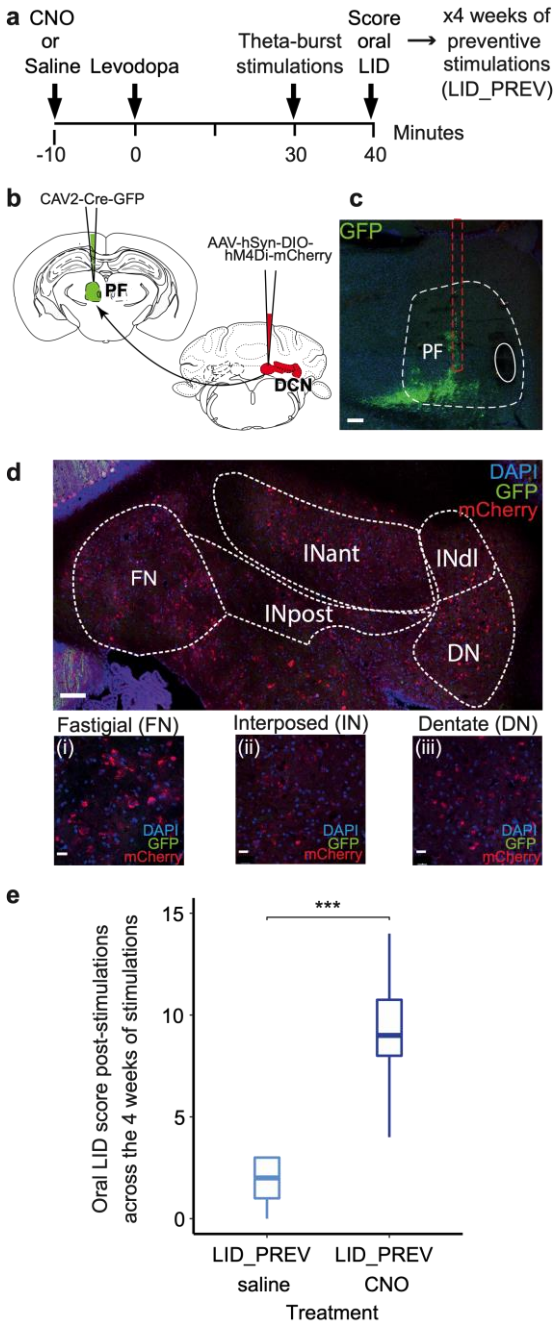

Fig. 5 DCN to PF pathway inhibition counteracts the effects of Purkinje cells stimulation on the severity of oral dyskinesia in preventive mice

a Experimental timeline. **b** Schematic of mouse coronal sections showing the injection site of the retrograde CAV2-Cre-GFP in the parafascicular nucleus of the thalamus (PF, green) ipsilateral-to-the-lesion (top, left) and the injection site of the anterograde Cre-dependent AAV-hSyn-DIO-hM4Di-mCherry in the three deep cerebellar nuclei (DCN, red) contralateral-to-the-lesion. **c** Coronal section from L7-ChR2-YFP mouse showing the injection site of retrograde CAV2-Cre-GFP in PF. Red dotted lines: needle's trajectory. White dotted lines highlight the limits of PF within the thalamus. Scale bar: 100 µm. **d** Coronal section from L7-ChR2-YFP mouse showing the expression of anterograde pAAV-hSyn-DIO-hM4Di-mCherry in neurons (red) of DCN. Med: medial cerebellar nucleus; IntP: interposed cerebellar nucleus, posterior part; IntA: interposed cerebellar nucleus, anterior part; IntDL: interposed cerebellar nucleus, dorsolateral hump; Lat: lateral cerebellar nucleus. Blue = DAPI; green = GFP; Red = mCherry. Scale bar: 100 µm. Insert: Postmortem histology showing hM4Di-mCherry-expressing neurons in the fastigial nucleus (i, FN), the interposed nucleus (ii, IN), and the dentate nucleus (iii, DN). Scale bars: 20µm. **e** Boxplots showing the average score of oral LID severity at the point time corresponding to 40 minutes after levodopa injection, 50 minutes after CNO injection and right after chronic theta-burst stimulations of Purkinje cells. Average score comprises the 4 weeks of preventive cerebellar stimulations in two groups: light blue represents preventive animals receiving 4 weeks of cerebellar stimulations + daily injections of both levodopa and saline (LID_PREV saline, N=5), dark blue represents preventive animals receiving 4 weeks of cerebellar stimulations + daily injections of both levodopa and CNO (LID_PREV CNO, N=6). Horizontal bars in boxplots represent the median score. Boxplots represents the lower and the upper quartiles. Non-parametric Kruskal-Wallis test with pairwise Wilcoxon test and a Benjamini & Hochberg correction were used. ***p<0.001; **p < 0.01; *p < 0.05; ns: p > 0.05.

Purkinje cell stimulations alter corticostriatal transmission and plasticity in brain slices

As PF projects to the striatum [72, 73, 74], it may relay a cerebellar control over corticostriatal synaptic plasticity [49]. Indeed, alterations in corticostriatal plasticity are found in hyperkinetic disorders such as LID [14, 43]. LID have notably been associated with an excessive corticostriatal long-term potentiation (LTP) in the direct pathway medium spiny neurons (MSN) without prominent change in the indirect pathway, resulting in an increased motor activity [43]. Direct and indirect pathway MSNs express different dopaminergic receptors, the dopamine receptor subtype-1 (D1R) or subtype-2 (D2R) respectively for the direct and indirect pathways [75]. Therefore, we examined *ex vivo* the corticostriatal synaptic plasticity in MSNs of the dorsolateral striatum belonging either to the direct or indirect striatal pathways using brain slices from L7-ChR2xDrd2-GFP mice subjected to 4 conditions: SHAM, SHAM_PREV, LID or LID_PREV (**Figure 6a**). We previously reported that using a spike-timing dependent plasticity (STDP) paradigm, paired pre-synaptic activations preceded by post-synaptic activations induced LTP in both direct and indirect pathway MSN [76, 77]. LTP was induced in MSNs of SHAM, SHAM_PREV, LID or LID_PREV mice except in direct pathway MSNs issued from LID_PREV mice, where a clear long-term depression (LTD) was found (**Figure 6b-e and Table S12**). Interestingly, in direct pathway MSNs, LTP induced in LID mice exhibited greater magnitude ($p<0.0001$) than in SHAM mice, whereas preventive PC stimulations either reduced LTP in SHAM mice ($p<0.0001$) or even reversed LTP into LTD in LID mice. The magnitude of corticostriatal LTP induced in indirect pathway MSNs did not show significant variation in SHAM and LID mice with or without preventive PC stimulations (ANOVA: $F=0.3044$, 38 degree of freedom, $p=0.8220$).

Therefore, we found that cerebellar preventive stimulations reverse striatal pathological LTP into LTD in direct pathway neurons, an effect which may then prevent the consolidation of an abnormal motor activity in the direct pathway and help reinstating normal motor functions.

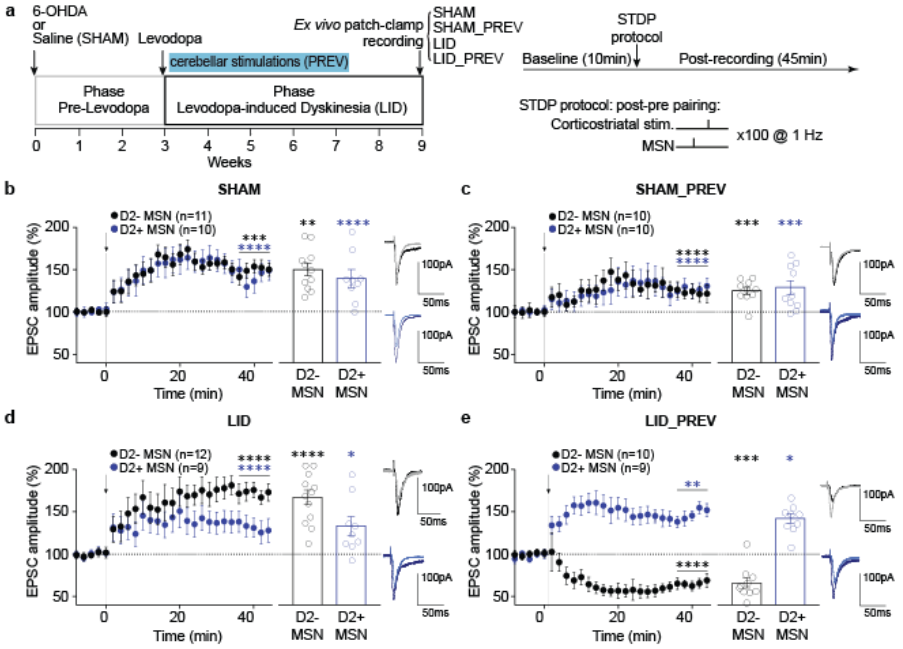

Fig. 6 Spike-timing dependent plasticity produce LTD instead of LTP in D1-expressing neurons following Purkinje cell stimulations

a *Left*: Experimental timeline. Control mice (SHAM): 6 weeks of levodopa treatment. Preventive control mice (SHAM_PREV): 6 weeks of levodopa treatment + 4 weeks of cerebellar stimulations. Dyskinetic mice (LID): 6 weeks of levodopa treatment. Preventive mice (LID_PREV): 6 weeks of levodopa treatment + 4 weeks of cerebellar stimulations. *Ex vivo* experiments were realized on mice subjected to 4 conditions, i.e. SHAM, SHAM_PREV, LID and LID_PREV. *Right*: STDP pairings: A single spike evoked in the recorded MSN (post) was paired with a single cortical stimulation (pre); pairings were repeated 100 times at 1 Hz.
b-e Averaged time courses of corticostriatal STDP in D1-MSNs and D2-MSNs induced by 100 post–pre pairings.
b In SHAM, LTP induced by 100 post–pre pairings in D1-MSNs and D2-MSNs (n=21).
c In SHAM_PREV, LTP induced by 100 post–pre pairings in D1-MSNs and D2-MSNs (n=20).
d In LID, LTP induced by 100 post–pre pairings in D1-MSNs (n=12) and D2-MSNs (n=9).
e In LID_PREV, LTP induced by 100 post–pre pairings in D1-MSNs (n=10) and the same protocol induced LTD in D2-MSNs (n=9).
Synaptic strength was determined 34-44 min after pairings.
Error bars represent the SEM. **p < 0.01; ***p < 0.001; ****p < 0.0001 by one sample t test.

Purkinje cell stimulations normalize the expression of the dyskinetic marker FosB/ΔFosB in the dorsolateral striatum

The expression of the transcription factors FosB/ΔFosB, from the immediate early gene *fosb*, has been used as a marker of dyskinesia [38]. Alterations in its expression

within the dorsolateral striatum affects LID, as both its inactivation [41] and its upregulation [7, 40] can respectively reduce and increase the severity of dyskinesia. We then examined whether PC stimulations also normalize the expression of the dyskinetic marker FosB/ΔFosB in the dorsolateral striatum (**Figure 7a**).

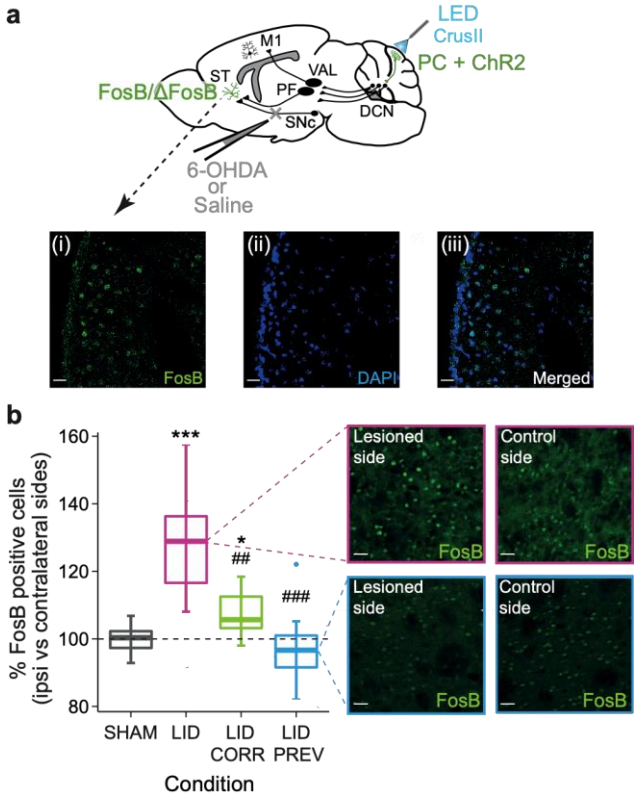

Fig. 7 Striatal overexpression of the dyskinetic marker FosB/ΔFosB is restored by Purkinje cell stimulations.
a Sagittal schematic showing neurons in the striatum expressing the dyskinetic marker FosB/ΔFosB (green). The cerebello-thalamo-cortical and cerebello-thalamo-striatal pathways are represented in mice expressing ChR2-YFP in Purkinje cells (PC+ChR2, green) as well as the injection site 6-OHDA or saline (grey). ST: Striatum; SNc: substantia nigra *pars compacta*; M1: Primary motor cortex, VAL: Ventroanterior-ventrolateral complex of the thalamus, PF: Parafascicular nucleus of the thalamus, DCN: deep cerebellar nuclei, CrusII: Crus2 of the ansiform lobule. Insets: Postmortem histology showing FosB-expressing neurons (i), DAPI (ii), and merged (iii). Scale bars: 20µm. **b** Boxplots showing the ratio of cells expressing FosB between the striatum ipsilateral to the lesion and the striatum contralateral to the lesion in percentage (%) in the 4 different conditions (magenta = LID, N=10; grey = SHAM, N=10; green = LID_CORR, N=7; and blue = LID_PREV, N=10). Horizontal bars in boxplots represent the median. Magenta inset: Postmortem histology showing FosB-expressing neurons in dyskinetic animals in the striatum ipsilateral to the lesion (left box) and in the striatum contralateral to the lesion (right box). Scale bars: 20µm. Blue inset: Postmortem histology showing FosB-expressing neurons in preventive animals in the striatum ipsilateral to the lesion (left box) and in the striatum contralateral to the lesion (right box). Scale bars: 20µm.
Boxplots represents the lower and the upper quartiles. Student t-test. ***p < 0.001; **p < 0.01; *p < 0.05. * Compared to SHAM; # compared to LID. See also Table S7.

We compared FosB/ΔFosB expression in the dorsolateral striatum ipsilateral to the lesion with the dorsolateral striatum contralateral to the lesion, in all the different conditions. As expected, neither levodopa nor cerebellar stimulations impacted the expression of FosB/ΔFosB in SHAM animals and no asymmetry was found between the two striatum (SHAM, N=10, 99.6 ± 1.3 %, **Figure 7b, Table S8**). As previously demonstrated in other studies, LID mice presented an overexpression of FosB/ΔFosB in the dorsolateral striatum ipsilateral to the lesion (LID, N=10, 128.9 ± 5.0 %, **Figure 7b, Table S8**), significantly different from the control group. 2 weeks of cerebellar stimulations decreased the asymmetric expression of FosB/ΔFosB in the dorsolateral striatum of corrective mice compared to dyskinetic animals (LID_CORR, N=7, 107 ± 2.8 %, **Figure 7b, Table S8**), although still significantly different from the control animals. No significant asymmetry of striatal FosB/ΔFosB expression was found in mice receiving 4 weeks of cerebellar stimulations (LID_PREV, N=10, 94.2 ± 3.4 %, **Figure 7b, Table S8**), which did not significantly differ from SHAM mice. Moreover, striatal FosB/ΔFosB expression in LID_PREV animals was significantly different from the one observed in LID mice. Thus, our results suggest that PC stimulations are able to restore normal expression of striatal FosB/ΔFosB, which is accompanied by an anti-dyskinetic effect.

In conclusion, repeated sessions of PC stimulations over CrusII can both normalize the aberrant activity of major motor structures involved in LID, including DCN, PF and M1, but also the overexpression of the dyskinetic marker FosB/ΔFosB within the dorsolateral striatum, tightly linked to the development of LID. These effects were associated with the advent of LTD in the striatal direct pathway MSNs, which may prevent the overactivation of this pathway in LID. Altogether, these results indicate a

384 widespread normalization in the cerebello-striato-cortical motor system and suggest
385 that the cerebellar stimulations act on core mechanisms of LID.
386

DISCUSSION

We used optogenetic stimulations, extracellular recordings, and chemogenetic inhibition to investigate the role of PC in CrusII, the orolingual region of the cerebellum, in the alleviation of orolingual levodopa-induced dyskinesia (LID). Previous clinical studies found a reduction of LID severity using cerebellar rTMS in PD patients [17, 19, 20, 59]. However, the precise mechanisms, pathways and cell-types responsible for this beneficial effect remained unknown. In the present study, we first show that CrusII PC opto-stimulations correct, or even prevent, severe orolingual dyskinesia exhibited by chronically levodopa-treated PD mice. These results are the first to demonstrate a direct involvement of PC in the anti-dyskinetic effect of the cerebellum. Strikingly, this beneficial effect led to complete alleviation of orolingual dyskinesia and thus was stronger than observed in patients where rTMS was applied bilaterally over the hemispheres of the cerebellum [18, 19]. However, the effect of rTMS on cerebellum is not yet well understood: rTMS may only indirectly activate PC and its efficacy may be constrained by the difficulty to target the optimal depths of the cerebellar cortex [78]. Interestingly, we found that the beneficial effect of cerebellar stimulations in CrusII, which hosts dense projections from the orolingual area [54], is mainly observed on the orolingual LID, suggesting a correspondence between the cerebellar somatotopy and functional impact of cerebellar stimulation. Similarly, different subtypes of LID are associated with different patterns of striatal FosB/ΔFosB expression levels, consistent with striatal somatotopy [38]. The efficacy of cerebellar rTMS in patients should thus strongly depend on the site of stimulation. Cerebellar rTMS have been reported to induce changes within the cerebellar cortex [79]. However, our work demonstrates a normalization of the neuronal activity in a wide motor network following stimulations, reveals a contribution of the cerebello-thalamo-striatal

pathway in mediating the effect of PC stimulations, and shows that it normalizes the expression of striatal FosB/ΔFosB causally linked to LID. Overall, our results indicate that PC stimulations exert long-range effects and act on core mechanisms of LID outside of the cerebellum

Our study further characterizes the alterations occurring in the cerebello-thalamo-cortical and cerebello-thalamo-striatal pathways during dyskinesia. The increased activity of the primary motor cortex in LID observed in our study is consistent with previous findings in rodents and humans [21, 24]. M1 (and also the subthalamic nucleus which is overactive in PD) reaches DCN and the cerebellar cortex through the pontine nuclei [48, 80, 81]. This observation contrasts with the decreased activity observed in IN and DN during LID, and may thus reflect compensatory adaptation in the cerebellum [60]. However, cerebellar nuclei neurons exhibited increased irregularity discharge, and such cerebellar anomalies have been implicated in other motor disorders, such as tremor [66], ataxia [82] and dystonia [64, 65]. The irregular activity found in cerebellar nuclei neurons could thus contribute to LID. The PF neurons exhibited a decreased activity as in the cerebellar nuclei; this change could result from a decreased cerebellar entrainment of PF through the cerebello- parafascicular connections [51, 83, 84, 85]. Interestingly, our results failed to evidence consistent modulations in the motor thalamus in LID or following cerebellar stimulations. Overall, the changes in activity observed in LID are likely inter-dependent since they were all corrected, or prevented, by the cerebellar stimulations.

The cerebellar stimulations produce alternate periods of silence and increased “rebound” activity in DCN [86]. Previous evidence demonstrated that this rebound activation is propagated in the forebrain motor network [71]. The chemogenetic inhibition of the cerebello-parafascicular neurons reduced the beneficial impact of

cerebellar stimulations suggesting an important contribution of the cerebello-thalamo-striatal pathway. Examination of the collaterals of these neurons revealed only sparse collaterals to the motor thalamus suggesting a primary role of the thalamostriatal over thalamocortical projections. The striatum is indeed playing a core role in LID generation notably through the overactivity of the direct pathway within the striatum [11, 13, 15]. This overactivity could result from an excessive potentiation at the corticostriatal synapses of direct pathway neurons [14, 43]. Interestingly, we found that preventive cerebellar stimulations converted the corticostriatal LTP into LTD in direct pathway MSNs in LID mice. This suggests that these stimulations promoted corticostriatal LTD over LTP in the direct pathway and may therefore circumvent the excessive potentiation occurring in LID [43]. We also found upregulation of striatal FosB/ΔFosB in LID, consistent with previous studies [35, 36, 38, 40]. Since FosB/ΔFosB overexpression suffices to trigger LID, the normalization of striatal FosB/ΔFosB levels by cerebellar stimulations may explain the suppression of LID. FosB/ΔFosB has been shown to be mainly expressed in D1-expressing striatal neurons [30, 36, 38], suggesting that cerebellar stimulations can modulate transcriptional activity in D1-MSNs, probably through projections of IN to PF and the striatum [85]. These changes of transcriptional activities might also be responsible for the change in corticostriatal plasticity observed in our study. Overall, these results show that our protocol of cerebellar stimulations induce profound changes in the striatal function. Moreover, the persistence of the beneficial effects of this protocol after its end indicates that it recruits a long-term plasticity that could be harnessed for the improvement of LID in PD patients.

Consistent with our finding that cerebellar stimulations may exert a transient therapeutic effect, stimulations of the output pathway of the cerebellum have been

463 recently shown to reduce tremor and ataxia [66, 87]. Therefore, improving the
464 experimental approaches aimed at stimulating cerebellar Purkinje cells or cerebellar
465 nuclei neurons may benefit to multiple motor disorders. Finally, our work confirms the
466 necessity to study LID as a network disorder involving abnormal signaling between
467 the basal ganglia, cerebral cortex, thalamus and cerebellum [16, 44].
468

METHODS

Animals and protocol

L7-ChR2;WT mice [52] were used for *in vivo* experiments, L7-ChR2;Drd2-GFP mice were used for *ex vivo* experiments. Animals were housed 1-3 per cage on a standard 12-hour light/dark cycle with *ad libitum* access to water and food. All behavioral manipulations took place during the light phase. All experiments were performed on mice aged 6-9 weeks, of either sex (35-45g), from the Institut de Biologie de l'Ecole Normale Supérieure, Paris, France and in accordance with the recommendations contained in the European Community Council Directives. All animals followed a 9 to 10-weeks experimental protocol. After surgical intervention, mice were carefully monitored during 1-1.5 weeks following a nursing protocol adapted from [88] to reduce post-surgery lethality. After 3 weeks, animals received daily intraperitoneal (I.P) injections of L3,4-dihydroxyphenylalanine methyl (L-DOPA, 3 day at 3mg/kg, then 6mg/kg, Sigma-Aldrich) and the peripheral DOPA decarboxylase inhibitor bensezaride hydrochloride (12mg/kg, Sigma-Aldrich) for 6 weeks (0.1mL/10g body weight). Animals were separated into 4 groups: LID_PREV, received daily theta-rhythm cerebellar "preventive" stimulations from the first day of levodopa administration, LID_CORR, received daily theta-rhythm cerebellar "corrective" stimulations after 2 weeks of L-DOPA injections, LID, received daily L-DOPA injections alone, and control SHAM mice, received daily L-DOPA and either no stimulations or preventive or corrective theta-rhythm cerebellar stimulations. Cerebellar stimulations were stopped simultaneously in all the groups and the last two weeks were assessed for long-term anti-dyskinetic effects. Every week, mice were behaviorally monitored (see below).

Surgical procedures

All surgical procedures were performed at 6-9 weeks of age. After subcutaneous (S.C) administration of buprenorphine (0.06mg/kg), animals were anesthetized with isoflurane (3%) and maintained with 0.5%-1.0% inhaled isoflurane. Mice were placed in a stereotaxic frame (David Kopf Instruments, USA) and pretreated with desipramine (25 mg/kg, I.P) (Sigma-Aldrich). Small holes were drilled over the left medial forebrain bundle (MFB: -1.2 AP, 1.3 ML, -3.75 mm DV) and either over the left oral motor cortex (M1: +2.2 AP, -2.2 ML, -1.5 mm DV), the left parafascicular nucleus (PF: -2.3 AP, -0.75 ML, -3.5 mm DV), and the left ventroanterior-ventrolateral complex of the thalamus (VAL: -1.40 AP, -1.40 ML, -3.50 mm DV) or over the right fastigial nucleus (FN: -6.4 AP, +0.85 ML, -3.25 mm DV), interposed nucleus (IN: -6.4 AP, +1.6 ML, -3.25 mm DV), and dentate nucleus (DN: -6.2 AP, +2.3 ML, -3.3 mm DV). The left MFB was injected with either 1µL of 6-Hydroxydopamine hydrochloride (6-OHDA, (Sigma-Aldrich) 3.2µg/µL free-base in a 0.02% ascorbic acid solution (Sigma-Aldrich)) (for the parkinsonian animals) or 1µL vehicle (ascorbic acid for control animals) at a rate of 0.1µL/min, after which the syringe was left in place for 10min. An additional hole was drilled over the left cerebellum for placement of a skull screw (INOX A2, Bossard) coupled to the ground wire. A final craniectomy centered over the left Crus II (-6.3 to -7.3 mm AP, +3.0 to +4.2 mm ML) was performed, without removing the dura to prevent damage to the cerebellar cortex. A 2.88 mm^2 LED (SMD chip LED lamp, Kingbright, USA) was then cement to the skull over Crus II. Recording electrodes were slowly lowered through the craniectomy at the wanted coordinates. The ground wire was clipped to the recording board using pins (Small EIB pins, Neuralynx, Dublin, Ireland) and the entire recording device was secured

519 with dental cement (Metabond) and dental acrylic (Pi-Ku-Plast HP 36, monomer and
520 polymer, Bredent, Germany).
521 All animals were given anti-inflammatory Metacam S.C (Metacam 2mg/mL,
522 Boehringer Ingelheim) for postoperative analgesia and sterile glucose-saline
523 solutions S.C [88] (Glucose 5%, Osalia). Parkinsonian animals were closely monitored
524 for 1-1.5 weeks following surgery, if needed mouse cages were kept on a heating
525 pad, animals received several glucose-saline injections daily and were fed a mixt of
526 bledine (Blédina, Danone, France) and concentrated milk.
527

528 **Behavior**

529 *Open field*

530 Animals were monitored in a 38cm diameter open field (Noldus, The Netherlands)
531 once a week for 5 min during 9 weeks. The mice were monitored with a camera
532 (Allied Vision Prosilica GigE GC650, Stemmer Imaging) placed directly above to
533 assess periods of inactivity/activity. The video acquisition was made at 25 Hz
534 frequency and at a resolution of 640 by 480 pixels. DeepLabCut method was used
535 for the analysis of locomotor activity. Seven points of interest were labeled: nose, left
536 ear, right ear, basis of tail, end of tail, red led of the headstage, green led of the
537 headstage. Labels were manually applied to the desired points on 500 frames. The
538 position of the mouse head has been reconstructed from the barycenter of the points:
539 nose, left ear, right ear, red led of the headstage, green led of the headstage
540 weighted by their likelihood. Then, to this head's trajectory, a cubic smoothing spline
541 fit was applied. For the analysis of locomotion, the periods of activity were isolated
542 from the periods of inactivity by thresholding the speed of the head point at 1cm/s.

543 *AIMs assessment*

After a 3-weeks pre-L-DOPA phase, daily IP injections of levodopa begun. In rodent models of LID, abnormal involuntary movements (AIMs) are considered the behavioral and mechanistic equivalent of LID in PD patients [14, 53]. To assess AIMs in our mouse model, a modified scale was used [53]. Each mouse was placed in a glass cylinder surrounded by 2 mirrors to detect AIMs in every angle and was recorded with a video camera (Allied Vision Prosilica GigE GC650, Stemmer Imaging) for 4 minutes every 20 minutes over a 2-hours period, starting 20 minutes before L-DOPA injection. *Post-hoc* scoring was performed for 2 minutes every 20 minutes. The mice were then evaluated a total of 8 times during the whole recording. Movements were identified as dyskinetic only when they were repetitive, affected the side of the body contralateral to the lesion, and could be clearly distinguished from naturally occurring behaviors such as grooming, sniffing, rearing, and gnawing. Specifically, AIMs were classified into three categories based on their topographic distribution: axial, forelimb, and orolingual. Forelimb dyskinesia are defined as hyperkinetic and/or dystonic movements of the contralateral forelimb on the sagittal or frontal plane. Axial AIMs are considered a twisted posture of the neck and upper body towards the side contralateral to the lesion. Finally, orolingual AIMs are defined as repetitive and empty chewing movements of the jaw, with or without tongue protrusion. Each subtype of AIMs were scored on a severity scale from 0 to 4 where: 0 = absent; 1 = occasional occurrence, less than half of the observation period; 2 = frequent occurrence, more than half of the observation time; 3 = continuous but interrupted by sensory stimuli; and 4 = continuous and not suppressible by sensory distraction [53]. AIM scores were averaged per time point or per session. Non-parametric Kruskal-Wallis test with pairwise Wilcox test and a Benjamini & Hochberg correction were

used to compared the average scores across time and between conditions for peak-dose and average off-period dyskinesia scores.

Optogenetic stimulations

To stimulate PC on Crus II cerebellar cortex, 3 micro LEDs (1.6x0.6 mm, SMD chip LED lamp, Kingbright, USA) emitting blue light with a dominant 458nm wavelength, were soldered together to cover the full extent of the stimulated area. A small piece of coverslip glass was glued to the bottom of the LEDs to prevent heat brain damage. Two insulated power wires were connecting the LEDs to allow connection with a stimulating cable (New England Wire Technologies, Lisbon) coupled to a LED driver (Universal LED Controler, Mightex). Stimulated mice (LID_PREV, LID_CORR and appropriate controls) received daily train of 20ms theta-rhythm stimulations delivered at 8.33 Hz and at 16mW/mm^2 irradiance for 2x40seconds separated by a 2 minutes period every day 30 minutes after L-DOPA injection as used in [19, 89, 90].

In vivo freely moving chronic recordings

To record cell activity, we used bundles of electrodes consisting of nichrome wire (0.005 inches diameter, Kanthal RO-800) folded and twisted into bundles of 4-8 electrodes. Prior to surgical intervention, the bundles were pinned to an electrode interface board (EIB-16; Neuralynx, Dublin, Ireland) according to the appropriate coordinates of the targeted structures. The microwires of each bundle were connected to the EIB-16 with gold pins (Neuralynx, Dublin, Ireland). The entire recording device was secured by dental cement. The impedance of every electrode was set to 200-500 kΩ using gold-plating (Cyanure-free gold solution, Sifco, France). Electrical signals were acquired using a headstage and amplifier from TDT (RZ2, RV2, Tucker-Davis Technologies, Alachya, FL, USA), filtered, amplified, and

recorded on Synapse System (Tucker-Davis Technologies, Alachya, FL, USA). Spike waveform were filtered at 3 Hz low-pass and 8000 Hz high-pass and digitized at 25 kHz. The experimenter manually set a threshold for storage and visualization of electrical events.

During recording sessions, after a 5-minutes open field and a 20-minutes recording baseline, L-DOPA (3-6 mg/kg) was injected IP and pontaneous activity was recorded for 1h30 and stimulated using a LED driver (Universal LED Controler, Mightex), an automatized commutator (ACO32 SYS3-32-CH motorized commutator, Tucker-Davis Technologies, Alachya, FL, USA), and controlled by TTL pulses from our behavioral monitoring system (RV2, Tucker-Davis Technologies, Alachya, FL, USA). At the end of recording sessions, animals were detached and returned to their home cages.

Single units were identified offline by manual spike sorting performed on Matlab (Mathworks, Natick, MA, USA) scripts based on k-means clustering on principle component analysis (PCA) of the spike waveforms [91]. One cluster was considered to represent a single-unit if the unit's spike waveform was different from other units on the same wire, in 3D PCA space. The unit's firing activity was analyzed from all structures. No statement is made whether the same cells were recorded across the 9-weeks session. For display purposes, the firing rate of single units was averaged per condition and per group of weeks using boxplots. Boxplots show the median rate in Hz, represented by horizontal bars, over 4 categories of weeks: first boxplot represents the 2^{nd} and 3^{rd} week of the protocol (pre-L-DOPA), second boxplot represents the 4^{th} and 5^{th} weeks when levodopa treatment has started as well as cerebellar stimulations for preventive mice, third boxplot represents the 6^{th} and 7^{th} weeks when corrective mice start receiving cerebellar stimulations, the last boxplot represents the 8^{th} and 9^{th} weeks of the protocol when stimulations stop and long-term

effects of cerebellar stimulations are visible. Welch Anova with Games Howell post-hoc test or one-way Anova's with Tukey post-hoc test were performed based the results of Levene test to compared the averaged firing rate between conditions in DCN whereas linear model ANOVA with the mice randomly distributed and Tukey's Post-Hoc test were performed to compared the averaged firing rate between conditions in M1, PF, and VAL.

Neuroanatomical tracing

Mice were injected with 100nL of retrograde AAV-Syn-eGFP (Titer: $1x10^{13}$ GC/mL, Lot#V16600, Addgene) in PF (N=6). For synaptophysin labeling and axon collaterals, 70nL of AAV8.2-hEF1a-DIO-synaptophysin-GFP (Titer: $2.19x10^{13}$ GC/mL, Massachusetts General Hospital) together with 50 nL of AAV1.CAG.Flex.tdTomato.WPRE.bGH (Titer: $7.8x10^{13}$ GC/mL, Lot #CS0923, Upenn Vector) were injected in IN, DN, and FN, in combination with 150nL of retrograde AAV-Cre-EBFP (Titer: $1x10^{13}$ GC/mL, Lot #V15413, Addgene) injection in PF. Mice were perfused (see below) 15-25 days after injections to allow the expression of the AAVs. Brains were sliced entirely at 90 µm using a vibratome (Leica VT 1000S), and mounted on gelatin-coated slides, dried and then coverslipped with Mowiol (Sigma). Slices were analyzed and imaged using a confocal microscope (SP8, Leica), and images were edited and analyzed using FIJI/ImageJ.

Chemogenetic experiment

Mice were injected with inhibitory DREADDs pAAV8-hSyn-DIO-hM4DimCherry (Titer: $2.9x10^{13}$ GC/mL, Vol: 100µL, Lot: v54499; Addgene) in IN, DN, and FN (150nL per nucleus)contralaterally-to-the-lesion, in complementation with 300nL CAV2-Cre-GFP

(Titer: 6.4 x 10^{12}, dilution 1/10, Plateforme de Vectorologie de Montpellier) viral infusion in ipsilateral-to-the-lesion PF. CAV2-Cre-GFP injections' surgeries were performed 1 week before the injections of pAAV-hSyn-DIO-hM4DimCherry and the MFB lesion. After 3 weeks, to allow good expression of the viruses and to reproduce our Parkinsonian model, the animals start the levodopa treatment for 6 weeks and the cerebellar stimulations for 4 weeks (LID_PREV). The severity of their orolingual LID was scored 40 minutes after levodopa injection (at the peak dose) and right after cerebellar stimulation. Scores were averaged across the 4 weeks of preventive stimulations. For neuronal modulation of animals expressing DREADDs, Clozapine N-oxide (1.25 mg/kg, Tocris Bioscience) was diluted in saline and injected I.P 10min prior L-DOPA. Control group is injected with saline.

Perfusion, Immunohistochemistry, Microscopy, and Cell counting

Mice were anesthetized with ketamine/xylazine I.P and transcardially perfused with 4% paraformaldehyde in PBS (Formalin solution, neutral buffer 10%, Sigma-Aldrich). Brains were dissected and post-fixed for 24h in 4% PFA, 24h in 20% sucrose (Merck) and 24h in 30% sucrose. Coronal 20µm sections were cut using a freezing microtome (Leica) and mounted on Superfrost glass slides (Superfrost Plus, Thermo Fisher) for imaging.

For immunohistochemistry, the tissue was blocked with 3% normal donkey serum (NDS, JacksonImmunoResearch) or normal goat serum (NGS, JacksonImmunoResearch) and permeabilized with 0.1% Triton X-100 (Sigma-Aldrich) for 2 hours at room temperature on a shaker. Primary antibodies: Guinea pig anti-TH (Synaptic System, 1:500) and Rabbit anti-FosB (Santa Cruz, 1:100) were added to 1% NDS or NGS and incubated overnight at 4°C on a shaker. Secondary

antibodies: donkey anti-Guinea Pig Cy3 (JacksonImmunoResearch, 1:400) and goat anti-Rabbit Alexa 488 (JacksonImmunoResearch, 1: 200) were added in 1% NDS/NGS for 2 hours at room temperature on a shaker. The slices were then washed, incubated with Hoechst (Invitrogen, ThermoFisher scientific, 1:10 000), and mounted onto slides for visualization and imaging. The color reaction was acquired under a dissecting microscope (Leica) and 5, 20, 40 or 64x images were taken. For FosB/ΔFosB quantification, images were taken using confocal microscope (SP8, Leica) with 40x objective. Exposure time were matched between images of the same type. Individual images were stitched together to produce an entire coronal image of both striatum. FIJI/ImageJ software was used to count cells using manual counting. Student t-test was used for statistics. The extend of the dopaminergic lesion was quantified using an optical density analysis on TH staining between the two striatum. Mean density of fluorescence of each striatum was normalized on the mean density of fluorescence of the ipsilateral corpus collasum. Only animals with >50% dopamine depletion were included in this study.

Ex vivo whole-cell patch-clamp electrophysiology

SHAM, SHAM_PREV, LID, and LID_PREV mice were anaesthetized using isofluorane and their brain removed from the skull. Horizontal striatal slices (270 µm-thick), containing the dorsal lateral striatum, were cut using a VT1000S vibratome (VT1000S, Leica Microsystems, Nussloch, Germany) in ice-cold oxygenated solution (ACSF: 125 mM NaCl, 2.5 mM KCl, 25 mM glucose, 25 mM NaHCO3, 1.25 mM NaH2PO4, 2 mM CaCl2, 1 mM MgCl2, 1 mM pyruvic acid). Slices were then incubated at 32–34°C for 60 minutes before returning to room temperature in holding ACSF. For whole-cell recordings, borosilicate glass pipettes of 4–8 MΩ resistance

were filled with a potassium gluconate-based internal solution consisting of (in mM): 122 K-gluconate, 13 KCl, 10 HEPES, 10 phosphocreatine, 4 Mg-ATP, 0.3 Na-GTP, 0.3 EGTA (adjusted to pH 7.35 with KOH, osmolarity 296 ± 3.8 mOsm). Signals were amplified using with EPC10–2 amplifiers (HEKA Elektronik, Lambrecht, Germany). All recordings were performed at 32–34°C, using a temperature control system (Bath-controller V, Luigs&Neumann, Ratingen, Germany) and slices were continuously superfused with extracellular solution at a rate of 2 ml/min. Recordings were sampled at 10 kHz, using the Patchmaster v2×32 program (HEKA Elektronik). $D2^{+}$-MSNs were visualized under direct interference contrast with an upright BX51WI microscope (Olympus, Japan), with a 40x water immersion objective combined with an infra-red filter, a monochrome CCD camera (Roper Scientific, The Netherlands) and a compatible system for analysis of images as well as contrast enhancement.

Spike-timing-dependent plasticity (STDP) protocols of stimulations were performed with one concentric bipolar electrode (Phymep, Paris, France; FHC, Bowdoin, ME) placed in the layer 5 of the somatosensory cortex while whole-cell recording MSN in the dorsolateral striatum. Electrical stimulations were monophasic, at constant current (ISO-Flex stimulators, AMPI, Jerusalem, Israel). Currents were adjusted to evoke 100–300 pA EPSCs. STDP protocols consisted of pairings of post- and presynaptic stimulations separated by a specific time interval (~20 ms); pairings being repeated at 1 Hz. The postsynaptic stimulation of an action potential evoked by a depolarizing current step (30 ms duration) in the recorded MSN preceded the presynaptic cortical stimulation, in a post-pre pairing paradigm. Post–pre pairings was repeated 100 times at 1 Hz (**Figure 6a1**). Recordings on neurons were made over a period of 10 minutes at baseline, and for at least 40 minutes after the STDP protocols; long-term changes in synaptic efficacy were measured in the last 10

718 minutes. Experiments were excluded if the mean input resistance (Ri) varied by more
719 than 20% through the experiment. Off-line analysis was performed with Fitmaster
720 (HEKA Elektronik), IGOR Pro 6.0.3 (WaveMetrics, Lake Oswego, OR, USA).
721 Statistical analyses were performed with Prism 7.00 software (San Diego, CA, USA).
722 All results are expressed as mean ± SEM. Statistical significance was assessed in
723 one-sample t tests, unpaired t tests as appropriate, using the indicated significance
724 threshold (p).

725

References:

1. Ahlskog JE, Muenter MD. Frequency of levodopa-related dyskinesias and motor fluctuations as estimated from the cumulative literature. *Mov Disord* **16**, 448-458 (2001).

2. Aquino CC, Fox SH. Clinical spectrum of levodopa-induced complications. *Mov Disord* **30**, 80-89 (2015).

3. Alonso-Frech F*, et al.* Slow oscillatory activity and levodopa-induced dyskinesias in Parkinson's disease. *Brain* **129**, 1748-1757 (2006).

4. Guerra A*, et al.* Abnormal cortical facilitation and L-dopa-induced dyskinesia in Parkinson's disease. *Brain Stimul* **12**, 1517-1525 (2019).

5. Kishore A*, et al.* Cerebellar sensory processing alterations impact motor cortical plasticity in Parkinson's disease: clues from dyskinetic patients. *Cereb Cortex* **24**, 2055-2067 (2014).

6. Wu YR, Levy R, Ashby P, Tasker RR, Dostrovsky JO. Does stimulation of the GPi control dyskinesia by activating inhibitory axons? *Mov Disord* **16**, 208-216 (2001).

7. Beck G*, et al.* Role of striatal DeltaFosB in l-Dopa-induced dyskinesias of parkinsonian nonhuman primates. *Proc Natl Acad Sci U S A* **116**, 18664-18672 (2019).

8. Guigoni C, Doudnikoff E, Li Q, Bloch B, Bezard E. Altered D(1) dopamine receptor trafficking in parkinsonian and dyskinetic non-human primates. *Neurobiol Dis* **26**, 452-463 (2007).

9. Guigoni C*, et al.* Involvement of sensorimotor, limbic, and associative basal ganglia domains in L-3,4-dihydroxyphenylalanine-induced dyskinesia. *J Neurosci* **25**, 2102-2107 (2005).

10. Heimer G, Rivlin-Etzion M, Bar-Gad I, Goldberg JA, Haber SN, Bergman H. Dopamine replacement therapy does not restore the full spectrum of normal pallidal activity in the 1-methyl-4-phenyl-1,2,3,6-tetra-hydropyridine primate model of Parkinsonism. *J Neurosci* **26**, 8101-8114 (2006).

11. Girasole AE*, et al.* A Subpopulation of Striatal Neurons Mediates Levodopa-Induced Dyskinesia. *Neuron* **97**, 787-795 e786 (2018).

12. Meissner W*, et al.* Increased slow oscillatory activity in substantia nigra pars reticulata triggers abnormal involuntary movements in the 6-OHDA-lesioned rat in the presence of excessive extracellular striatal dopamine. *Neurobiol Dis* **22**, 586-598 (2006).

13. Parker JG*, et al.* Diametric neural ensemble dynamics in parkinsonian and dyskinetic states. *Nature* **557**, 177-182 (2018).

14. Picconi B*, et al.* Loss of bidirectional striatal synaptic plasticity in L-DOPA-induced dyskinesia. *Nat Neurosci* **6**, 501-506 (2003).

15. Ryan MB, Bair-Marshall C, Nelson AB. Aberrant Striatal Activity in Parkinsonism and Levodopa-Induced Dyskinesia. *Cell Rep* **23**, 3438-3446 e3435 (2018).

16. Cenci MA, Jorntell H, Petersson P. On the neuronal circuitry mediating L-DOPA-induced dyskinesia. *J Neural Transm (Vienna)* **125**, 1157-1169 (2018).

17. Brusa L*, et al.* Metabolic changes induced by theta burst stimulation of the cerebellum in dyskinetic Parkinson's disease patients. *Parkinsonism Relat Disord* **18**, 59-62 (2012).

18. Kishore A, Meunier S, Popa T. Cerebellar influence on motor cortex plasticity: behavioral implications for Parkinson's disease. *Front Neurol* **5**, 68 (2014).

19. Koch G*, et al.* Cerebellar magnetic stimulation decreases levodopa-induced dyskinesias in Parkinson disease. *Neurology* **73**, 113-119 (2009).

20. Sanna A*, et al.* Cerebellar continuous theta burst stimulation reduces levodopa-induced dyskinesias and decreases serum BDNF levels. *Neurosci Lett* **716**, 134653 (2020).

21. Rascol O*, et al.* Cortical motor overactivation in parkinsonian patients with L-dopa-induced peak-dose dyskinesia. *Brain* **121 (Pt 3)**, 527-533 (1998).

22. Morgante F, Espay AJ, Gunraj C, Lang AE, Chen R. Motor cortex plasticity in Parkinson's disease and levodopa-induced dyskinesias. *Brain* **129**, 1059-1069 (2006).

23. Lindenbach D, Conti MM, Ostock CY, Dupre KB, Bishop C. Alterations in primary motor cortex neurotransmission and gene expression in hemi-parkinsonian rats with drug-induced dyskinesia. *Neuroscience* **310**, 12-26 (2015).

24. Halje P, Tamte M, Richter U, Mohammed M, Cenci MA, Petersson P. Levodopa-induced dyskinesia is strongly associated with resonant cortical oscillations. *J Neurosci* **32**, 16541-16551 (2012).

25. Gradinaru V, Mogri M, Thompson KR, Henderson JM, Deisseroth K. Optical deconstruction of parkinsonian neural circuitry. *Science* **324**, 354-359 (2009).

26. Valverde S*, et al.* Deep brain stimulation-guided optogenetic rescue of parkinsonian symptoms. *Nat Commun* **11**, 2388 (2020).

27. Popa T*, et al.* Cerebellar processing of sensory inputs primes motor cortex plasticity. *Cereb Cortex* **23**, 305-314 (2013).

28. Picazio S, Koch G. Is motor inhibition mediated by cerebello-cortical interactions? *Cerebellum* **14**, 47-49 (2015).

29. Ferrucci R*, et al.* Cerebellar and Motor Cortical Transcranial Stimulation Decrease Levodopa-Induced Dyskinesias in Parkinson's Disease. *Cerebellum* **15**, 43-47 (2016).

30. Spigolon G, Fisone G. Signal transduction in L-DOPA-induced dyskinesia: from receptor sensitization to abnormal gene expression. *J Neural Transm (Vienna)* **125**, 1171-1186 (2018).

31. Jenner P. Molecular mechanisms of L-DOPA-induced dyskinesia. *Nat Rev Neurosci* **9**, 665-677 (2008).

32. Lindgren HS*, et al.* Putaminal upregulation of FosB/DeltaFosB-like immunoreactivity in Parkinson's disease patients with dyskinesia. *J Parkinsons Dis* **1**, 347-357 (2011).

33. Doucet JP*, et al.* Chronic alterations in dopaminergic neurotransmission produce a persistent elevation of deltaFosB-like protein(s) in both the rodent and primate striatum. *Eur J Neurosci* **8**, 365-381 (1996).

34. Berton O*, et al.* Striatal overexpression of DeltaJunD resets L-DOPA-induced dyskinesia in a primate model of Parkinson disease. *Biol Psychiatry* **66**, 554-561 (2009).

35. Bastide MF*, et al.* Immediate-early gene expression in structures outside the basal ganglia is associated to l-DOPA-induced dyskinesia. *Neurobiol Dis* **62**, 179-192 (2014).

36. Fieblinger T*, et al.* Striatonigral neurons divide into two distinct morphological-physiological phenotypes after chronic L-DOPA treatment in parkinsonian rats. *Sci Rep* **8**, 10068 (2018).

37. Pavon N, Martin AB, Mendialdua A, Moratalla R. ERK phosphorylation and FosB expression are associated with L-DOPA-induced dyskinesia in hemiparkinsonian mice. *Biol Psychiatry* **59**, 64-74 (2006).

38. Andersson M, Hilbertson A, Cenci MA. Striatal fosB expression is causally linked with l-DOPA-induced abnormal involuntary movements and the associated upregulation of

striatal prodynorphin mRNA in a rat model of Parkinson's disease. *Neurobiol Dis* **6**, 461-474 (1999).

39. Cenci MA, Tranberg A, Andersson M, Hilbertson A. Changes in the regional and compartmental distribution of FosB- and JunB-like immunoreactivity induced in the dopamine-denervated rat striatum by acute or chronic L-dopa treatment. *Neuroscience* **94**, 515-527 (1999).

40. Cao X*, et al.* Striatal overexpression of DeltaFosB reproduces chronic levodopa-induced involuntary movements. *J Neurosci* **30**, 7335-7343 (2010).

41. Engeln M*, et al.* Selective Inactivation of Striatal FosB/DeltaFosB-Expressing Neurons Alleviates L-DOPA-Induced Dyskinesia. *Biol Psychiatry* **79**, 354-361 (2016).

42. Thiele SL*, et al.* Selective loss of bi-directional synaptic plasticity in the direct and indirect striatal output pathways accompanies generation of parkinsonism and l-DOPA induced dyskinesia in mouse models. *Neurobiol Dis* **71**, 334-344 (2014).

43. Calabresi P, Pisani A, Rothwell J, Ghiglieri V, Obeso JA, Picconi B. Hyperkinetic disorders and loss of synaptic downscaling. *Nat Neurosci* **19**, 868-875 (2016).

44. Calabresi P, Standaert DG. Dystonia and levodopa-induced dyskinesias in Parkinson's disease: Is there a connection? *Neurobiol Dis* **132**, 104579 (2019).

45. Smith Y, Raju DV, Pare JF, Sidibe M. The thalamostriatal system: a highly specific network of the basal ganglia circuitry. *Trends Neurosci* **27**, 520-527 (2004).

46. Caparros-Lefebvre D, Blond S, Feltin MP, Pollak P, Benabid AL. Improvement of levodopa induced dyskinesias by thalamic deep brain stimulation is related to slight variation in electrode placement: possible involvement of the centre median and parafascicularis complex. *J Neurol Neurosurg Psychiatry* **67**, 308-314 (1999).

47. Alam M, Capelle HH, Schwabe K, Krauss JK. Effect of deep brain stimulation on levodopa-induced dyskinesias and striatal oscillatory local field potentials in a rat model of Parkinson's disease. *Brain Stimul* **7**, 13-20 (2014).

48. Bostan AC, Dum RP, Strick PL. The basal ganglia communicate with the cerebellum. *Proc Natl Acad Sci U S A* **107**, 8452-8456 (2010).

49. Chen CH, Fremont R, Arteaga-Bracho EE, Khodakhah K. Short latency cerebellar modulation of the basal ganglia. *Nat Neurosci* **17**, 1767-1775 (2014).

50. Hoshi E, Tremblay L, Feger J, Carras PL, Strick PL. The cerebellum communicates with the basal ganglia. *Nat Neurosci* **8**, 1491-1493 (2005).

51. Ichinohe N, Mori F, Shoumura K. A di-synaptic projection from the lateral cerebellar nucleus to the laterodorsal part of the striatum via the central lateral nucleus of the thalamus in the rat. *Brain Res* **880**, 191-197 (2000).

52. Chaumont J*, et al.* Clusters of cerebellar Purkinje cells control their afferent climbing fiber discharge. *Proc Natl Acad Sci U S A* **110**, 16223-16228 (2013).

53. Lundblad M, Picconi B, Lindgren H, Cenci MA. A model of L-DOPA-induced dyskinesia in 6-hydroxydopamine lesioned mice: relation to motor and cellular parameters of nigrostriatal function. *Neurobiol Dis* **16**, 110-123 (2004).

54. Apps R, Hawkes R. Cerebellar cortical organization: a one-map hypothesis. *Nat Rev Neurosci* **10**, 670-681 (2009).

55. Schwarz C, Welsh JP. Dynamic modulation of mossy fiber system throughput by inferior olive synchrony: a multielectrode study of cerebellar cortex activated by motor cortex. *J Neurophysiol* **86**, 2489-2504 (2001).

56. Eriksson T, Magnusson T, Carlsson A, Linde A, Granerus AK. "On-off" phenomenon in Parkinson's disease: correlation to the concentration of dopa in plasma. *J Neural Transm* **59**, 229-240 (1984).

57. Putterman DB, Munhall AC, Kozell LB, Belknap JK, Johnson SW. Evaluation of levodopa dose and magnitude of dopamine depletion as risk factors for levodopa-induced dyskinesia in a rat model of Parkinson's disease. *J Pharmacol Exp Ther* **323**, 277-284 (2007).

58. Winkler C, Kirik D, Bjorklund A, Cenci MA. L-DOPA-induced dyskinesia in the intrastriatal 6-hydroxydopamine model of parkinson's disease: relation to motor and cellular parameters of nigrostriatal function. *Neurobiol Dis* **10**, 165-186 (2002).

59. Kishore A, Popa T. Cerebellum in levodopa-induced dyskinesias: the unusual suspect in the motor network. *Front Neurol* **5**, 157 (2014).

60. Menardy F, Varani AP, Combes A, Lena C, Popa D. Functional Alteration of Cerebello-Cerebral Coupling in an Experimental Mouse Model of Parkinson's Disease. *Cereb Cortex* **29**, 1752-1766 (2019).

61. Cenci MA, Crossman AR. Animal models of l-dopa-induced dyskinesia in Parkinson's disease. *Mov Disord* **33**, 889-899 (2018).

62. Thanvi B, Lo N, Robinson T. Levodopa-induced dyskinesia in Parkinson's disease: clinical features, pathogenesis, prevention and treatment. *Postgrad Med J* **83**, 384-388 (2007).

63. Hoebeek FE*, et al.* Increased noise level of purkinje cell activities minimizes impact of their modulation during sensorimotor control. *Neuron* **45**, 953-965 (2005).

64. Calderon DP, Fremont R, Kraenzlin F, Khodakhah K. The neural substrates of rapid-onset Dystonia-Parkinsonism. *Nat Neurosci* **14**, 357-365 (2011).

65. Fremont R, Tewari A, Khodakhah K. Aberrant Purkinje cell activity is the cause of dystonia in a shRNA-based mouse model of Rapid Onset Dystonia-Parkinsonism. *Neurobiol Dis* **82**, 200-212 (2015).

66. Brown AM, White JJ, van der Heijden ME, Zhou J, Lin T, Sillitoe RV. Purkinje cell misfiring generates high-amplitude action tremors that are corrected by cerebellar deep brain stimulation. *Elife* **9**, (2020).

67. Holt GR, Softky WR, Koch C, Douglas RJ. Comparison of discharge variability in vitro and in vivo in cat visual cortex neurons. *J Neurophysiol* **75**, 1806-1814 (1996).

68. Teune TM, van der Burg J, van der Moer J, Voogd J, Ruigrok TJ. Topography of cerebellar nuclear projections to the brain stem in the rat. *Prog Brain Res* **124**, 141-172 (2000).

69. Gornati SV, Schafer CB, Eelkman Rooda OHJ, Nigg AL, De Zeeuw CI, Hoebeek FE. Differentiating Cerebellar Impact on Thalamic Nuclei. *Cell Rep* **23**, 2690-2704 (2018).

70. Kelly RM, Strick PL. Cerebellar loops with motor cortex and prefrontal cortex of a nonhuman primate. *J Neurosci* **23**, 8432-8444 (2003).

71. Proville RD*, et al.* Cerebellum involvement in cortical sensorimotor circuits for the control of voluntary movements. *Nat Neurosci* **17**, 1233-1239 (2014).

72. Mandelbaum G*, et al.* Distinct Cortical-Thalamic-Striatal Circuits through the Parafascicular Nucleus. *Neuron* **102**, 636-652 e637 (2019).

73. Feger J, Bevan M, Crossman AR. The projections from the parafascicular thalamic nucleus to the subthalamic nucleus and the striatum arise from separate neuronal populations: a comparison with the corticostriatal and corticosubthalamic efferents in a retrograde fluorescent double-labelling study. *Neuroscience* **60**, 125-132 (1994).

74. Lanciego JL, Gonzalo N, Castle M, Sanchez-Escobar C, Aymerich MS, Obeso JA. Thalamic innervation of striatal and subthalamic neurons projecting to the rat entopeduncular nucleus. *Eur J Neurosci* **19**, 1267-1277 (2004).

75. Surmeier DJ, Song WJ, Yan Z. Coordinated expression of dopamine receptors in neostriatal medium spiny neurons. *J Neurosci* **16**, 6579-6591 (1996).

994 76. Fino E, Glowinski J, Venance L. Bidirectional activity-dependent plasticity at
995 corticostriatal synapses. *J Neurosci* **25**, 11279-11287 (2005).

996
997 77. Paille V*, et al.* GABAergic circuits control spike-timing-dependent plasticity. *J*
998 *Neurosci* **33**, 9353-9363 (2013).

999
1000 78. Hardwick RM, Lesage E, Miall RC. Cerebellar transcranial magnetic stimulation: the
1001 role of coil geometry and tissue depth. *Brain Stimul* **7**, 643-649 (2014).

1002
1003 79. Dufor T*, et al.* Neural circuit repair by low-intensity magnetic stimulation requires
1004 cellular magnetoreceptors and specific stimulation patterns. *Sci Adv* **5**, eaav9847
1005 (2019).

1006
1007 80. Leergaard TB, Bjaalie JG. Topography of the complete corticopontine projection: from
1008 experiments to principal Maps. *Front Neurosci* **1**, 211-223 (2007).

1009
1010 81. Sutton AC, O'Connor KA, Pilitsis JG, Shin DS. Stimulation of the subthalamic nucleus
1011 engages the cerebellum for motor function in parkinsonian rats. *Brain Struct Funct*
1012 **220**, 3595-3609 (2015).

1013
1014 82. Walter JT, Alvina K, Womack MD, Chevez C, Khodakhah K. Decreases in the
1015 precision of Purkinje cell pacemaking cause cerebellar dysfunction and ataxia. *Nat*
1016 *Neurosci* **9**, 389-397 (2006).

1017
1018 83. Aumann TD, Rawson JA, Finkelstein DI, Horne MK. Projections from the lateral and
1019 interposed cerebellar nuclei to the thalamus of the rat: a light and electron
1020 microscopic study using single and double anterograde labelling. *J Comp Neurol* **349**,
1021 165-181 (1994).

1022
1023 84. Fujita H, Kodama T, du Lac S. Modular output circuits of the fastigial nucleus for
1024 diverse motor and nonmotor functions of the cerebellar vermis. *Elife* **9**, (2020).

1025
1026 85. Xiao L, Bornmann C, Hatstatt-Burkle L, Scheiffele P. Regulation of striatal cells and
1027 goal-directed behavior by cerebellar outputs. *Nat Commun* **9**, 3133 (2018).

1028
1029 86. Tadayonnejad R, Anderson D, Molineux ML, Mehaffey WH, Jayasuriya K, Turner
1030 RW. Rebound discharge in deep cerebellar nuclear neurons in vitro. *Cerebellum* **9**,
1031 352-374 (2010).

1032
1033 87. Miterko LN*, et al.* Neuromodulation of the cerebellum rescues movement in a mouse
1034 model of ataxia. *Nat Commun* **12**, 1295 (2021).

1035
1036 88. Francardo V, Recchia A, Popovic N, Andersson D, Nissbrandt H, Cenci MA. Impact of
1037 the lesion procedure on the profiles of motor impairment and molecular

responsiveness to L-DOPA in the 6-hydroxydopamine mouse model of Parkinson's disease. *Neurobiol Dis* **42**, 327-340 (2011).

89. Huang YZ, Edwards MJ, Rounis E, Bhatia KP, Rothwell JC. Theta burst stimulation of the human motor cortex. *Neuron* **45**, 201-206 (2005).

90. Suppa A*, et al.* Ten Years of Theta Burst Stimulation in Humans: Established Knowledge, Unknowns and Prospects. *Brain Stimul* **9**, 323-335 (2016).

91. Paz R, Pelletier JG, Bauer EP, Pare D. Emotional enhancement of memory via amygdala-driven facilitation of rhinal interactions. *Nat Neurosci* **9**, 1321-1329 (2006).

Acknowledgments: This work was supported by Agence Nationale de Recherche to D.P (ANR-12-JSV4-0004 Ceredystim, ANR-16-CE37-0003-02 Amedyst, ANR-19-CE37-0007-01 Multimod) and to C.L. (ANR-17-CE37-0009 Mopla, ANR-17-CE16-0019 Synpredict) and to B.C. (France Parkinson, Labex Memolife) and by the Institut National de la Santé et de la Recherche Médicale (France). The authors declare no competing financial interests. We are grateful to Sabine Meunier for the careful reading of the manuscript. We thank the Imaging Facility at IBENS.

Author contributions: DP and CL acquired funding; DP and CL conceived and designed all experiments and analysis, except all patch clamp experiments designed by BD and LV; BC, DP, CL wrote the manuscript; BC, JLF, EP, AC, TT, CL analyzed the data; BC, JLF, EP, AC, FM, CMH, SP, DP performed the experiments. All authors interpreted results, revised the final manuscript, and approved the final manuscript.

Competing interests: The authors have no competing interests

Data, code and materials availability: All data are available in the main text or in the supplementary materials. The code for electrophysiological analysis is available from the corresponding author upon reasonable request.

FIGURE LEGENDS

Fig. 1 Optogenetic stimulations of Crus II Purkinje cells both reduce and prevent severe oral peak-dose dyskinesia.

a Experimental timeline. Dyskinetic mice (LID, magenta): 6 weeks of levodopa treatment. Preventive mice (LID_PREV, blue): 6 weeks of levodopa treatment + 4 weeks of cerebellar stimulations. Corrective mice (LID_CORR, green): 6 weeks of levodopa treatment + 2 weeks of cerebellar stimulations. **b** Sagittal schematic of a mouse brain showing cerebello-thalamo-cortical and -striatal pathways, ChR2-YFP in Purkinje cells (PC+ChR2, green), and injection site of 6-OHDA or saline. M1: Primary motor cortex, ST: striatum, VAL: Ventroanterior-ventrolateral complex of the thalamus, PF: Parafascicular nucleus of the thalamus, SNc: Substantia nigra *pars compacta*, DCN: deep cerebellar nuclei, CrusII: Crus2 of the ansiform lobule. **c** *Upper panel*: Coronal section from a mouse unilaterally-lesioned with 6-OHDA stained with anti-tyrosine hydroxylase (TH). Scale bar: 0.5 mm. M1: Primary motor cortex, ST: Striatum. *Bottom panel*: Loss of striatal TH-positive fibers (%) between the lesioned and the intact striatum in control mice (grey, N=17) and parkinsonian animals (red, N=40). **d** Examples of orolingual (top), axial (middle), and limb (bottom) levodopa-induced dyskinesia in dyskinetic mice. **e** Boxplot showing the sum of oral LID scores across the 6 weeks of levodopa treatment (light grey bar) for SHAM (grey, N=18), LID (magenta, N=19); LID_CORR (green, N=17); LID_PREV (bleu, N=24). Stripped blue lines: weeks of theta-burst PC stimulations. **f** Boxplot showing the sum of axial LID across the 6 weeks of levodopa treatment (light grey bar) for SHAM (grey, N=12), LID (magenta, N=8), LID_CORR (green, N=14), LID_PREV (bleu, N=6). Stripped blue lines: weeks of theta-burst PC stimulations. **g** Boxplot showing the sum

of limb LID scores across the 6 weeks of levodopa treatment (light grey bar) for SHAM (grey, N=14), LID (magenta, N=9), LID_CORR (green, N=15), LID_PREV (bleu, N=9). Stripped blue lines: weeks of theta-burst PC stimulations.

Boxplots represents the lower and the upper quartiles as well as the median of LID score. Kruskal-Wallis test with pairwise Wilcoxon test and Benjamini & Hochberg correction. ***p < 0.001; **p < 0.01; *p < 0.05; * compared to SHAM; # compared to LID. See also Table S1.

Fig. 2 Purkinje cell stimulations normalize firing rate and regularize pattern of activity in the interposed nucleus.

a *Left*: Experimental timeline. *Right*: Schematic of electrode implantation in the interposed nucleus (IN), ChR2-YFP expression in Purkinje cells (PC+ChR2, green) and injection site of 6-OHDA or saline. ST: Striatum; SNc: substantia nigra *pars compacta*; M1: Primary motor cortex; PF: Parafascicular nucleus of the thalamus. **b** *Top*: Coronal section from L7-ChR2-YFP mouse. Red lines: electrode's trajectory. Dotted white lines: IN and fastigial (FN) nuclei. Scale bar: 0.5 mm. Crus2: Crus2 of the ansiform lobule, DN: Dentate cerebellar nucleus. *Bottom*: PC expressing YFP. Scale bar: 20µm. **c** *Top*: Theta-burst protocol. *Middle*: Raster plot of a deep cerebellar nuclei (DCN) neuron for each stimulation. Dotted line: Basal firing rate (FR) before the onset of stimulations. Blue box: Time of optogenetic stimulation. *Bottom*: Summary of DCN firing profiles (n=27; N=3) exhibiting a strong inhibition (>90%) during PC stimulations. The firing rate of each unit was normalized to its baseline. Shaded lines: mean +/- std. **d** Firing rate (Hz) across 9 weeks in the IN. Boxplots show the median rate (horizontal bars) over 4 categories of weeks. First

boxplot: 2nd and 3rd weeks; second boxplot: 4th and 5th weeks when levodopa begins; third boxplot: 6th and 7th weeks; last boxplot: 8th and 9th weeks when stimulations stopped. Grey = SHAM (N=5); Magenta = LID (N=3); Green = LID_CORR (N=4); Blue = LID_PREV (N=3). Light grey lines: 6 weeks of levodopa treatment (3 boxplots). Stripped blue lines: weeks of theta-burst stimulations. **e** Coefficient of variation 2 (cv2.isi) across 9 weeks in the IN. Same order of boxplot as panel **d**. Grey = SHAM (N=5); Magenta = LID (N=3); Green = LID_CORR (N=4); Blue = LID_PREV (N=3). Light grey lines: 6 weeks of levodopa treatment (3 boxplots). Stripped blue lines: weeks of theta-burst stimulations.

Boxplots represents the lower and the upper quartiles. Welch Anova with Games Howell post-hoc test and one-way Anova's with Tukey post-hoc test based on Levene test. ***p < 0.001; **p < 0.01; *p < 0.05; ns: p > 0.5. See also Tables S2, S3, and S4.

Fig. 3 Aberrant activity in the motor cortex and the parafascicular nucleus of the thalamus in dyskinesia is restored by Purkinje cell stimulations.

a *Top*: Experimental timeline. *Bottom*: Schematic of electrode implantation in the primary motor cortex (M1) and the parafascicular nucleus of the thalamus (PF), ChR2-YFP expression in the Purkinje cells (PC+ChR2, green), and injection site of 6-OHDA or saline. ST: Striatum; SNc: substantia nigra *pars compacta*; DCN: deep cerebellar nuclei: VAL: Ventroanterior-ventrolateral complex of the thalamus. **b** *Top*: Coronal section from L7-ChR2-YFP mouse showing the electrode's trajectory (dotted yellow line) and the lesion site (red circle) in layer 5 of the oral M1 (oM1). Scale bar: 0.5 mm. *Bottom*: Coronal section from L7-ChR2-YFP mouse showing the electrode's

trajectory (dotted yellow line) and the lesion site (red circle) in the parafascicular nucleus of the thalamus (PF). Scale bar: 0.5 mm. **c** Firing rate (Hz) across 9 weeks in M1. Boxplots show the median rate (horizontal bars), over 4 categories of weeks. First boxplot: 2nd and 3rd week of the protocol, second boxplot: 4th and 5th weeks when levodopa begins, third boxplot: 6th and 7th weeks, last boxplot: 8th of the protocol when stimulations stopped. Grey = SHAM (N=5); Magenta = LID (N=4); Green = LID_CORR (N=6); Blue = LID_PREV (N=8). Light grey lines: 6 weeks of levodopa treatment (3 boxplots). Stripped blue lines: weeks of theta-burst PC stimulations. **d** Firing rate (Hz) across 9 weeks in the parafascicular nucleus of the thalamus (PF). Same order of boxplot as panel **c**. Grey = SHAM (N=5); Magenta = LID (N=4); Green = LID_CORR (N=6); Blue = LID_PREV (N=8). Light grey lines: 6 weeks of levodopa treatment (3 boxplots). Stripped blue lines: weeks of theta-burst PC stimulations.

Boxplots represents the lower and the upper quartiles. One-way Anova with Tukey HSD post-hoc test. ***p < 0.001; **p < 0.01; *p < 0.05; ns: p > 0.5. See also Tables S5 and S6.

Fig. 4 DCN monosynaptic inputs to PF and collaterals.

a Retrograde labeling strategy by viral injection of retrograde AAV-syn-GFP in the parafascicular nucleus of the thalamus (PF). **b** Anterior to posterior cerebellar sections showing retrograde labeled neurons in the three deep cerebellar nuclei (DCN): dentate (DN), interposed (IN), and fastigial (FN). Scale bar: 1 mm. **c** High-magnification on DCN from **b**. Scale bar: 0.5 mm. **d** Quantification of the cell fraction (%) of retrograde labeled DN, IN and FN neurons projecting to PF. **e** Distribution of

retrograde labeled DCN neurons projecting to PF in each nucleus. **f** Tracing of axon collaterals from DCN-PF projecting neurons by expression of retrograde AAV-Cre in PF, AAV-DIO-SynP-GFP and AAV-DIO-tdTomato in IN, FN, and DN. **g** Posterior thalamic section showing DCN neurons projecting to PF expressing Cre-dependent Synaptophysin (SynP)-GFP and tdTomato. Scale bar: 1mm. **h** Zoom-in of PF section exhibiting synaptic boutons (arrows) in DCN inputs Scale bar: 100 µm. **i-j** Anterior thalamic section showing axon collaterals within the thalamus. Scale bar: 1mm. **j** Zoom-in from **i** of VAL section exhibiting some synaptic boutons (arrows) from DCN-PF axon collaterals. Scale bar: 1mm.

Fig. 5 DCN to PF pathway inhibition counteracts the effects of Purkinje cells stimulation on the severity of oral dyskinesia in preventive mice

a Experimental timeline. **b** Schematic of mouse coronal sections showing the injection site of the retrograde CAV2-Cre-GFP in the parafascicular nucleus of the thalamus (PF, green) ipsilateral-to-the-lesion (top, left) and the injection site of the anterograde Cre-dependent AAV-hSyn-DIO-hM4Di-mCherry in the three deep cerebellar nuclei (DCN, red) contralateral-to-the-lesion. **c** Coronal section from L7-ChR2-YFP mouse showing the injection site of retrograde CAV2-Cre-GFP in PF. Red dotted lines: needle's trajectory. White dotted lines highlight the limits of PF within the thalamus. Scale bar: 100 µm. **d** Coronal section from L7-ChR2-YFP mouse showing the expression of anterograde pAAV-hSyn-DIO-hM4Di-mCherry in neurons (red) of DCN. Med: medial cerebellar nucleus; IntP: interposed cerebellar nucleus, posterior part; IntA: interposed cerebellar nucleus, anterior part; IntDL: interposed cerebellar nucleus, dorsolateral hump; Lat: lateral cerebellar nucleus. Blue = DAPI; green =

GFP; Red = mCherry. Scale bar: 100 µm. Insert: Postmortem histology showing hM4Di-mCherry-expressing neurons in the fastigial nucleus (i, FN), the interposed nucleus (ii, IN), and the dentate nucleus (iii, DN). Scale bars: 20µm. **e** Boxplots showing the average score of oral LID severity at the point time corresponding to 40 minutes after levodopa injection, 50 minutes after CNO injection and right after chronic theta-burst stimulations of Purkinje cells. Average score comprises the 4 weeks of preventive cerebellar stimulations in two groups: light blue represents preventive animals receiving 4 weeks of cerebellar stimulations + daily injections of both levodopa and saline (LID_PREV saline, N=5), dark blue represents preventive animals receiving 4 weeks of cerebellar stimulations + daily injections of both levodopa and CNO (LID_PREV CNO, N=6). Horizontal bars in boxplots represent the median score. Boxplots represents the lower and the upper quartiles. Non-parametric Kruskal-Wallis test with pairwise Wilcoxon test and a Benjamini & Hochberg correction were used. ***p<0.001; **p < 0.01; *p < 0.05; ns: p > 0.05.

Fig. 6 Spike-timing dependent plasticity produce LTD instead of LTP in D1-expressing neurons following Purkinje cell stimulations

a *Left*: Experimental timeline. Control mice (SHAM): 6 weeks of levodopa treatment. Preventive control mice (SHAM_PREV): 6 weeks of levodopa treatment + 4 weeks of cerebellar stimulations. Dyskinetic mice (LID): 6 weeks of levodopa treatment. Preventive mice (LID_PREV): 6 weeks of levodopa treatment + 4 weeks of cerebellar stimulations. *Ex vivo* experiments were realized on mice subjected to 4 conditions, i.e. SHAM, SHAM_PREV, LID and LID_PREV. *Right*: STDP pairings: A single spike evoked in the recorded MSN (post) was paired with a single cortical stimulation (pre);

pairings were repeated 100 times at 1 Hz. **b-e** Averaged time courses of corticostriatal STDP in D1-MSNs and D2-MSNs induced by 100 post–pre pairings. **b** In SHAM, LTP induced by 100 post–pre pairings in D1-MSNs and D2-MSNs (n=21). **c** In SHAM_PREV, LTP induced by 100 post–pre pairings in D1-MSNs and D2-MSNs (n=20). **d** In LID, LTP induced by 100 post–pre pairings in D1-MSNs (n=12) and D2-MSNs (n=9). **e** In LID_PREV, LTP induced by 100 post–pre pairings in D1-MSNs (n=10) and the same protocol induced LTD in D2-MSNs (n=9). Synaptic strength was determined 34-44 min after pairings. Error bars represent the SEM. **p < 0.01; ***p < 0.001; ****p < 0.0001 by one sample t test.

Fig. 7 Striatal overexpression of the dyskinetic marker FosB/ΔFosB is restored by Purkinje cell stimulations.

a Sagittal schematic showing neurons in the striatum expressing the dyskinetic marker FosB/ΔFosB (green). The cerebello-thalamo-cortical and cerebello-thalamo-striatal pathways are represented in mice expressing ChR2-YFP in Purkinje cells (PC+ChR2, green) as well as the injection site 6-OHDA or saline (grey). ST: Striatum; SNc: substantia nigra *pars compacta*; M1: Primary motor cortex, VAL: Ventroanterior-ventrolateral complex of the thalamus, PF: Parafascicular nucleus of the thalamus, DCN: deep cerebellar nuclei, CrusII: Crus2 of the ansiform lobule. Insets: Postmortem histology showing FosB-expressing neurons (i), DAPI (ii), and merged (iii). Scale bars: 20µm. **b** Boxplots showing the ratio of cells expressing FosB between the striatum ipsilateral to the lesion and the striatum contralateral to the lesion in percentage (%) in the 4 different conditions (magenta = LID, N=10; grey = SHAM, N=10; green = LID_CORR, N=7; and blue = LID_PREV, N=10). Horizontal bars in boxplots represent the median. Magenta inset: Postmortem histology showing

1244 FosB-expressing neurons in dyskinetic animals in the striatum ipsilateral to the lesion
1245 (left box) and in the striatum contralateral to the lesion (right box). Scale bars: 20µm.
1246 Blue inset: Postmortem histology showing FosB-expressing neurons in preventive
1247 animals in the striatum ipsilateral to the lesion (left box) and in the striatum
1248 contralateral to the lesion (right box). Scale bars: 20µm.

1249 Boxplots represents the lower and the upper quartiles. Student t-test. ***p < 0.001;
1250 **p < 0.01; *p < 0.05. * Compared to SHAM; # compared to LID. See also Table S7.

1251

SUPPLEMENTARY FIGURE LEGENDS

Supplementary Fig. S1 Optogenetic stimulations of CrusII Purkinje cells are sufficient to both reduce and prevent severe orolingual peak-dose dyskinesia. Related to Fig. 1

a Examples of orolingual peak-dose levodopa-induced dyskinesia in L7-ChR2-YFP LID parkinsonian mice chronically treated with levodopa. **b** Boxplot showing the average oral LID scores measured over 7 time points starting from the time of levodopa injection (black arrows) across the 6 weeks of treatment in SHAM (grey, N=17), LID (magenta, N=19), LID_CORR receiving 2 weeks of Purkinje cell stimulations (green, N=24), and LID_PREV mice receiving 4 weeks of Purkinje cell stimulations (blue, N=18). Boxplots represents the lower and the upper quartiles and horizontal bars in boxplots represent median score. Light grey lines: time of levodopa peak-dose effect. Striped blue lines: time of theta-burst stimulations. **c** Boxplot showing the average oral “off-period” LID scores measured 20 minutes before levodopa injection across the 6 weeks of treatment in SHAM (grey, N=8), LID (magenta, N=6), LID_CORR (green, N=6), and LID_PREV mice (blue, N=4). Boxplots represents the lower and the upper quartiles and horizontal bars in boxplots represent median score. Light grey lines: 6 weeks of levodopa treatment. Stripped blue lines: weeks of Purkinje cell stimulations. See also Table S1.

Supplementary Fig. S2 Optogenetic stimulations of CrusII Purkinje cells are not sufficient to completely reduce and prevent severe axial peak-dose dyskinesia. Related to Fig. 1

a Examples of axial peak-dose levodopa-induced dyskinesia in L7-ChR2-YFP LID parkinsonian mice chronically treated with levodopa. **b** Boxplot showing the average axial LID scores measured over 7 time points starting from the time of levodopa injection (black arrows) across the 6 weeks of treatment in SHAM (grey, N=12), LID (magenta, N=8), LID_CORR receiving 2 weeks of Purkinje cell stimulations (green, N=14), and LID_PREV mice receiving 4 weeks of Purkinje cell stimulations (blue, N=6). Boxplots represents the lower and the upper quartiles and horizontal bars in boxplots represent median score. Light grey lines: time of levodopa peak-dose effect. Striped blue lines: time of theta-burst stimulations.

Supplementary Fig. S3 Optogenetic stimulations of CrusII Purkinje cells are not sufficient to completely reduce and prevent severe limb peak-dose dyskinesia. Related to Fig. 1

a Examples of limb peak-dose levodopa-induced dyskinesia in L7-ChR2-YFP LID parkinsonian mice chronically treated with levodopa. **b** Boxplot showing the average limb LID scores measured over 7 time points starting from the time of levodopa injection (black arrows) across the 6 weeks of treatment in SHAM (grey, N=14), LID (magenta, N=9), LID_CORR receiving 2 weeks of Purkinje cell stimulations (green, N=15), and LID_PREV mice receiving 4 weeks of Purkinje cell stimulations (blue, N=9). Boxplots represents the lower and the upper quartiles and horizontal bars in boxplots represent median score. Light grey lines: time of levodopa peak-dose effect. Striped blue lines: time of theta-burst stimulations.

Supplementary Fig. S4 Optogenetic stimulations of CrusII Purkinje cells does not affect severe peak-dose oral, axial and limb dyskinesia in SHAM. Related to Fig. 1

Boxplot showing the sum of oral (left), axial (middle), and limb (right) LID scores measured over 8 time points starting 20 minutes before levodopa injection to 120 minutes after across the 6 weeks of treatment in SHAM mice treated with levodopa (dark grey, SHAM, N=4), SHAM mice treated with levodopa and receiving 2 weeks of Purkinje cells stimulations (grey, SHAM_CORR, N=5), SHAM mice treated with levodopa and receiving 4 weeks of Purkinje cells stimulations (light grey, SHAM_PREV, N=3). Horizontal bars in boxplots represent median score. Light grey lines: 6 weeks of levodopa treatment. Stripped blue lines: time of theta-burst stimulations. Boxplots represents the lower and the upper quartiles. Non-parametric Kruskal-Wallis test with pairwise Wilcox test and a Benjamini & Hochberg correction. ***p < 0.001; **p < 0.01; *p < 0.05; ns: p > 0.5. See also Table S8.

Supplementary Fig. S5. Purkinje cell stimulations do not completely normalize the aberrant activity in the dentate and fastigial cerebellar nuclei. Related to Fig. 2

a *Left*: Experimental timeline. *Right*: Schematic of electrode implantation in the dentate (DN) and fastigial nuclei (FN), ChR2-YFP expression in the Purkinje cells (PC+ChR2, green) and injection site with 6-OHDA or saline in sagittal mouse brain. ST: Striatum; SNc: substantia nigra *pars compacta*; M1: Primary motor cortex; PF: Parafascicular nucleus of the thalamus. **b** Coronal section from L7-ChR2-YFP mouse showing electrode's trajectory (red lines). Dotted red lines: IN, FN, and DN. Green:

ChR2-YFP expression. Scale bars: 0.5 mm (left); 20µm (right). Crus1: Crus1 of the ansiform lobule, Crus2: Crus2 of the ansiform lobule. **c** Schematic of verified recording sites in IN, FN, and DN (grey = SHAM; magenta = LID; green = LID_CORR; blue = LID_PREV). Crus2: Crus2 of the ansiform lobule. **d** Firing rate (Hz) across 9 weeks in DN. Boxplots show the median rate (horizontal bars), over 4 categories of weeks. First boxplot: 2nd and 3rd week of the protocol, second boxplot: 4th and 5th weeks when levodopa treatment started, third boxplot: 6th and 7th weeks, last boxplot: 8th and 9th weeks when stimulations stopped. Grey = SHAM (N=3); Magenta = LID (N=3); Green = LID_CORR (N=3); Blue = LID_PREV (N=3). Light grey lines: 6 weeks of levodopa (3 boxplots). Stripped blue lines: weeks of theta-burst PC stimulations. **e** Coefficient of variation 2 (cv2.isi) across 9 weeks in DN. The order of boxplots is identical to panel **d**. Grey = SHAM (N=3); Magenta = LID (N=3); Green = LID_CORR (N=3); Blue = LID_PREV (N=3). Light grey lines: 6 weeks of levodopa (3 boxplots). Stripped blue lines: weeks of theta-burst PC stimulations. **f** Firing rate (Hz) across 9 weeks in FN. The order of boxplots is identical to panel **d**. Grey = SHAM (N=3); Magenta = LID (N=6); Green = LID_CORR (N=4); Blue = LID_PREV (N=3). Light grey lines: 6 weeks of levodopa (3 boxplots). Stripped blue lines: weeks of theta-burst PC stimulations. **g** Coefficient of variation 2 (cv2.isi) across 9 weeks in FN. The order of boxplots is identical to panel **d**. Grey = SHAM (N=3); Magenta = LID (N=6); Green = LID_CORR (N=4); Blue = LID_PREV (N=3). Light grey lines: 6 weeks of levodopa (3 boxplots). Stripped blue lines: weeks of theta-burst PC stimulations.

Boxplots represents the lower and the upper quartiles. Welch Anova with Games Howell post-hoc test and one-way Anova's with Tukey post-hoc test based on Levene test. ***$p < 0.001$; **$p < 0.01$; *$p < 0.05$; ns: $p > 0.5$. See also Tables S2, S3, and S4.

Supplementary Fig. S6 Modulation of the firing rate of the deep cerebellar nuclei induced by locomotor activity. **Related to Fig. 2**

a Image of the tracking points of interest, represented by different colors (tip of the tail: dark blue; base of the tail: light blue; right ear: dark green; left ear: light green; nose: yellow; right led: dark red; left led: light red) during a recording session in the openfield using Deeplabcut. **b** Evolution of the probability of the head point during the recording. Diagram of the reconstruction of the head point (light red) from the barycenter weighted by the probabilities of the points: nose; right ear; left ear; right led; left led. **c** Path of the head's point as a function of the movement speed. The movement speed is discretized in "off" and "on" periods which are represented by blue and red circles, respectively when the speed is lower and higher than the threshold of 1cm/s. **d** Evolution of the speed of the head's point. The moments when the speed of the head's point crosses the threshold of 1cm/s (dotted line) are reported by a red star. **e** Cumulative distribution of the speed of the head's point. Threshold of 1cm/s: vertical dotted line. **f** Mean firing rate (Hz) of the deep cerebellar nuclei (DCN) activity as a function of the average velocity defined per second (cm/s). Mean firing rate: vertical dotted line, velocity threshold: horizontal dotted line. **g** Evolution of the average firing rate (Hz) of the DCN activity over time. **h** Raster plot of mean DCN activity around the transitions from "off" to "on" state of locomotor activity (red stars in D). **i** Relation of the firing rate (Hz) between the locomotor "on" and "off" periods defined per cell (n=12). Dotted line (y=x), straight red line of linear regression of the firing rate of the cells during the "on" periods as a function of the "off" periods.

Supplementary Fig. S7 Locomotor activity does not impact the firing rate of the three deep cerebellar nuclei in SHAM. Related to Fig. 2

Top: Firing rate (Hz) over 9 weeks in the three deep cerebellar nuclei (DCN) in all control mice: the interposed nucleus (IN, left), the dentate nucleus (DN, middle), and the fastigial nucleus (FN, right). *Middle*: Firing rate (Hz) during periods of locomotor activity ("on") over 9 weeks in DCN in all control mice: IN (left), DN (middle), and FN (right). *Bottom*: Firing rate (Hz) during periods of locomotor inactivity ("off") over 9 weeks in DCN in all control mice: IN (left), DN (middle), and FN (right).

Boxplots represents the lower and the upper quartiles and show the median rate (horizontal bars), over 4 categories of weeks. First boxplot: 2^{nd} and 3^{rd} week of the protocol, second boxplot: 4^{th} and 5^{th} weeks when levodopa treatment started as well as cerebellar stimulations for preventive sham mice, third boxplot: 6^{th} and 7^{th} weeks when corrective sham mice start receiving cerebellar stimulations, last boxplot: 8^{th} and 9^{th} weeks of the protocol when stimulations stop and long-term effects of cerebellar stimulations are visible. Control mice only treated with levodopa represented in dark grey (SHAM, IN: N=1, FN: N=1, DN: N=2); control mice treated with levodopa and receiving 2 weeks of Purkinje cell stimulations represented in grey (SHAM_CORR, IN: N=2); control mice treated with levodopa and receiving 4 weeks of Purkinje cell stimulations represented in grey (SHAM_PREV, IN: N=2, FN: N=2, DN: N=1). Light grey lines: 6 weeks of levodopa (3 boxplots). Stripped blue lines: weeks of theta-burst Purkinje cell stimulations. Welch Anova with Games Howell post-hoc test and one-way Anova's with Tukey post-hoc test based on Levene test. ***$p < 0.001$; **$p < 0.01$; *$p < 0.05$; ns: $p > 0.5$. See also Table S9.

Supplementary Fig. S8 In dyskinetic mice, the burst rate decreases during periods of activity and increases during periods of inactivity. These effects are prevented by cerebellar stimulations in the interposed nucleus. Related to Fig. 2

a Burst rate (Hz) during periods of locomotor activity ("on") over 9 weeks in the interposed nucleus (IN, left), the dentate nucleus (DN, middle), and the fastigial nucleus (FN, right). Boxplots show the median burst rate (horizontal bars), over 4 categories of weeks. First boxplot: 2nd and 3rd week of the protocol, second boxplot: 4th and 5th weeks when levodopa treatment started, third boxplot: 6th and 7th, last boxplot: 8th and 9th weeks when stimulations stopped. Grey = SHAM (IN: N=4, DN: N=3, FN: N=3); Magenta = LID (IN: N=3, DN: N=4, FN: N=6); Green = LID_CORR (IN: N=4, DN: N=3, FN: N=4); Blue = LID_PREV (IN: N=3, DN: N=3, FN: N=3). Light grey lines: 6 weeks of levodopa (3 boxplots). Stripped blue lines: weeks of theta-burst Purkinje cell stimulations. **b** Burst rate (Hz) during periods of locomotor inactivity ("off") over 9 weeks in IN (left), DN (middle), and FN (right). Same order of boxplot as panel A. Grey = SHAM (IN: N=4, DN: N=3, FN: N=3); Magenta = LID (IN: N=3, DN: N=4, FN: N=6); Green = LID_CORR (IN: N=4, DN: N=3, FN: N=4); Blue = LID_PREV (IN: N=3, DN: N=3, FN: N=3). Light grey lines: 6 weeks of levodopa (3 boxplots). Stripped blue lines: weeks of theta-burst Purkinje cell stimulations.

Boxplots represents the lower and the upper quartiles. Welch Anova with Games Howell post-hoc test and one-way Anova's with Tukey post-hoc test based on Levene test. ***$p < 0.001$; **$p < 0.01$; *$p < 0.05$; ns: $p > 0.5$. See also Table S10 and S11.

Supplementary Fig. S9 Neither levodopa nor Purkinje cell stimulations affect the firing rate in the ventroanterior-ventrolateral complex of the thalamus. Related to Fig. 3

a Experimental timeline. Dyskinetic mice (LID, red): 5 weeks of levodopa treatment. Preventive mice LID_PREV, blue): 5 weeks of levodopa treatment + 4 weeks of cerebellar stimulations. Corrective mice (LID_CORR, green): 5 weeks of levodopa treatment + 2 weeks of cerebellar stimulations. **b** Schematic of electrode implantation in ventroanterior-ventrolateral complex of the thalamus (VAL), ChR2-YFP expression in the Purkinje cells (PC+ChR2, green) and injection site with 6-OHDA or saline in sagittal mouse brain. ST: Striatum; SNc: substantia nigra *pars compacta*; M1: Primary motor cortex, PF: Parafascicular nucleus of the thalamus, DCN: deep cerebellar nuclei, CrusII: Crus2 of the ansiform lobule. **c** Coronal section from L7-ChR2-YFP mouse showing the electrode's trajectory (yellow dotted line) and the electrolytic lesion (red circle) at the recording site in VAL. Scale bar: 0.5 mm. **d** Firing rate (Hz) across 9 weeks in VAL. Boxplots show the median rate (horizontal bars), over 4 categories of weeks. First boxplot: 2^{nd} and 3^{rd} week of the protocol, second boxplot: 4^{th} and 5^{th} weeks when levodopa treatment started, third boxplot: 6^{th} and 7^{th} weeks, last boxplot represents the 8^{th} week when stimulations stopped. Grey = SHAM (N=5); Magenta = LID (N=4); Green = LID_CORR (N=6); Blue = LID_PREV (N=8). Light grey lines: 6 weeks of levodopa (3 boxplots). Stripped blue lines: weeks of theta-burst PC stimulations.

Boxplots represents the lower and the upper quartiles. One-way Anova with Tukey HSD post-hoc test. ***$p < 0.001$; **$p < 0.01$; *$p < 0.05$; ns: $p > 0.5$. See also Table S6.

Figure 1

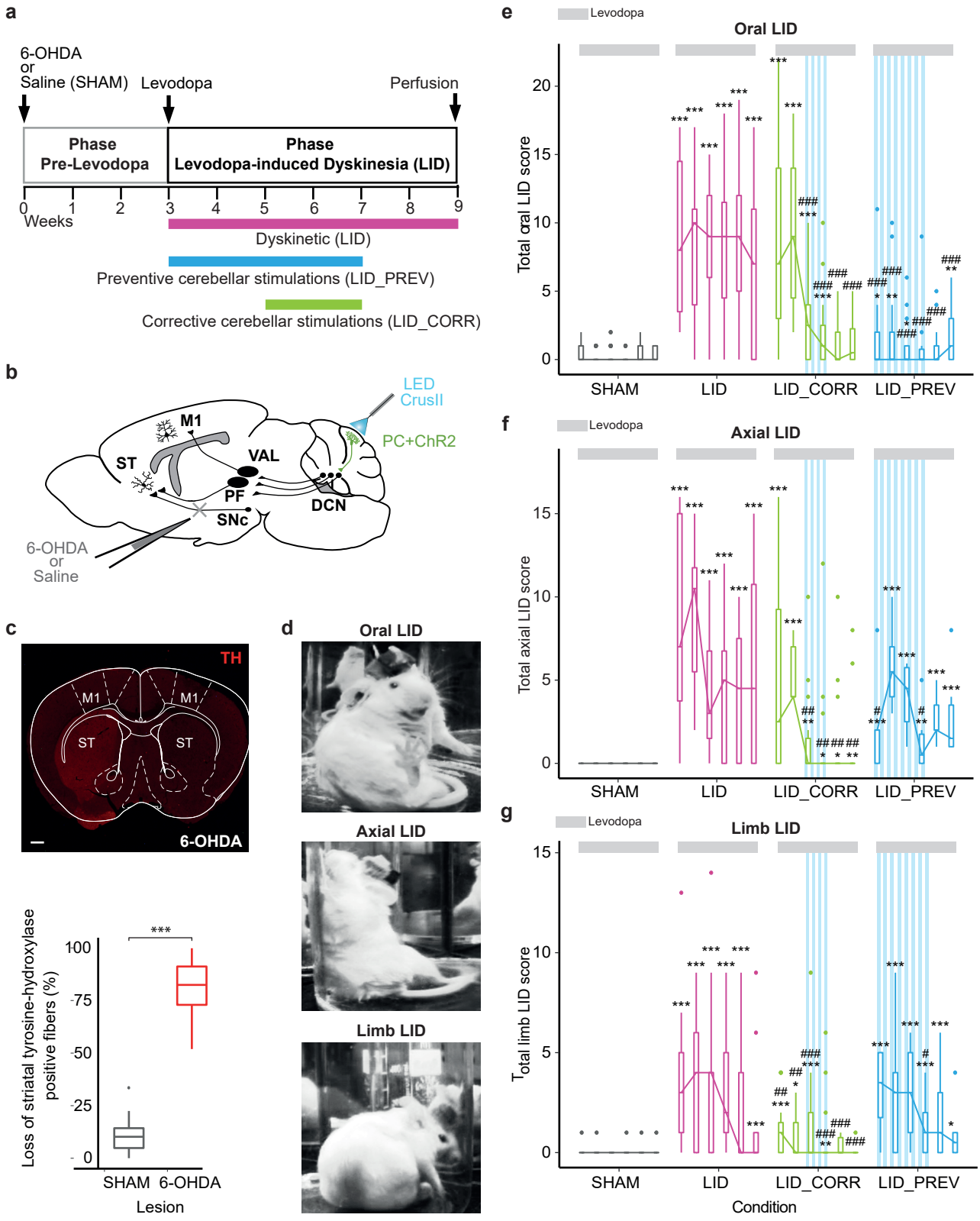

Figure 2

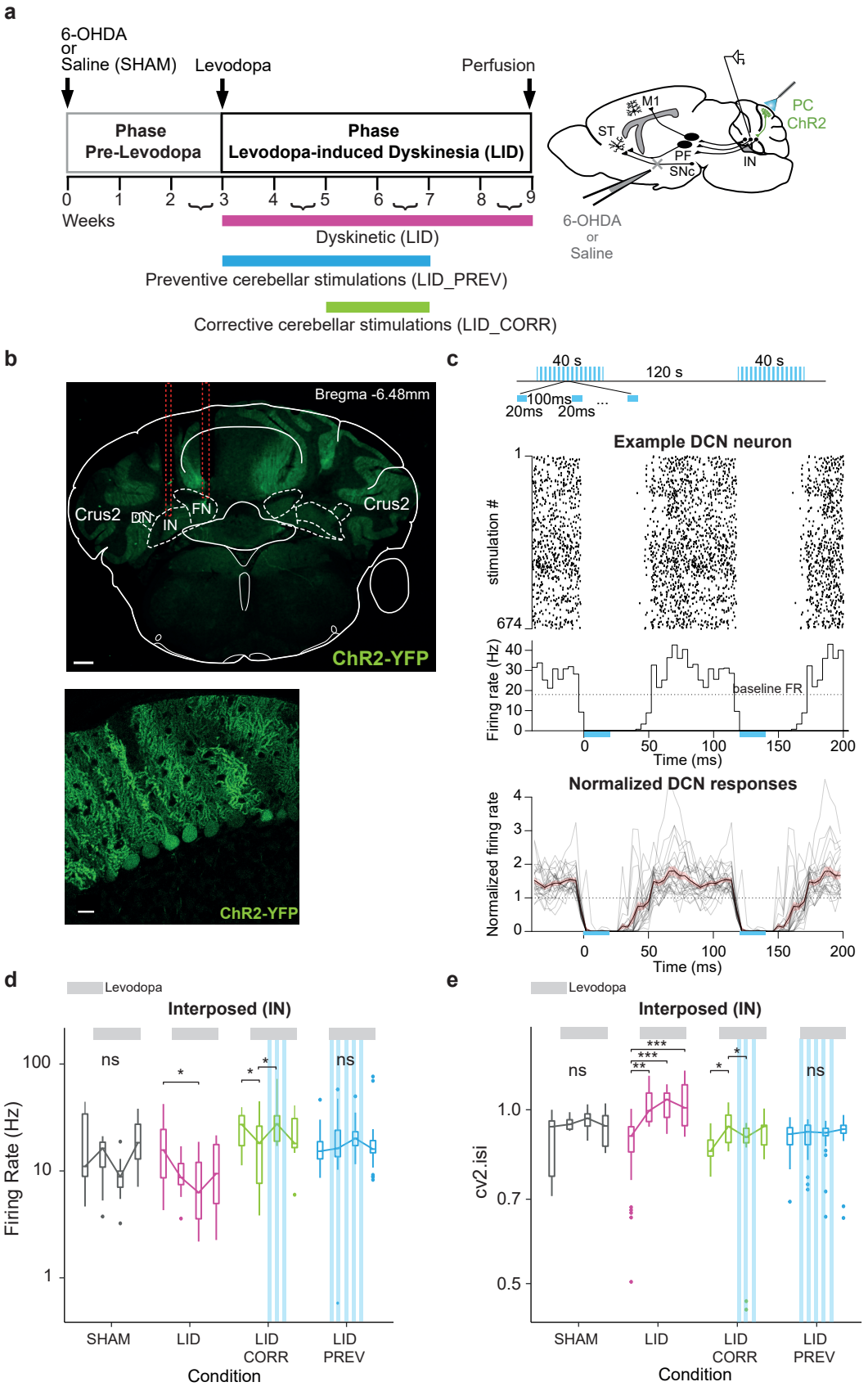

Figure 3

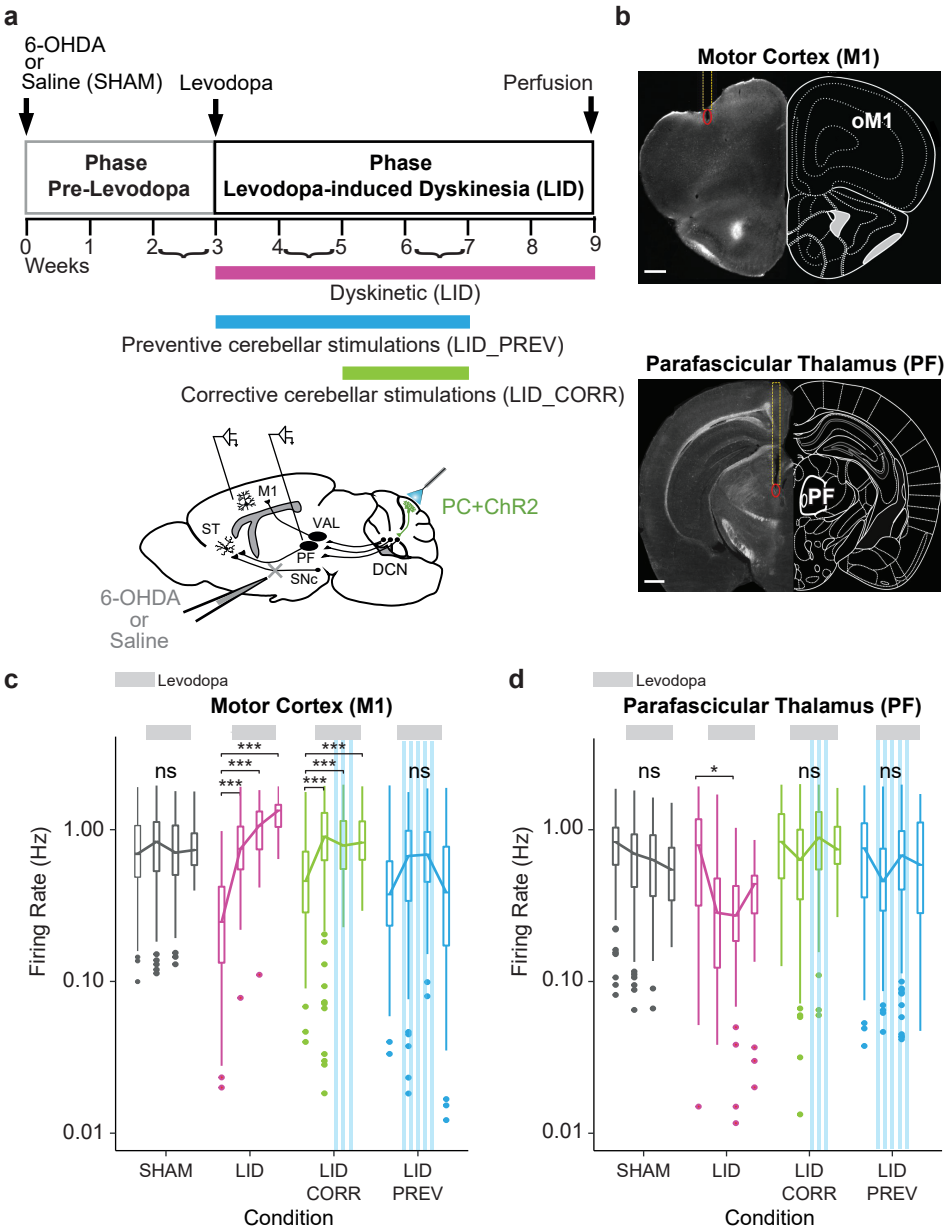

Figure 4

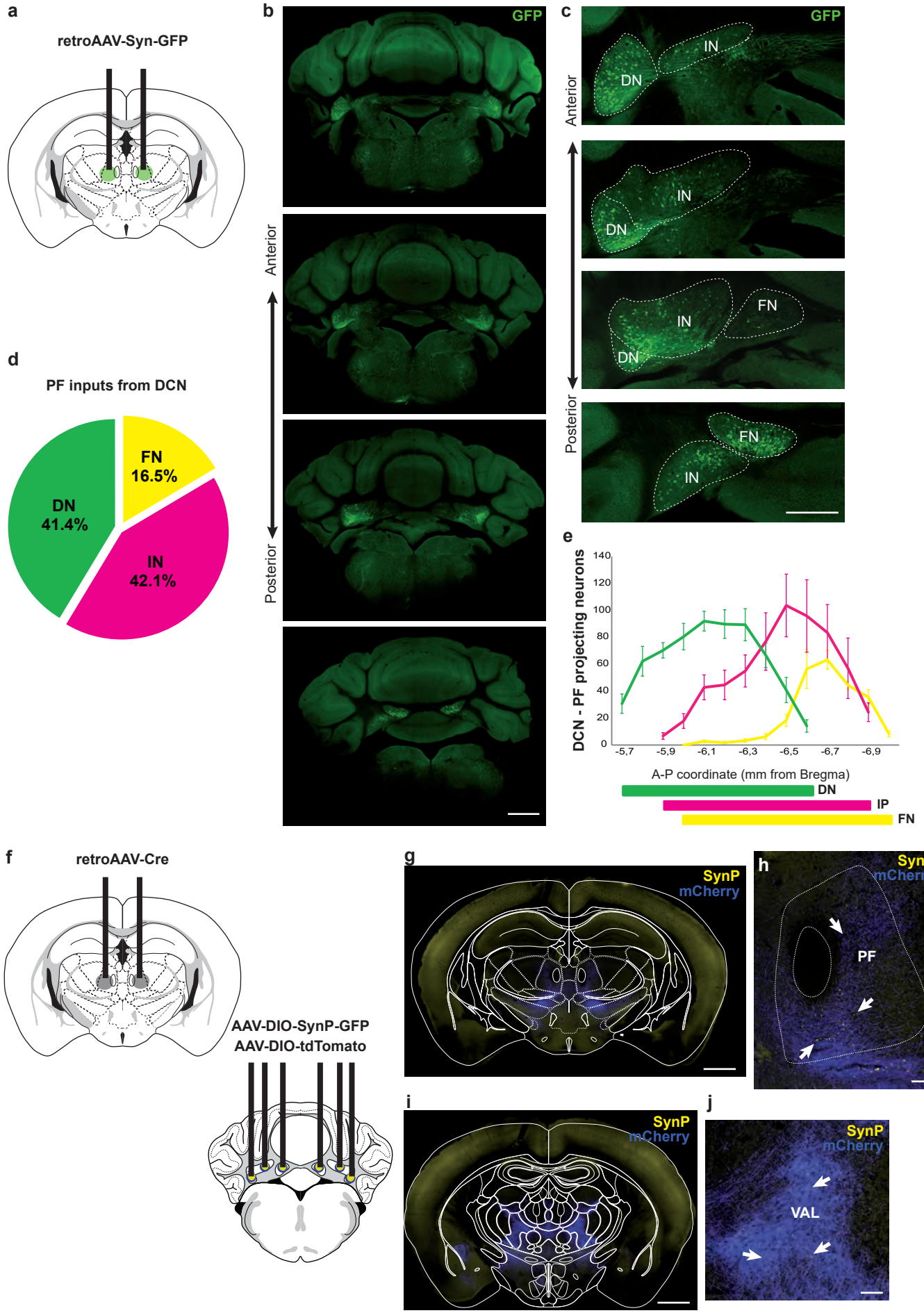

Figure 5

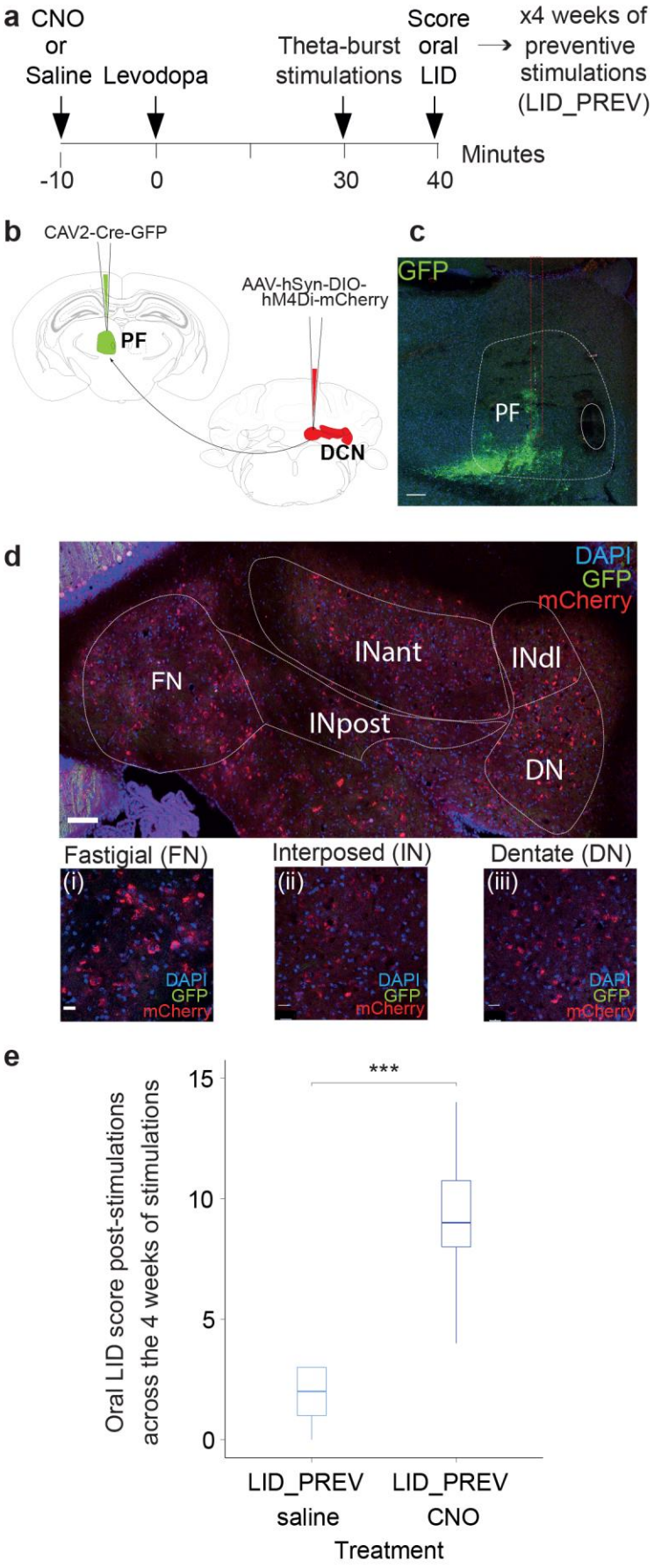
a
CNO or Saline
Levodopa
Theta-burst stimulations
Score oral LID
x4 weeks of preventive stimulations (LID_PREV)
-10
0
30
40
Minutes
b
CAV2-Cre-GFP
PF
AAV-hSyn-DIO-hM4Di-mCherry
DCN
c
GFP
PF
d
DAPI
GFP
mCherry
FN
INant
INdl
INpost
DN
Fastigial (FN)
Interposed (IN)
Dentate (DN)
(i)
(ii)
(iii)
e
***
Oral LID score post-stimulations across the 4 weeks of stimulations
15
10
5
0
LID_PREV saline
LID_PREV CNO
Treatment

Figure 6

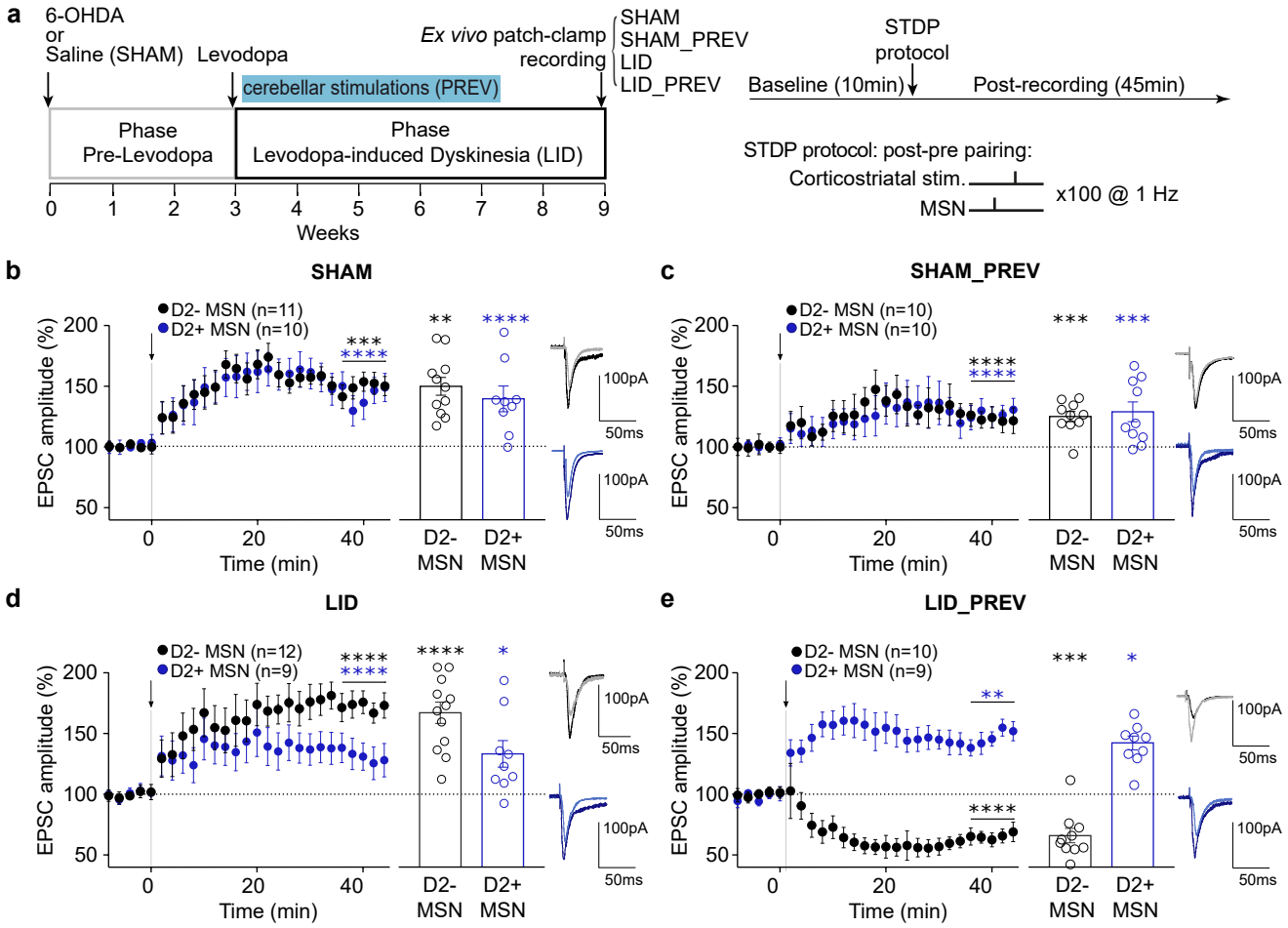

Figure 7

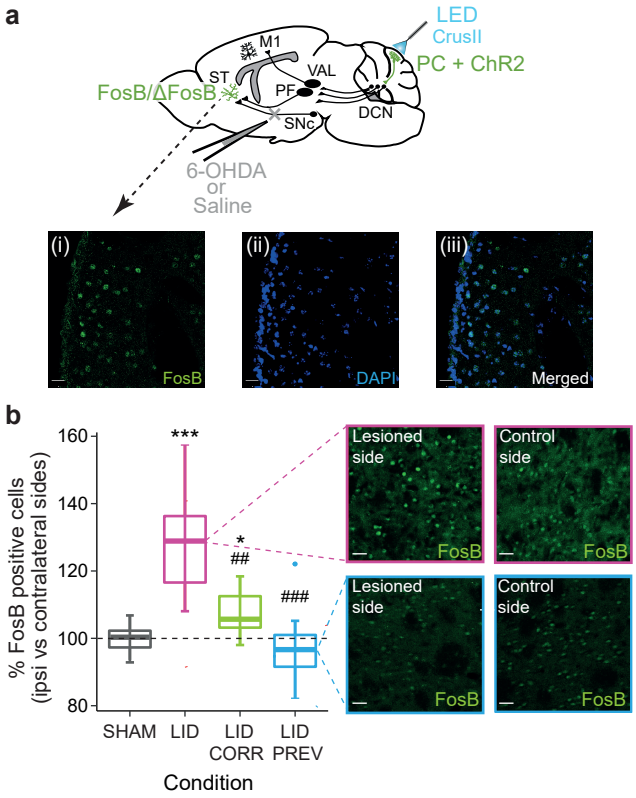

Supplementary Fig. S1

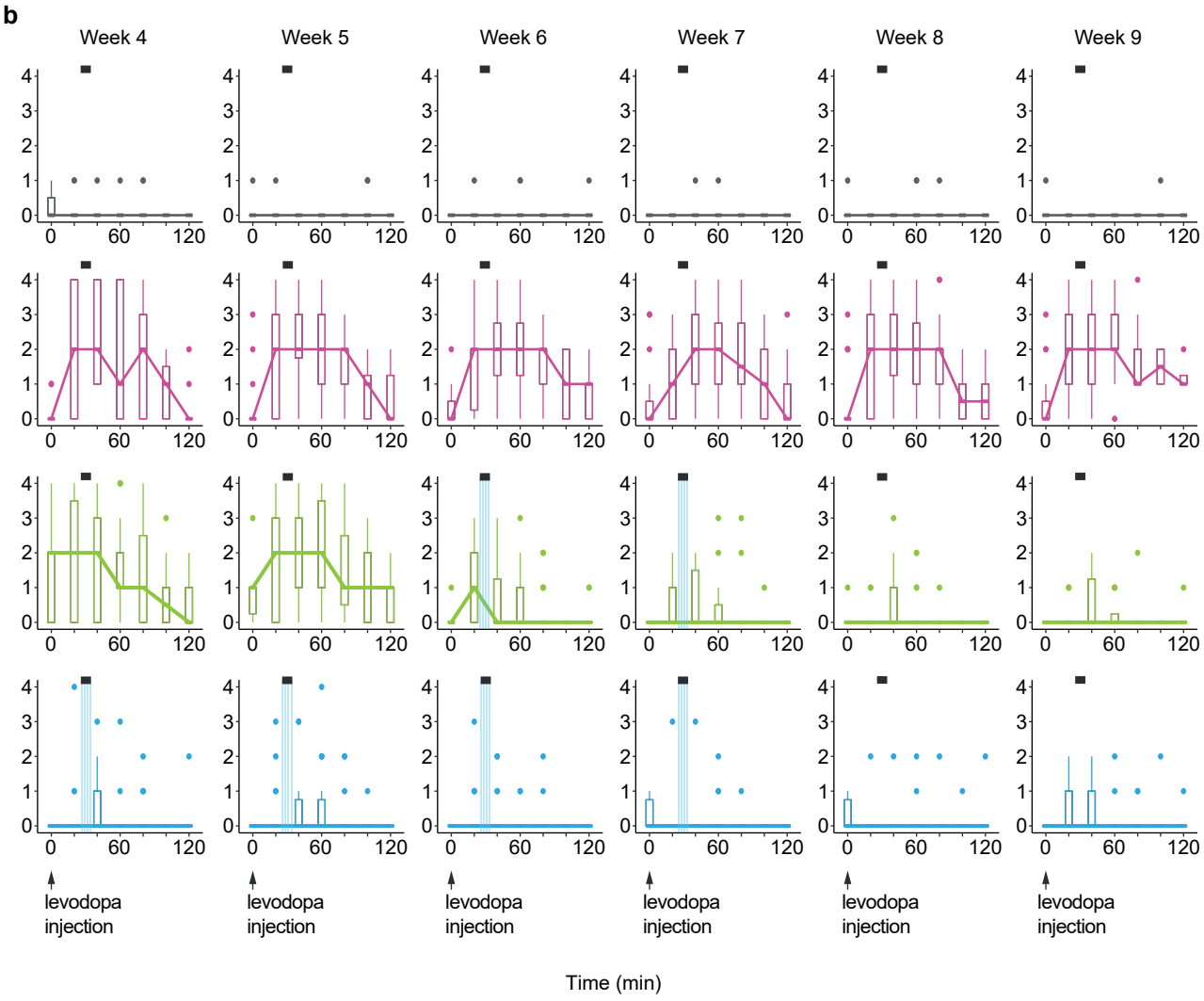

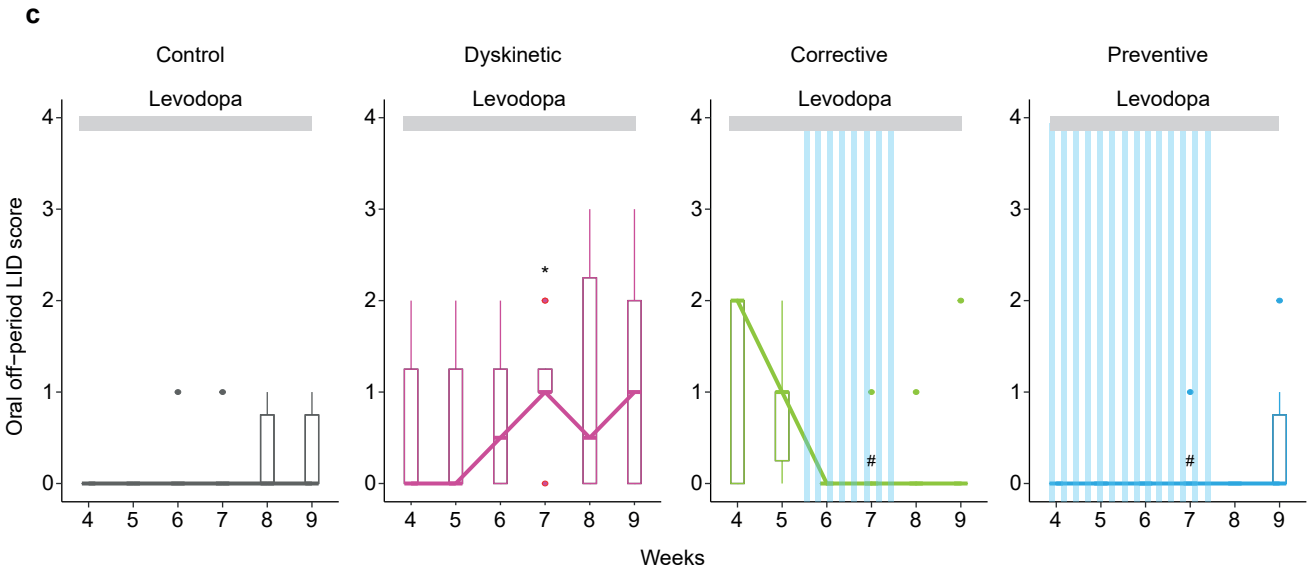

Supplementary Fig. S2

a

b

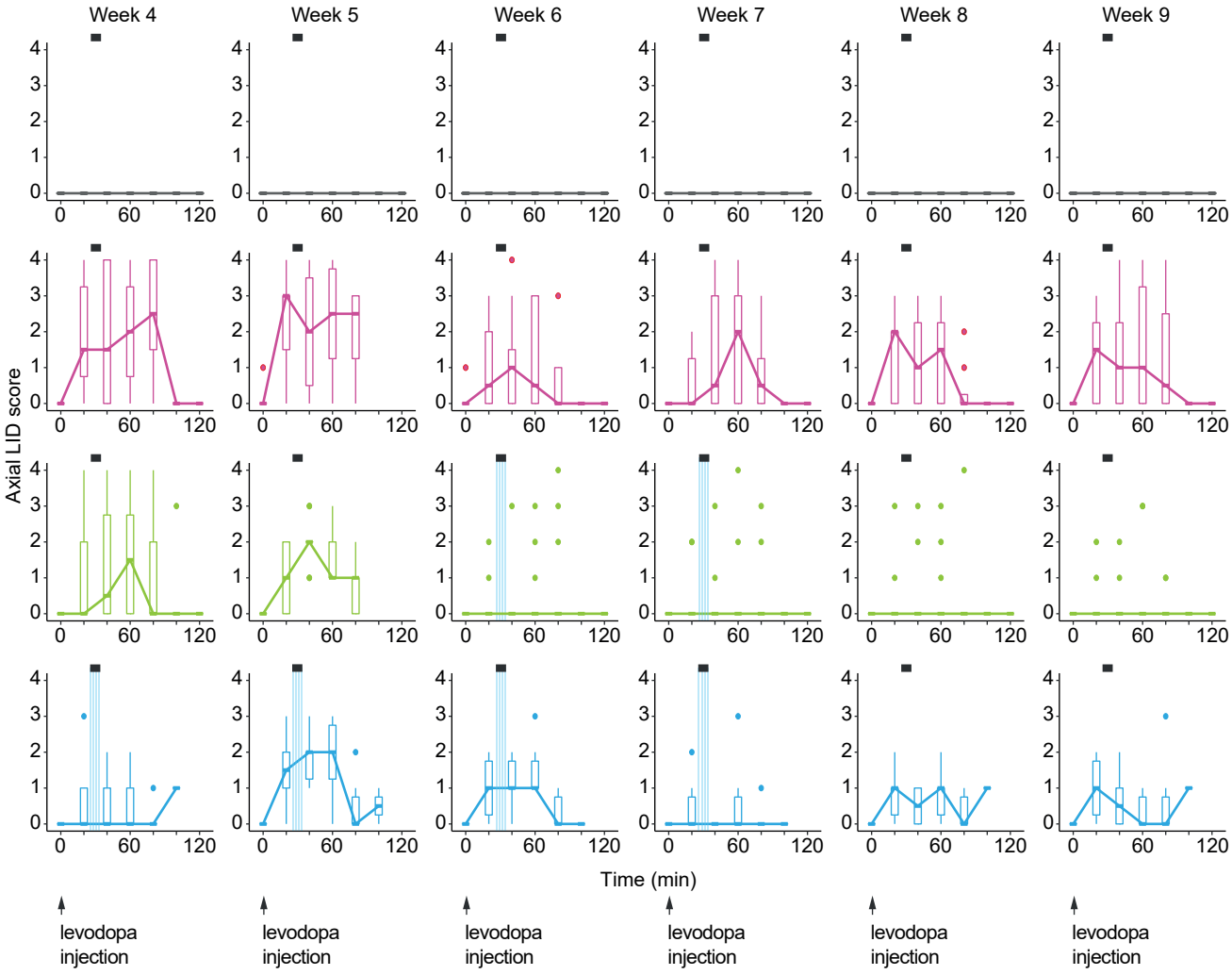

Supplementary Fig. S3

a

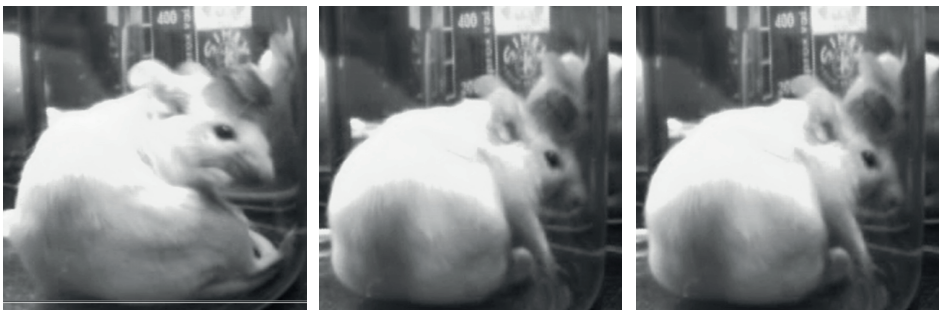

b

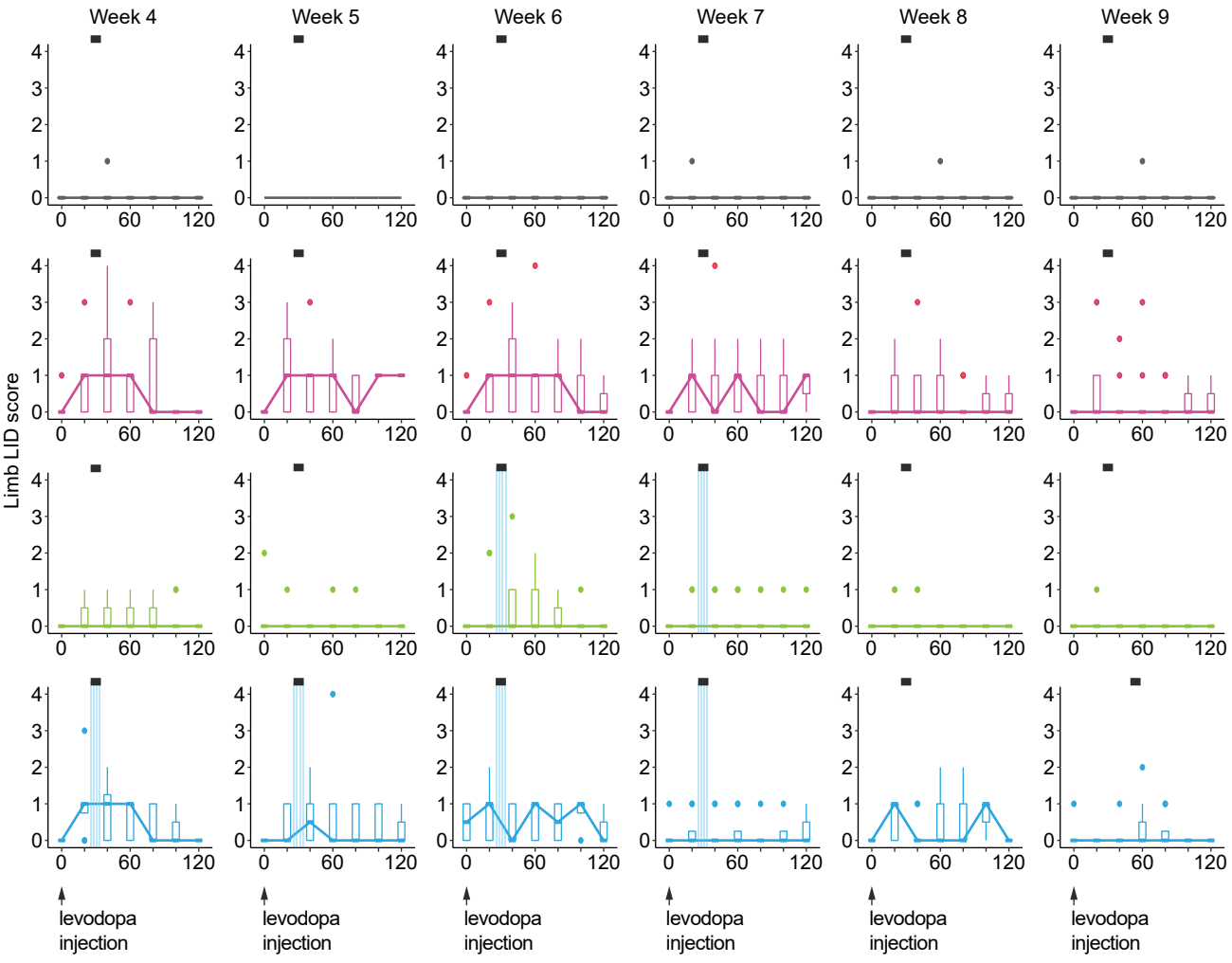

Supplementary Fig. S4

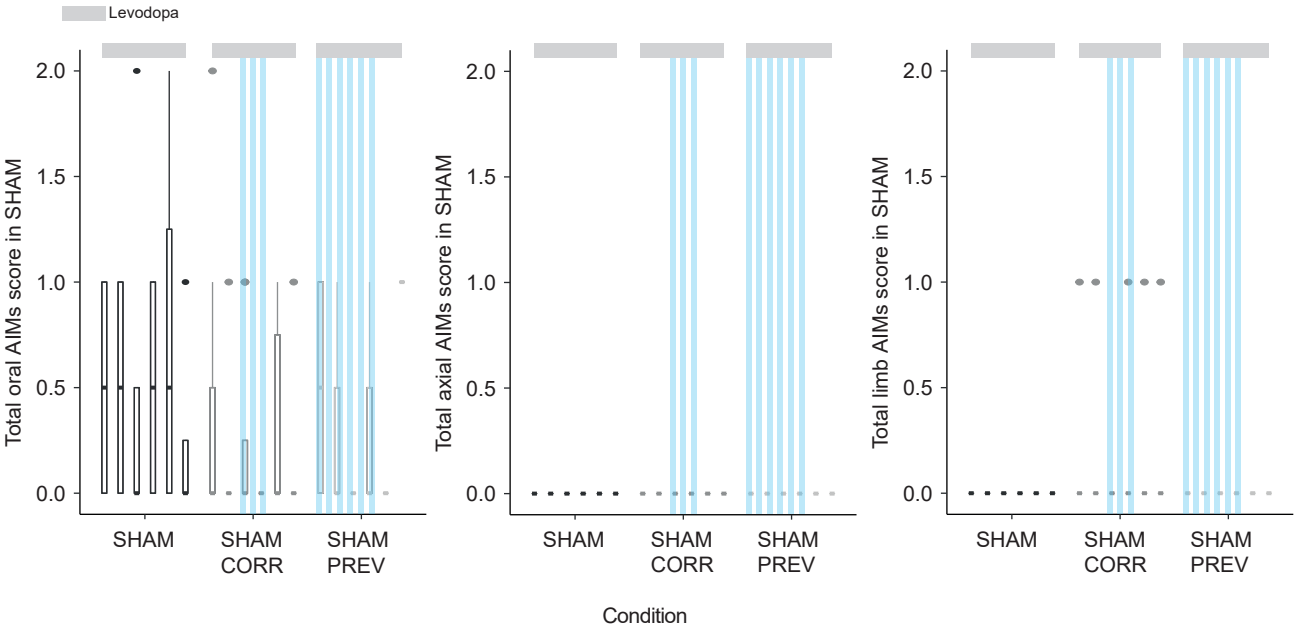

Supplementary Fig. S5

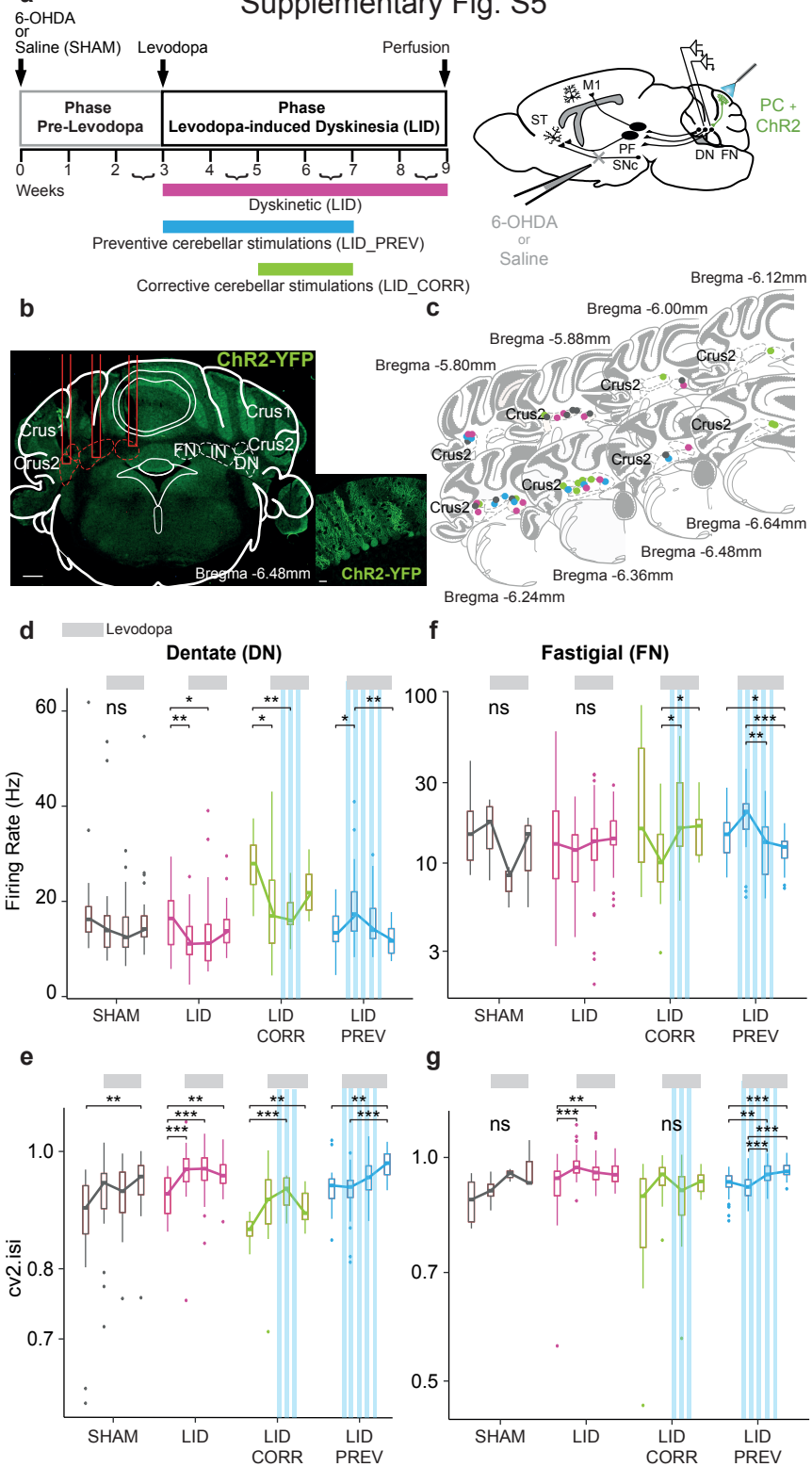

Influence of locomotion on DCN discharge

As DCN activity is modulated by locomotion in normal animals (Sarnaik and Raman, 2018), we quantified the locomotor activity using DeepLabCut (Mathis et al., 2018) (**Supplementary Figure 6**) and tested if the activity observed in DCN correlated with a change in locomotor activity in control animals (**Supplementary Figure 7**). No differences were observed in the DCN during levodopa treatment in control animals, whether the animals were moving or not (**Supplementary Figure 7**).

Increased cv2.isi does not simply reflect increased bursting

Since greater cv2.isi in LID mice may reflect irregular burst firing under levodopa treatment in DCN neurons, we analyzed the burst rate in periods of locomotor activity and inactivity. Surprisingly, the burst rate of dyskinetic mice decreased during levodopa treatment in periods of activity in the IN, DN, and FN (**Supplementary Figure 8a**). However, the burst rate of LID mice in periods of locomotor inactivity increased during levodopa treatment in the DN and FN (**Supplementary Figure 8b**).

PC stimulations during 4 weeks prevented the decreased of the burst rate in the IN during periods of locomotor activity (**Supplementary Figure 8a, left panel**). Changes, although less consistent, were also observed as a function of the motor state in the DN and FN (**Supplementary Figure 8a, middle and right panels)**. Only mild differences were observed in the burst rate in the IN, DN or FN in the different groups during periods of locomotor inactivity (**Supplementary Figure 8b)**.

References

Mathis, A., Mamidanna, P., Cury, K.M., Abe, T., Murthy, V.N., Mathis, M.W., and Bethge, M. (2018). DeepLabCut: markerless pose estimation of user-defined body parts with deep learning. Nat Neurosci 21, 1281-1289.

Sarnaik, R., and Raman, I.M. (2018). Control of voluntary and optogenetically perturbed locomotion by spike rate and timing of neurons of the mouse cerebellar nuclei. Elife 7.

Supplementary Fig. S6

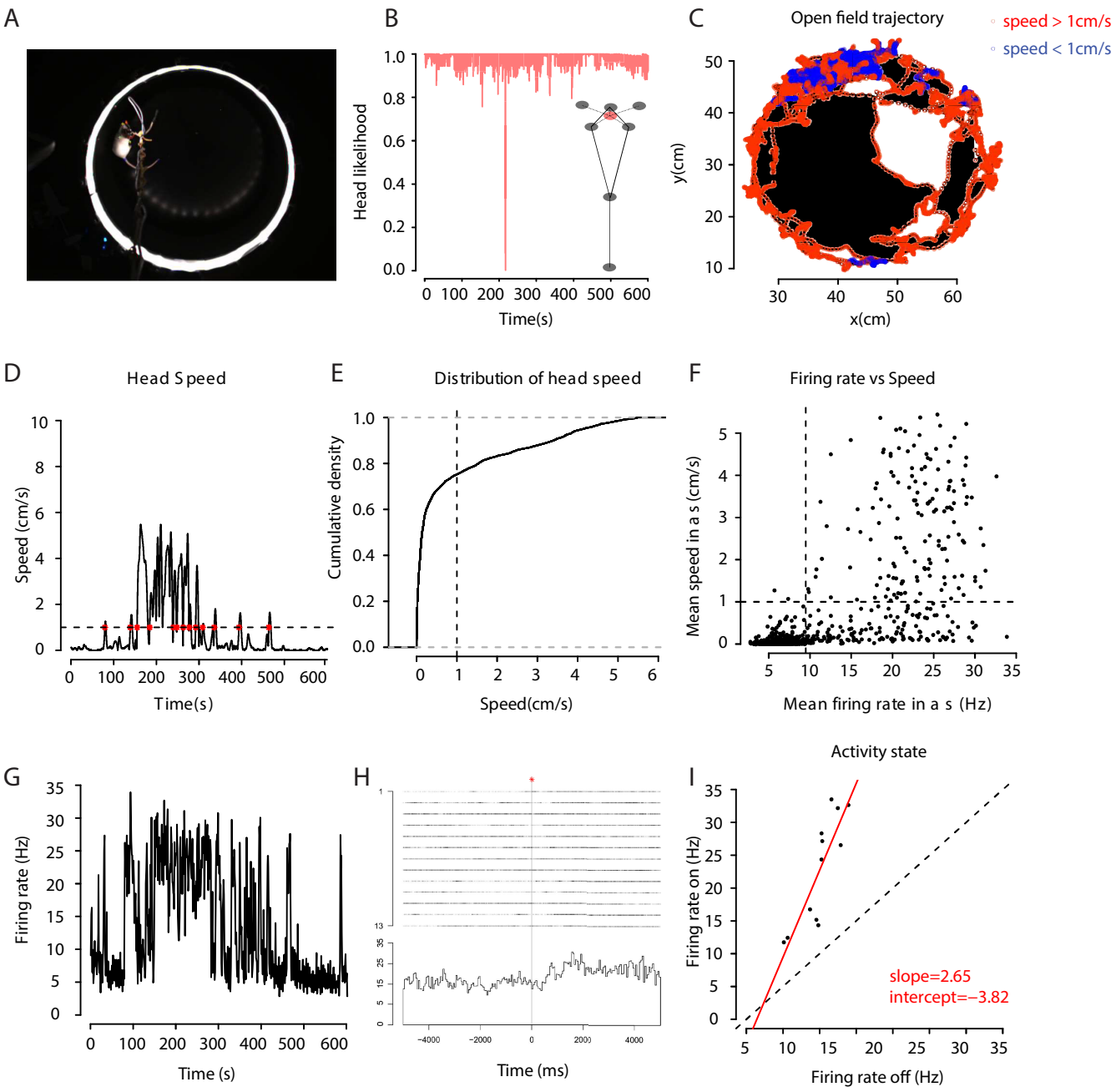

Supplementary Fig. S7

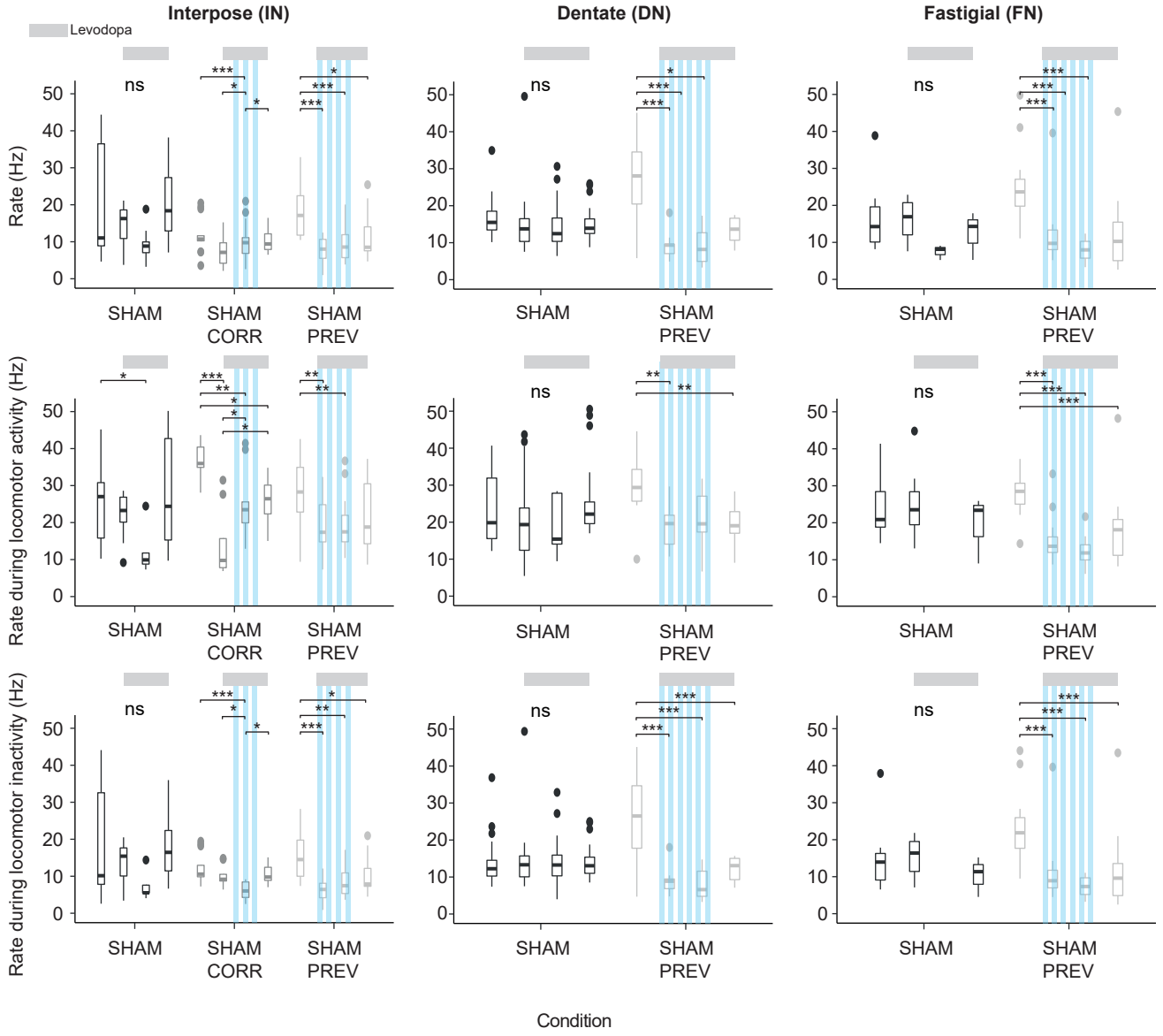

Supplementary Fig. S8

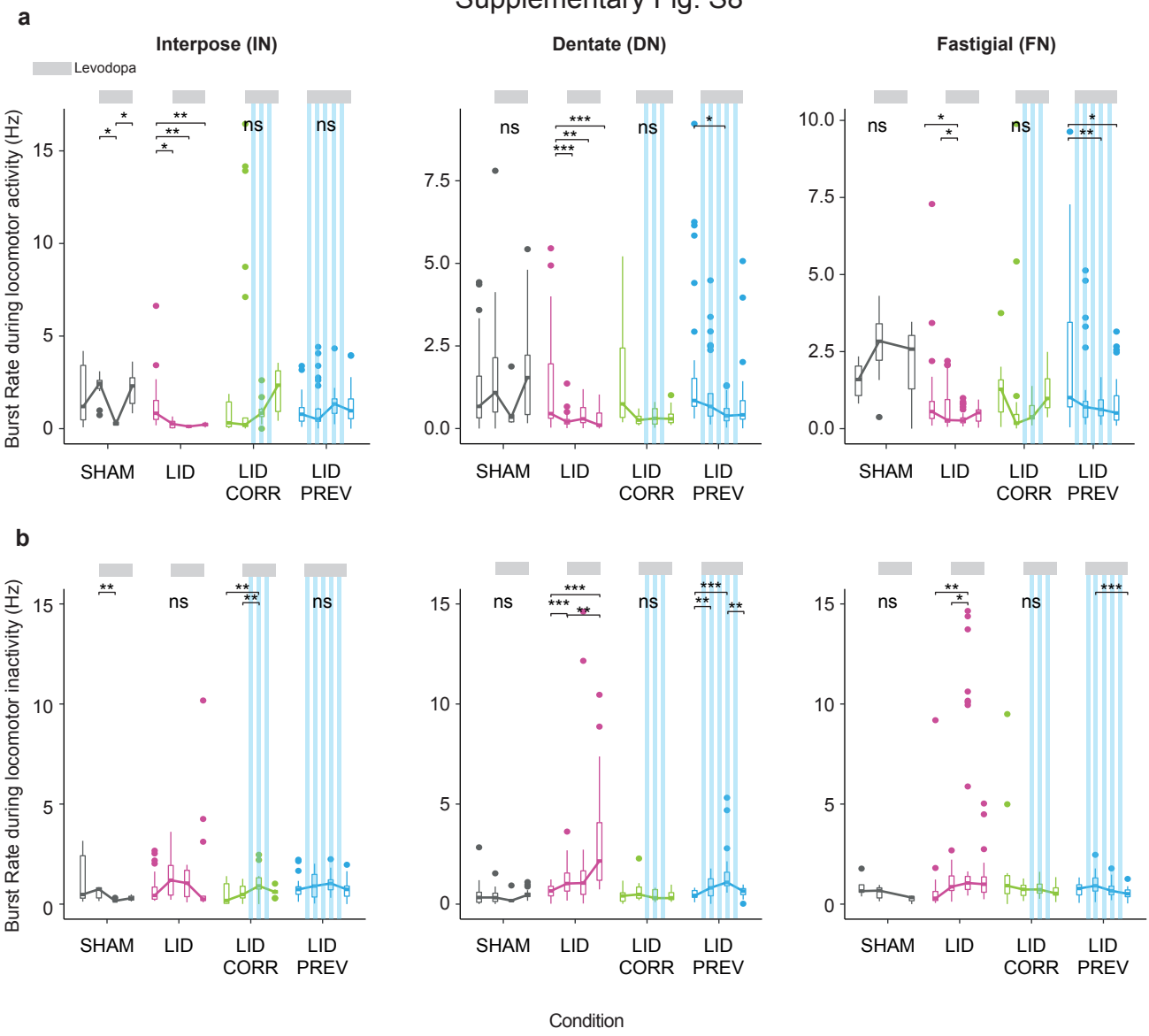

Supplementary Fig. S9

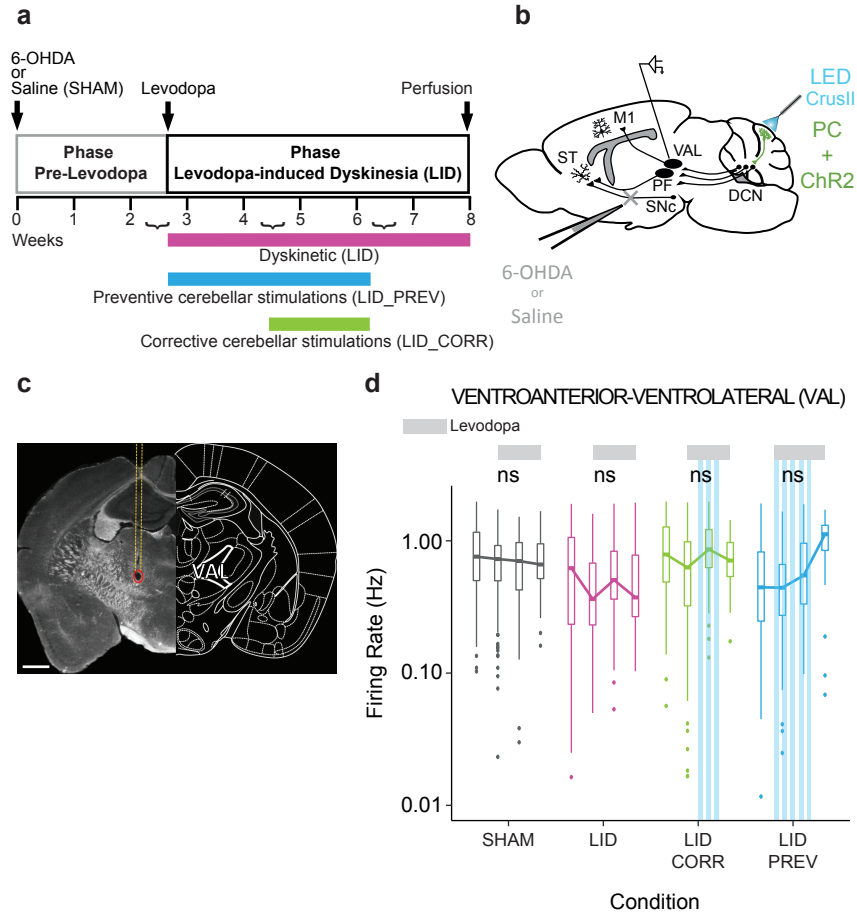

Table S1: Precision measures, exact p-values, and replicate data relevant to Figure 1, and Supplementary Figure 1c

Fig	Param	Week	Group1	Group2	Mean1	Mean2	n1	n2	Sum	Adjusted p Value
Fig. 1c	6OHDA lesion	/	6-OHDA	SHAM	80.93	11.05	40	17	***	< 0.001
Fig. 1e	Oral	4	LID	SHAM	8.84	0.42	19	19	***	< 0.001
			LID_CORR	SHAM	7.96	0.42	23	19	***	< 0.001
			LID_PREV	SHAM	1.59	0.42	17	19	*	0.035
			LID_CORR	LID	7.96	8.84	23	19	ns	0.711
			LID_PREV	LID	1.59	8.84	17	19	###	< 0.001
			LID_PREV	LID_CORR	1.59	7.96	17	23	&&&	< 0.001
Fig. 1e	Oral	5	LID	SHAM	7.79	0.23	19	17	***	< 0.001
			LID_CORR	SHAM	9.20	0.23	15	17	***	< 0.001
			LID_PREV	SHAM	1.83	0.23	18	17	**	0.002
			LID_CORR	LID	9.20	7.79	15	19	ns	0.425
			LID_PREV	LID	1.83	7.79	18	19	###	< 0.001
			LID_PREV	LID_CORR	1.83	9.20	18	15	&&&	< 0.001
Fig. 1e	Oral	6	LID	SHAM	8.31	0.23	19	19	***	< 0.001
			LID_CORR	SHAM	2.71	0.23	24	19	***	< 0.001
			LID_PREV	SHAM	0.94	0.23	18	19	*	0.048
			LID_CORR	LID	2.71	8.31	24	19	###	< 0.001
			LID_PREV	LID	0.94	8.31	18	19	###	< 0.001
			LID_PREV	LID_CORR	0.94	2.71	18	24	&&	0.002

Fig. 1e	Oral	7	LID	SHAM	8.37	0.20	19	15	***	< 0.001
			LID_CORR	SHAM	1.87	0.20	23	15	***	< 0.001
			LID_PREV	SHAM	0.78	0.20	18	15	ns	0.127
			LID_CORR	LID	1.87	8.37	23	19	###	< 0.001
			LID_PREV	LID	0.78	8.37	18	19	###	< 0.001
			LID_PREV	LID_CORR	0.78	1.87	18	23	&	0.010
Fig. 1e	Oral	8	LID	SHAM	8.74	0.35	19	17	***	< 0.001
			LID_CORR	SHAM	0.91	0.35	23	17	ns	0.16
			LID_PREV	SHAM	0.78	0.35	18	17	ns	0.43
			LID_CORR	LID	0.91	8.74	23	19	###	< 0.001
			LID_PREV	LID	0.78	8.74	18	19	###	< 0.001
			LID_PREV	LID_CORR	0.78	0.91	18	23	ns	0.43
Fig. 1e	Oral	9	LID	SHAM	6.42	0.36	19	11	***	< 0.001
			LID_CORR	SHAM	1.31	0.36	16	11	ns	0.053
			LID_PREV	SHAM	1.92	0.36	13	11	**	0.004
			LID_CORR	LID	1.31	6.42	16	19	###	< 0.001
			LID_PREV	LID	1.92	6.42	13	19	###	< 0.001
			LID_PREV	LID_CORR	1.92	1.31	13	16	ns	0.219
Fig. 1f	Axial	4	LID	SHAM	8.12	0	8	12	***	<0.001
			LID_CORR	SHAM	5.07	0	14	12	***	<0.001
			LID_PREV	SHAM	2.40	0	5	12	***	<0.001
			LID_CORR	LID	5.07	8.12	14	8	ns	0.077
			LID_PREV	LID	2.40	8.12	5	8	#	0.018

			LID_PREV	LID_CORR	2.40	5.07	5	14	ns	0.219
Fig. 1f	Axial	5	LID	SHAM	9.00	0	6	9	***	<0.001
			LID_CORR	SHAM	5.40	0	5	9	***	<0.001
			LID_PREV	SHAM	5.83	0	6	9	***	<0.001
			LID_CORR	LID	5.40	9.00	5	6	ns	0.190
			LID_PREV	LID	5.83	9.00	6	6	ns	0.190
			LID_PREV	LID_CORR	5.83	5.40	6	5	ns	0.980
Fig. 1f	Axial	6	LID	SHAM	4.25	0	8	11	***	<0.001
			LID_CORR	SHAM	1.50	0	14	11	**	0.006
			LID_PREV	SHAM	4.00	0	6	11	***	<0.001
			LID_CORR	LID	1.50	4.25	14	8	##	0.002
			LID_PREV	LID	4.00	4.25	6	8	ns	0.610
			LID_PREV	LID_CORR	4.00	1.50	6	14	&&&	<0.001
Fig. 1f	Axial	7	LID	SHAM	4.62	0	8	11	***	<0.001
			LID_CORR	SHAM	1.36	0	14	11	*	0.014
			LID_PREV	SHAM	1.33	0	6	11	**	0.004
			LID_CORR	LID	1.36	4.62	14	8	##	0.002
			LID_PREV	LID	1.33	4.62	6	8	#	0.030
			LID_PREV	LID_CORR	1.33	1.36	6	14	ns	0.586
Fig. 1f	Axial	8	LID	SHAM	4.37	0	8	11	***	<0.001
			LID_CORR	SHAM	1.36	0	14	11	*	0.011
			LID_PREV	SHAM	2.67	0	6	11	***	<0.001
			LID_CORR	LID	1.36	4.37	14	8	##	0.001

			LID_PREV	LID	2.67	4.37	6	8	ns	0.628
			LID_PREV	LID_CORR	2.67	1.36	6	14	&&	0.001
Fig. 1f	Axial	9	LID	SHAM	5.85	0	8	11	***	<0.001
			LID_CORR	SHAM	1.27	0	11	11	**	0.005
			LID_PREV	SHAM	2.83	0	6	11	***	<0.001
			LID_CORR	LID	1.27	5.85	11	8	##	0.001
			LID_PREV	LID	2.83	5.85	6	8	ns	0.246
			LID_PREV	LID_CORR	2.83	1.27	6	11	&	0.021
Fig. 1g	Limb	4	LID	SHAM	3.89	0.07	9	14	***	<0.001
			LID_CORR	SHAM	1.20	0.07	15	14	***	<0.001
			LID_PREV	SHAM	3.12	0.07	8	14	***	<0.001
			LID_CORR	LID	1.20	3.89	15	9	##	0.003
			LID_PREV	LID	3.12	3.89	8	9	ns	0.981
			LID_PREV	LID_CORR	3.12	1.20	8	15	&&	0.002
Fig. 1g	Limb	5	LID	SHAM	3.57	0.09	7	11	***	<0.001
			LID_CORR	SHAM	0.83	0.09	6	11	*	0.034
			LID_PREV	SHAM	2.67	0.09	9	11	***	<0.001
			LID_CORR	LID	0.83	3.57	6	7	##	0.004
			LID_PREV	LID	2.67	3.57	9	7	ns	0.375
			LID_PREV	LID_CORR	2.67	0.83	9	6	&	0.015
Fig. 1g	Limb	6	LID	SHAM	4.22	0	9	13	***	<0.001
			LID_CORR	SHAM	1.53	0	15	13	***	<0.001
			LID_PREV	SHAM	2.89	0	9	13	***	<0.001

			LID_CORR	LID	1.53	4.22	15	9	###	<0.001
			LID_PREV	LID	2.89	4.22	9	9	ns	0.476
			LID_PREV	LID_CORR	2.89	1.53	9	15	&&	0.003
Fig. 1g	Limb	7	LID	SHAM	3.44	0.08	9	12	***	<0.001
			LID_CORR	SHAM	0.86	0.08	14	12	**	0.004
			LID_PREV	SHAM	1.22	0.08	9	12	***	<0.001
			LID_CORR	LID	0.86	3.44	14	9	###	<0.001
			LID_PREV	LID	1.22	3.44	9	9	#	0.018
			LID_PREV	LID_CORR	1.22	0.86	9	14	ns	0.302
Fig. 1g	Limb	8	LID	SHAM	2.22	0.08	9	12	***	<0.001
			LID_CORR	SHAM	0.28	0.08	14	12	ns	0.264
			LID_PREV	SHAM	2.00	0.08	9	12	***	<0.001
			LID_CORR	LID	0.28	2.22	14	9	###	<0.001
			LID_PREV	LID	2.00	2.22	9	9	ns	0.852
			LID_PREV	LID_CORR	2.00	0.28	9	14	&&&	<0.001
Fig. 1g	Limb	9	LID	SHAM	1.89	0.08	9	12	***	<0.001
			LID_CORR	SHAM	0.09	0.08	11	12	ns	0.936
			LID_PREV	SHAM	0.87	0.08	8	12	*	0.014
			LID_CORR	LID	0.09	1.89	11	9	###	<0.001
			LID_PREV	LID	0.87	1.89	8	9	ns	0.291
			LID_PREV	LID_CORR	0.87	0.09	8	11	&	0.018
Supp. Fig1c	Oral	4	LID	SHAM	0.62	0	8	7	ns	0.160

			LID_CORR	SHAM	1.20	0	5	7	ns	0.150
			LID_PREV	SHAM	0	0	5	7	-	-
			LID_CORR	LID	1.20	0.62	5	8	ns	0.370
			LID_PREV	LID	0	0.62	5	8	ns	0.210
			LID_PREV	LID_CORR	0	1.20	5	5	ns	0.160
Supp. Fig1c	Oral	5	LID	SHAM	0.62	0	8	6	ns	0.157
			LID_CORR	SHAM	0.83	0	6	6	ns	0.067
			LID_PREV	SHAM	0	0	6	6	-	-
			LID_CORR	LID	0.83	0.62	6	8	ns	0.575
			LID_PREV	LID	0	0.62	6	8	ns	0.157
			LID_PREV	LID_CORR	0	0.83	6	6	ns	0.067
Supp. Fig1c	Oral	6	LID	SHAM	0.75	0.17	8	6	ns	0.330
			LID_CORR	SHAM	0	0.17	6	6	ns	0.400
			LID_PREV	SHAM	0	0.17	6	6	ns	0.400
			LID_CORR	LID	0	0.75	6	8	ns	0.160
			LID_PREV	LID	0	0.75	6	8	ns	0.160
			LID_PREV	LID_CORR	0	0	6	6	-	-
Supp. Fig1c	Oral	7	LID	SHAM	1.12	0.17	8	6	*	0.028
			LID_CORR	SHAM	0.17	0.17	6	6	ns	1
			LID_PREV	SHAM	0.17	0.17	6	6	ns	1
			LID_CORR	LID	0.17	1.12	6	8	#	0.028
			LID_PREV	LID	0.17	1.12	6	8	#	0.028
			LID_PREV	LID_CORR	0.17	0.17	6	6	ns	1

Supp. Fig1c	Oral	8	LID	SHAM	1.12	0.33	8	6	ns	0.490
			LID_CORR	SHAM	0.17	0.33	6	6	ns	0.590
			LID_PREV	SHAM	0	0.33	6	6	ns	0.350
			LID_CORR	LID	0.17	1.12	6	8	ns	0.350
			LID_PREV	LID	0	1.12	6	8	ns	0.350
			LID_PREV	LID_CORR	0	0.17	6	6	ns	0.49
Supp. Fig1c	Oral	9	LID	SHAM	1.12	0.33	8	6	ns	0.550
			LID_CORR	SHAM	0.33	0.33	6	6	ns	0.900
			LID_PREV	SHAM	0.50	0.33	6	6	ns	0.920
			LID_CORR	LID	0.33	1.12	6	8	ns	0.550
			LID_PREV	LID	0.50	1.12	6	8	ns	0.590
			LID_PREV	LID_CORR	0.50	0.33	6	6	ns	0.900

Table S2: Number of cells and mice in each condition per week for the three deep cerebellar nuclei. Related to Figure 2 and Supplementary Figure 5.

All cell (DCN)	Region	Interposed		Dentate		Fastigial	
Groupe	Weeks	Cells	Mice	Cells	Mice	Cells	Mice
SHAM	W2-W3	n=10	N=1	n=28	N=2	n=7	N=1
	W4-W5	n=11	N=1	n=30	N=2	n=8	N=1
	W6-W7	n=10	N=1	n=24	N=2	n=3	N=1
	W8-W9	n=9	N=1	n=28	N=2	n=3	N=1
LID	W2-W3	n=25	N=3	n=41	N=4	n=41	N=5
	W4-W5	n=8	N=2	n=33	N=4	n=42	N=5
	W6-W7	n=10	N=3	n=24	N=3	n=49	N=6
	W8-W9	n=13	N=3	n=30	N=4	n=27	N=4
LID_CORR	W2-W3	n=19	N=2	n=12	N=1	n=15	N=3
	W4-W5	n=24	N=3	n=17	N=2	n=22	N=3

	W6-W7	n=12	N=2	n=10	N=1	n=20	N=3
	W8-W9	n=11	N=2	n=12	N=1	n=17	N=3
LID_PREV	W2-W3	n=31	N=3	n=34	N=3	n=31	N=3
	W4-W5	n=32	N=3	n=26	N=3	n=32	N=3
	W6-W7	n=26	N=3	n=25	N=3	n=32	N=3
	W8-W9	n=27	N=3	n=16	N=3	n=29	N=3

Table S3: Precision measures, exact p-values, and replicate data relevant to Figure 2d and Supplementary Figures 5d and 5f.

Fig	Reg	Group	Weeks1	Weeks2	Mean1	Mean2	n1	n2	Sum	Adjusted p Value
Fig. 2d	IN	SHAM	W2-W3	W4-W5	19.68 Hz	14.05 Hz	10	11	ns	0.973
			W2-W3	W6-W7	19.68 Hz	9.24 Hz	10	10	ns	0.283
			W2-W3	W8-W9	19.68 Hz	20.48 Hz	10	9	ns	0.841
			W4-W5	W6-W7	14.05 Hz	9.24 Hz	11	10	ns	0.492
			W4-W5	W8-W9	14.05 Hz	20.48 Hz	11	9	ns	0.591
			W6-W7	W8-W9	9.24 Hz	20.48 Hz	10	9	ns	0.063
Fig. 2d	IN	LID	W2-W3	W4-W5	17.35 Hz	9.75 Hz	25	8	ns	0.338
			W2-W3	W6-W7	17.35 Hz	8.50 Hz	25	10	*	0.023
			W2-W3	W8-W9	17.35 Hz	10.64 Hz	25	13	ns	0.147
			W4-W5	W6-W7	9.75 Hz	8.50 Hz	8	10	ns	0.812
			W4-W5	W8-W9	9.75 Hz	10.64 Hz	8	13	ns	0.999
			W6-W7	W8-W9	8.50 Hz	10.64 Hz	10	13	ns	0.818
Fig. 2d	IN	LID	W2-W3	W4-W5	26.52 Hz	18.81 Hz	19	24	*	0.031

		CORR	W2-W3	W6-W7	26.52 Hz	32.37 Hz	19	12	ns	0.927
			W2-W3	W8-W9	26.52 Hz	22.67 Hz	19	11	ns	0.722
			W4-W5	W6-W7	18.81 Hz	32.37 Hz	24	12	*	0.015
			W4-W5	W8-W9	18.81 Hz	22.67 Hz	24	11	ns	0.567
			W6-W7	W8-W9	32.37 Hz	22.67 Hz	12	11	ns	0.448
Fig. 2d	IN	LID	W2-W3	W4-W5	17.50 Hz	19.78 Hz	31	32	ns	0.998
		PREV	W2-W3	W6-W7	17.50 Hz	21.47 Hz	31	26	ns	0.403
			W2-W3	W8-W9	17.50 Hz	20.12 Hz	31	27	ns	0.978
			W4-W5	W6-W7	19.78 Hz	21.47 Hz	32	26	ns	0.488
			W4-W5	W8-W9	19.78 Hz	20.12 Hz	32	27	ns	0.994
			W6-W7	W8-W9	21.47 Hz	20.12 Hz	26	27	ns	0.672
Fig. Supp5d	DN	SHAM	W2-W3	W4-W5	18.31 HZ	16.05 Hz	28	30	ns	0.376
			W2-W3	W6-W7	18.31 HZ	14.55 Hz	28	24	ns	0.178
			W2-W3	W8-W9	18.31 HZ	16.56 Hz	28	28	ns	0.791
			W4-W5	W6-W7	16.05 Hz	14.55 Hz	30	24	ns	0.951
			W4-W5	W8-W9	16.05 Hz	16.56 Hz	30	28	ns	0.908
			W6-W7	W8-W9	14.55 Hz	16.56 Hz	24	28	ns	0.656
Fig. Supp5d	DN	LID	W2-W3	W4-W5	16.39 Hz	12.11 Hz	41	33	**	0.007
			W2-W3	W6-W7	16.39 Hz	13.14 Hz	41	24	*	0.033
			W2-W3	W8-W9	16.39 Hz	14.30 Hz	41	30	ns	0.674
			W4-W5	W6-W7	12.11 Hz	13.14 Hz	33	24	ns	0.997
			W4-W5	W8-W9	12.11 Hz	14.30 Hz	33	30	ns	0.210
			W6-W7	W8-W9	13.14 Hz	14.30 Hz	24	30	ns	0.381

Fig. Supp5d	DN	LID CORR	W2-W3	W4-W5	27.49 Hz	17.61 Hz	12	17	*	0.015
			W2-W3	W6-W7	27.49 Hz	17.15 Hz	12	10	**	0.002
			W2-W3	W8-W9	27.49 Hz	22.39 Hz	12	12	ns	0.181
			W4-W5	W6-W7	17.61 Hz	17.15 Hz	17	10	ns	0.866
			W4-W5	W8-W9	17.61 Hz	22.39 Hz	17	12	ns	0.137
			W6-W7	W8-W9	17.15 Hz	22.39 Hz	10	12	ns	0.089
Fig. Supp5d	DN	LID PREV	W2-W3	W4-W5	13.77 Hz	18.40 Hz	34	26	*	0.017
			W2-W3	W6-W7	13.77 Hz	15.73 Hz	34	25	ns	0.431
			W2-W3	W8-W9	13.77 Hz	11.77 Hz	34	16	ns	0.586
			W4-W5	W6-W7	18.40 Hz	15.73 Hz	26	25	ns	0.520
			W4-W5	W8-W9	18.40 Hz	11.77 Hz	26	16	**	0.002
			W6-W7	W8-W9	15.73 Hz	11.77 Hz	25	16	ns	0.075
Fig. Supp5f	FN	SHAM	W2-W3	W4-W5	17.24 Hz	15.96 Hz	7	8	ns	1
			W2-W3	W6-W7	17.24 Hz	7.49 Hz	7	3	ns	0.191
			W2-W3	W8-W9	17.24 Hz	12.48 Hz	7	3	ns	0.807
			W4-W5	W6-W7	15.96 Hz	7.49 Hz	8	3	ns	0.193
			W4-W5	W8-W9	15.96 Hz	12.48 Hz	8	3	ns	0.821
			W6-W7	W8-W9	7.49 Hz	12.48 Hz	3	3	ns	0.739
Fig. Supp5f	FN	LID	W2-W3	W4-W5	14.84 Hz	11.20 Hz	41	42	ns	0.467
			W2-W3	W6-W7	14.84 Hz	13.85 Hz	41	49	ns	0.998
			W2-W3	W8-W9	14.84 Hz	14.75 Hz	41	27	ns	0.843
			W4-W5	W6-W7	11.20 Hz	13.85 Hz	42	49	ns	0.527
			W4-W5	W8-W9	11.20 Hz	14.75 Hz	42	27	ns	0.150

			W6-W7	W8-W9	13.85 Hz	14.75 Hz	49	27	ns	0.754
Fig. Supp5d	FN	LID CORR	W2-W3	W4-W5	29.90 Hz	12.07 Hz	15	22	ns	0.075
			W2-W3	W6-W7	29.90 Hz	20.21 Hz	15	20	ns	0.898
			W2-W3	W8-W9	29.90 Hz	16.44 Hz	15	17	ns	0.679
			W4-W5	W6-W7	12.07 Hz	20.21 Hz	22	20	*	0.042
			W4-W5	W8-W9	12.07 Hz	16.44 Hz	22	17	*	0.041
			W6-W7	W8-W9	20.21 Hz	16.44 Hz	20	17	ns	0.935
Fig. Supp5d	FN	LID PREV	W2-W3	W4-W5	15.11 Hz	19.29 Hz	31	32	ns	0.095
			W2-W3	W6-W7	15.11 Hz	12.95 Hz	31	32	ns	0.212
			W2-W3	W8-W9	15.11 Hz	11.77 Hz	31	29	*	0.016
			W4-W5	W6-W7	19.29 Hz	12.95 Hz	32	32	**	0.001
			W4-W5	W8-W9	19.29 Hz	11.77 Hz	32	29	***	<0.001
			W6-W7	W8-W9	12.95 Hz	11.77 Hz	32	29	ns	0.960

Table S4: Precision measures, exact p-values, and replicate date relevant to Figure 2e and Supplementary Figures 5e and 5g.

Fig	Reg	Group	Weeks1	Weeks2	Mean1	Mean2	n1	n2	Sum	Adjusted p Value
Fig. 2e	IN	SHAM	W2-W3	W4-W5	0.882	0.947	10	11	ns	0.166
			W2-W3	W6-W7	0.882	0.959	10	10	ns	0.089
			W2-W3	W8-W9	0.882	0.929	10	9	ns	0.482
			W4-W5	W6-W7	0.947	0.959	11	10	ns	0.982
			W4-W5	W8-W9	0.947	0.929	11	9	ns	0.935
			W6-W7	W8-W9	0.959	0.929	10	9	ns	0.791

Fig. 2e	IN	LID	W2-W3	W4-W5	0.859	1.017	25	8	**	0.003
			W2-W3	W6-W7	0.859	1.023	25	10	***	<0.001
			W2-W3	W8-W9	0.859	1.018	25	13	***	<0.001
			W4-W5	W6-W7	1.017	1.023	8	10	ns	0.999
			W4-W5	W8-W9	1.017	1.018	8	13	ns	1
			W6-W7	W8-W9	1.023	1.018	10	13	ns	0.999
Fig. 2e	IN	LID CORR	W2-W3	W4-W5	0.855	0.932	19	24	*	0.031
			W2-W3	W6-W7	0.855	0.834	19	12	ns	0.906
			W2-W3	W8-W9	0.855	0.914	19	11	ns	0.307
			W4-W5	W6-W7	0.932	0.834	24	12	*	0.013
			W4-W5	W8-W9	0.932	0.914	24	11	ns	0.942
			W6-W7	W8-W9	0.834	0.914	12	11	ns	0.139
Fig. 2e	IN	LID PREV	W2-W3	W4-W5	0.891	0.894	31	32	ns	0.998
			W2-W3	W6-W7	0.891	0.895	31	26	ns	0.998
			W2-W3	W8-W9	0.891	0.910	31	27	ns	0.713
			W4-W5	W6-W7	0.894	0.895	32	26	ns	1
			W4-W5	W8-W9	0.894	0.910	32	27	ns	0.802
			W6-W7	W8-W9	0.895	0.910	26	27	ns	0.832
Fig. Supp5e	DN	SHAM	W2-W3	W4-W5	0.877	0.920	31	32	ns	0.069
			W2-W3	W6-W7	0.877	0.920	31	24	ns	0.093
			W2-W3	W8-W9	0.877	0.943	31	30	**	0.002
			W4-W5	W6-W7	0.920	0.920	32	24	ns	1
			W4-W5	W8-W9	0.920	0.943	32	30	ns	0.552

			W6-W7	W8-W9	0.920	0.943	24	30	ns	0.603
Fig. Supp5e	DN	LID	W2-W3	W4-W5	0.920	0.961	41	33	***	<0.001
			W2-W3	W6-W7	0.920	0.961	41	24	***	<0.001
			W2-W3	W8-W9	0.920	0.956	41	30	**	0.001
			W4-W5	W6-W7	0.961	0.961	33	24	ns	1
			W4-W5	W8-W9	0.961	0.956	33	30	ns	0.947
			W6-W7	W8-W9	0.961	0.956	24	30	ns	0.959
Fig. Supp5e	DN	LID CORR	W2-W3	W4-W5	0.862	0.906	12	17	ns	0.086
			W2-W3	W6-W7	0.862	0.925	12	10	***	<0.001
			W2-W3	W8-W9	0.862	0.899	12	12	**	0.008
			W4-W5	W6-W7	0.906	0.925	17	10	ns	0.764
			W4-W5	W8-W9	0.906	0.899	17	12	ns	0.982
			W6-W7	W8-W9	0.925	0.899	10	12	ns	0.219
Fig. Supp5e	DN	LID PREV	W2-W3	W4-W5	0.934	0.926	34	26	ns	0.830
			W2-W3	W6-W7	0.934	0.951	34	25	ns	0.284
			W2-W3	W8-W9	0.934	0.975	34	16	**	0.001
			W4-W5	W6-W7	0.926	0.951	26	25	ns	0.070
			W4-W5	W8-W9	0.926	0.975	26	16	***	<0.001
			W6-W7	W8-W9	0.951	0.975	25	16	ns	0.143
Fig. Supp5f	FN	SHAM	W2-W3	W4-W5	0.875	0.903	7	8	ns	0.689
			W2-W3	W6-W7	0.875	0.948	7	3	ns	0.185
			W2-W3	W8-W9	0.875	0.967	7	3	ns	0.069
			W4-W5	W6-W7	0.903	0.948	8	3	ns	0.563

			W4-W5	W8-W9	0.903	0.967	8	3	ns	0.275
			W6-W7	W8-W9	0.948	0.967	3	3	ns	0.966
Fig. Supp5f	FN	LID	W2-W3	W4-W5	0.919	0.977	41	42	***	<0.001
			W2-W3	W6-W7	0.919	0.957	41	49	**	0.004
			W2-W3	W8-W9	0.919	0.950	41	27	ns	0.076
			W4-W5	W6-W7	0.977	0.957	42	49	ns	0.254
			W4-W5	W8-W9	0.977	0.950	42	27	ns	0.154
			W6-W7	W8-W9	0.957	0.950	49	27	ns	0.947
Fig. Supp5f	FN	LID CORR	W2-W3	W4-W5	0.835	0.935	15	22	ns	0.080
			W2-W3	W6-W7	0.835	0.880	15	20	ns	0.723
			W2-W3	W8-W9	0.835	0.923	15	17	ns	0.133
			W4-W5	W6-W7	0.935	0.880	22	20	ns	0.143
			W4-W5	W8-W9	0.935	0.923	22	17	ns	0.792
			W6-W7	W8-W9	0.880	0.923	20	17	ns	0.288
Fig. Supp5f	FN	LID PREV	W2-W3	W4-W5	0.918	0.916	31	32	ns	0.993
			W2-W3	W6-W7	0.918	0.951	31	32	**	0.001
			W2-W3	W8-W9	0.918	0.962	31	29	***	<0.001
			W4-W5	W6-W7	0.916	0.951	32	32	***	<0.001
			W4-W5	W8-W9	0.916	0.962	32	29	***	<0.001
			W6-W7	W8-W9	0.951	0.962	32	29	ns	0.628

Table S5: Number of cells and mice in each condition per week in the motor cortex (M1), the parafascicular nucleus (PF) of the thalamus and the

ventroanterior-ventrolateral complex (VAL) of the thalamus. Related to Figures 3c, 3d and Supplementary Figure 7d.

All cell	Region	M1		PF		VAL	
Groupe	Weeks	Cells	Mice	Cells	Mice	Cells	Mice
SHAM	W2-W3	n=169	N=5	n=125	N=5	n=150	N=5
	W4-W5	n=137	N=5	n=107	N=5	n=136	N=5
	W6-W7	n=123	N=5	n=104	N=5	n=161	N=5
	W8	n=37	N=3	n=16	N=2	n=46	N=3
LID	W2-W3	n=107	N=4	n=83	N=4	n=135	N=4
	W4-W5	n=73	N=3	n=80	N=3	n=81	N=3
	W6-W7	n=65	N=3	n=83	N=3	n=105	N=3
	W8	n=34	N=3	n=32	N=3	n=46	N=3
LID_CORR	W2-W3	n=253	N=6	n=244	N=6	n=229	N=6
	W4-W5	n=255	N=6	n=282	N=6	n=278	N=6
	W6-W7	n=208	N=6	n=148	N=6	n=178	N=6
	W8	n=99	N=5	n=70	N=4	n=59	N=4
LID_PREV	W2-W3	n=221	N=8	n=159	N=8	n=164	N=8
	W4-W5	n=172	N=8	n=168	N=8	n=154	N=8
	W6-W7	n=120	N=8	n=131	N=8	n=123	N=8
	W8	n=41	N=4	n=37	N=5	n=29	N=5

Table S6: Precision measures, exact p-values, and replicate date relevant to Figures 3c, 3d and Supplementary Figure 7d.

Fig	**Reg**	**Group**	**Weeks1**	**Weeks2**	**Mean1**	**Mean2**	**n1**	**n2**	**Sum**	**Adjusted p Value**
Fig.3c	M1	SHAM	W2-W3	W4-W5	1.01 Hz	0.93 Hz	169	137	ns	0.989
			W2-W3	W6-W7	1.01 Hz	0.80 Hz	169	123	ns	0.790
			W2-W3	W8	1.01 Hz	0.85 Hz	169	37	ns	0.880
			W4-W5	W6-W7	0.93 Hz	0.80 Hz	123	137	ns	0.934

			W4-W5	W8	0.93 Hz	0.85 Hz	123	37	ns	0.772
			W6-W7	W8	0.80 Hz	0.85 Hz	137	37	ns	0.491
Fig.3c	M1	LID	W2-W3	W4-W5	0.30 Hz	0.83 Hz	107	73	***	<0.001
			W2-W3	W6-W7	0.30 Hz	1.16 Hz	107	65	***	<0.001
			W2-W3	W8	0.30 Hz	1.39 Hz	107	34	***	<0.001
			W4-W5	W6-W7	0.83 Hz	1.16 Hz	73	65	ns	0.567
			W4-W5	W8	0.83 Hz	1.39 Hz	73	34	ns	0.120
			W6-W7	W8	1.16 Hz	1.39 Hz	65	34	ns	0.768
Fig.3c	M1	LID CORR	W2-W3	W4-W5	0.58 Hz	1.28 Hz	253	255	***	<0.001
			W2-W3	W6-W7	0.58 Hz	0.93 Hz	253	208	***	<0.001
			W2-W3	W8	0.58 Hz	0.95 Hz	253	99	***	<0.001
			W4-W5	W6-W7	1.28 Hz	0.93 Hz	255	208	ns	0.933
			W4-W5	W8	1.28 Hz	0.95 Hz	255	99	ns	0.999
			W6-W7	W8	0.93 Hz	0.95 Hz	208	99	ns	0.914
Fig.3c	M1	LID PREV	W2-W3	W4-W5	0.56 Hz	0.70 Hz	221	172	ns	0.594
			W2-W3	W6-W7	0.56 Hz	0.85 Hz	221	120	ns	0.156
			W2-W3	W8	0.56 Hz	0.56 Hz	221	41	ns	0.574
			W4-W5	W6-W7	0.70 Hz	0.85 Hz	172	120	ns	0.833
			W4-W5	W8	0.70 Hz	0.56 Hz	172	41	ns	0.983
			W6-W7	W8	0.85 Hz	0.56 Hz	120	41	ns	0.994
Fig.3d	PF	SHAM	W2-W3	W4-W5	0.91 Hz	0.71 Hz	125	107	ns	0.662
			W2-W3	W6-W7	0.91 Hz	0.68 Hz	125	104	ns	0.906
			W2-W3	W8	0.91 Hz	0.60 Hz	125	16	ns	0.766

			W4-W5	W6-W7	0.71 Hz	0.68 Hz	107	104	ns	0.966
			W4-W5	W8	0.71 Hz	0.60 Hz	107	16	ns	0.994
			W6-W7	W8	0.68 Hz	0.60 Hz	104	16	ns	0.946
Fig.3d	PF	LID	W2-W3	W4-W5	1.06 Hz	0.34 Hz	83	80	ns	0.053
			W2-W3	W6-W7	1.06 Hz	0.31 Hz	83	83	*	0.025
			W2-W3	W8	1.06 Hz	0.40 Hz	83	32	ns	0.102
			W4-W5	W6-W7	0.34 Hz	0.31 Hz	80	83	ns	0.993
			W4-W5	W8	0.34 Hz	0.40 Hz	80	32	ns	1
			W6-W7	W8	0.31 Hz	0.40 Hz	83	32	ns	0.992
Fig.3d	PF	LID CORR	W2-W3	W4-W5	1.11 Hz	0.82 Hz	244	282	ns	0.057
			W2-W3	W6-W7	1.11 Hz	1.03 Hz	244	148	ns	0.896
			W2-W3	W8	1.11 Hz	0.84 Hz	244	70	ns	0.995
			W4-W5	W6-W7	0.82 Hz	1.03 Hz	282	148	ns	0.280
			W4-W5	W8	0.82 Hz	0.84 Hz	282	70	ns	0.234
			W6-W7	W8	1.03 Hz	0.84 Hz	148	70	ns	0.984
Fig.3d	PF	LID PREV	W2-W3	W4-W5	1.11 Hz	0.58 Hz	159	168	ns	0.086
			W2-W3	W6-W7	1.11 Hz	0.72 Hz	159	131	ns	0.146
			W2-W3	W8	1.11 Hz	0.74 Hz	159	37	ns	0.672
			W4-W5	W6-W7	0.58 Hz	0.72 Hz	168	131	ns	0.996
			W4-W5	W8	0.58 Hz	0.74 Hz	168	37	ns	0.906
			W6-W7	W8	0.72 Hz	0.74 Hz	131	37	ns	0.958
Fig. Supp7d	VAL	SHAM	W2-W3	W4-W5	0.92 Hz	0.72 Hz	150	136	ns	0.298
			W2-W3	W6-W7	0.92 Hz	0.72 Hz	150	161	ns	0.411

			W2-W3	W8	0.92 Hz	0.75 Hz	150	46	ns	0.890
			W4-W5	W6-W7	0.72 Hz	0.72 Hz	136	161	ns	0.996
			W4-W5	W8	0.72 Hz	0.75 Hz	136	46	ns	0.908
			W6-W7	W8	0.72 Hz	0.75 Hz	161	46	ns	0.957
Fig. Supp7d	VAL	LID	W2-W3	W4-W5	0.92 Hz	0.48 Hz	135	81	ns	0.856
			W2-W3	W6-W7	0.92 Hz	0.61 Hz	135	105	ns	0.990
			W2-W3	W8	0.92 Hz	0.66 Hz	135	46	ns	0.964
			W4-W5	W6-W7	0.48 Hz	0.61 Hz	81	105	ns	0.967
			W4-W5	W8	0.48 Hz	0.66 Hz	81	46	ns	0.992
			W6-W7	W8	0.61 Hz	0.66 Hz	105	46	ns	0.998
Fig. Supp7d	VAL	LID CORR	W2-W3	W4-W5	1.09 Hz	0.84 Hz	229	278	ns	0.055
			W2-W3	W6-W7	1.09 Hz	1.06 Hz	229	178	ns	0.993
			W2-W3	W8	1.09 Hz	0.80 Hz	229	59	ns	0.829
			W4-W5	W6-W7	0.84 Hz	1.06 Hz	278	178	ns	0.109
			W4-W5	W8	0.84 Hz	0.80 Hz	278	59	ns	0.566
			W6-W7	W8	1.06 Hz	0.80 Hz	178	59	ns	0.925
Fig. Supp7d	VAL	LID PREV	W2-W3	W4-W5	0.66 Hz	0.52 Hz	164	154	ns	0.952
			W2-W3	W6-W7	0.66 Hz	0.70 Hz	164	123	ns	0.929
			W2-W3	W8	0.66 Hz	1.06 Hz	164	29	ns	0.910
			W4-W5	W6-W7	0.52 Hz	0.70 Hz	154	123	ns	0.665
			W4-W5	W8	0.52 Hz	1.06 Hz	154	29	ns	0.685
			W6-W7	W8	0.70 Hz	1.06 Hz	123	29	ns	0.999

Table S7: Precision measures, exact p-values, and replicate date relevant to Figure 6b.

Fig	Group1	Group 2	Mean1	Mean2	n1	n2	Sum	Adjusted p Value
Fig. 6b	LID	SHAM	128.85	99.57	10	11	***	< 0.001
	LID_CORR	SHAM	107.64	99.57	7	11	*	0.030
	LID_PREV	SHAM	96.73	99.57	11	11	ns	0.444
	LID_CORR	LID	107.64	128.85	7	10	##	0.002
	LID_PREV	LID	96.73	128.85	11	10	###	< 0.001
	LID_PREV	LID_CORR	96.73	107.64	11	7	&	0.024

Table S8: Precision measures, exact p-values, and replicate date relevant to Supplementary Figure 4

Fig	Param	Week	Group1	Group2	Mean1	Mean2	n1	n2	Sum	Adjusted p Value
Fig. Supp4	Oral	4	SHAM	SHAM_CORR	0.50	0.36	4	11	ns	1
			SHAM	SHAM_PREV	0.50	0.50	4	4	ns	1
			SHAM_CORR	SHAM_PREV	0.36	0.50	11	4	ns	1
Fig. Supp4	Oral	5	SHAM	SHAM_CORR	0.50	0.1	4	10	ns	0.51
			SHAM	SHAM_PREV	0.50	0.33	4	3	ns	0.77
			SHAM_CORR	SHAM_PREV	0.1	0.33	10	3	ns	0.60
Fig. Supp4	Oral	6	SHAM	SHAM_CORR	0.50	0.25	4	12	ns	0.49
			SHAM	SHAM_PREV	0.50	0	4	3	ns	0.49
			SHAM_CORR	SHAM_PREV	0.25	0	12	3	ns	0.49

Fig. Supp4	Oral	7	SHAM	SHAM_CORR	0.50	0	4	8	ns	0.17
			SHAM	SHAM_PREV	0.50	0.33	4	3	ns	0.77
			SHAM_CORR	SHAM_PREV	0	0.33	8	3	ns	0.18
Fig. Supp4	Oral	8	SHAM	SHAM_CORR	0.75	0.30	4	10	ns	0.33
			SHAM	SHAM_PREV	0.75	0	4	3	ns	0.33
			SHAM_CORR	SHAM_PREV	0.30	0	10	3	ns	0.33
Fig. Supp4	Oral	9	SHAM	SHAM_CORR	0.25	0.20	4	5	ns	0.94
			SHAM	SHAM_PREV	0.25	1	4	2	ns	0.33
			SHAM_CORR	SHAM_PREV	0.20	1	5	2	ns	0.33
Fig. Supp4	Axial	4	SHAM	SHAM_CORR	0	0	4	5	ns	-
			SHAM	SHAM_PREV	0	0	4	3	ns	-
			SHAM_CORR	SHAM_PREV	0	0	5	3	ns	-
Fig. Supp4	Axial	5	SHAM	SHAM_CORR	0	0	4	3	ns	-
			SHAM	SHAM_PREV	0	0	4	2	ns	-
			SHAM_CORR	SHAM_PREV	0	0	3	2	ns	-
Fig. Supp4	Axial	6	SHAM	SHAM_CORR	0	0	4	5	ns	-
			SHAM	SHAM_PREV	0	0	4	2	ns	-
			SHAM_CORR	SHAM_PREV	0	0	5	2	ns	-
Fig. Supp4	Axial	7	SHAM	SHAM_CORR	0	0	4	5	ns	-
			SHAM	SHAM_PREV	0	0	4	2	ns	-
			SHAM_CORR	SHAM_PREV	0	0	5	2	ns	-
Fig.	Axial	8	SHAM	SHAM_CORR	0	0	4	5	ns	-

Supp4			SHAM	SHAM_PREV	0	0	4	2	ns	-
			SHAM_CORR	SHAM_PREV	0	0	5	2	ns	-
Fig. Supp4	Axial	9	SHAM	SHAM_CORR	0	0	4	5	ns	-
			SHAM	SHAM_PREV	0	0	4	2	ns	-
			SHAM_CORR	SHAM_PREV	0	0	5	2	ns	-
Fig. Supp4	Limb	4	SHAM	SHAM_CORR	0	0.14	4	7	ns	0.51
			SHAM	SHAM_PREV	0	0	4	3	ns	-
			SHAM_CORR	SHAM_PREV	0.14	0	7	3	ns	0.51
Fig. Supp4	Limb	5	SHAM	SHAM_CORR	0	0.20	4	5	ns	0.54
			SHAM	SHAM_PREV	0	0	4	2	ns	-
			SHAM_CORR	SHAM_PREV	0.20	0	5	2	ns	0.54
Fig. Supp4	Limb	6	SHAM	SHAM_CORR	0	0	4	7	ns	-
			SHAM	SHAM_PREV	0	0	4	2	ns	-
			SHAM_CORR	SHAM_PREV	0	0	7	2	ns	-
Fig. Supp4	Limb	7	SHAM	SHAM_CORR	0	0.17	4	6	ns	0.58
			SHAM	SHAM_PREV	0	0	4	2	ns	-
			SHAM_CORR	SHAM_PREV	0.17	0	6	2	ns	0.58
Fig. Supp4	Limb	8	SHAM	SHAM_CORR	0	0.17	4	6	ns	0.58
			SHAM	SHAM_PREV	0	0	4	2	ns	-
			SHAM_CORR	SHAM_PREV	0.17	0	6	2	ns	0.58
Fig. Supp4	Limb	9	SHAM	SHAM_CORR	0	0.17	4	6	ns	0.58
			SHAM	SHAM_PREV	0	0	4	2	ns	-

			SHAM_CORR	SHAM_PREV	0.17	0	6	2	ns	0.58

Table S9: Precision measures, exact p-values, and replicate date relevant to Supplementary Figure 7

Fig	Reg	Group	Weeks1	Weeks2	Mean1	Mean2	n1	n2	Sum	Adjusted p Value
Fig. Supp7 (upper)	IN	SHAM	W2-W3	W4-W5	2.64 Hz	2.52 Hz	10	11	ns	0.975
			W2-W3	W6-W7	2.64 Hz	2.12 Hz	10	10	ns	0.551
			W2-W3	W8-W9	2.64 Hz	2.88 Hz	10	9	ns	0.854
			W4-W5	W6-W7	2.52 Hz	2.12 Hz	11	10	ns	0.743
			W4-W5	W8-W9	2.52 Hz	2.88 Hz	11	9	ns	0.617
			W6-W7	W8-W9	2.12 Hz	2.88 Hz	10	9	ns	0.223
Fig. Supp7 (upper)	IN	SHAM CORR	W2-W3	W4-W5	2.37 Hz	1.89 Hz	13	21	ns	0.228
			W2-W3	W6-W7	2.37 Hz	2.27 Hz	13	21	***	<0.001
			W2-W3	W8-W9	2.37 Hz	2.28 Hz	13	24	ns	0.472
			W4-W5	W6-W7	1.89 Hz	2.27 Hz	21	21	*	0.018
			W4-W5	W8-W9	1.89 Hz	2.28 Hz	21	24	ns	0.914
			W6-W7	W8-W9	2.27 Hz	2.28 Hz	21	24	**	0.002
Fig. Supp7 (upper)	IN	SHAM PREV	W2-W3	W4-W5	2.84 Hz	1.92 Hz	18	23	***	< 0.001
			W2-W3	W6-W7	2.84 Hz	2.14 Hz	18	19	***	< 0.001
			W2-W3	W8-W9	2.84 Hz	2.32 Hz	18	16	*	0.016
			W4-W5	W6-W7	1.92 Hz	2.14 Hz	23	19	ns	0.492
			W4-W5	W8-W9	1.92 Hz	2.32 Hz	23	16	ns	0.076
			W6-W7	W8-W9	2.14 Hz	2.32 Hz	19	16	ns	0.716

Fig. Supp7 (upper)	DN	SHAM	W2-W3	W4-W5	2.82 Hz	2.66 Hz	28	30	ns	0.406
			W2-W3	W6-W7	2.82 Hz	2.60 Hz	28	24	ns	0.742
			W2-W3	W8-W9	2.82 Hz	2.73 Hz	28	28	ns	0.806
			W4-W5	W6-W7	2.66 Hz	2.60 Hz	30	24	ns	0.998
			W4-W5	W8-W9	2.66 Hz	2.73 Hz	30	28	ns	0.916
			W6-W7	W8-W9	2.60 Hz	2.73 Hz	24	28	ns	0.954
Fig. Supp7 (upper)	DN	SHAM PREV	W2-W3	W4-W5	3.14 Hz	2.15 Hz	10	12	***	< 0.001
			W2-W3	W6-W7	3.14 Hz	2.08 Hz	10	11	***	< 0.001
			W2-W3	W8-W9	3.14 Hz	2.57 Hz	10	13	*	0.024
			W4-W5	W6-W7	2.15 Hz	2.08 Hz	12	11	ns	0.982
			W4-W5	W8-W9	2.15 Hz	2.57 Hz	12	13	ns	0.126
			W6-W7	W8-W9	2.08 Hz	2.57 Hz	11	13	ns	0.062
Fig. Supp7 (upper)	FN	SHAM	W2-W3	W4-W5	2.71 Hz	2.69 Hz	7	8	ns	1
			W2-W3	W6-W7	2.71 Hz	1.99 Hz	7	3	ns	0.191
			W2-W3	W8-W9	2.71 Hz	2.40 Hz	7	3	ns	0.808
			W4-W5	W6-W7	2.69 Hz	1.99 Hz	8	3	ns	0.193
			W4-W5	W8-W9	2.69 Hz	2.40 Hz	8	3	ns	0.821
			W6-W7	W8-W9	1.99 Hz	2.40 Hz	3	3	ns	0.739
Fig. Supp7 (upper)	FN	SHAM PREV	W2-W3	W4-W5	3.25 Hz	2.34 Hz	18	14	***	<0.001
			W2-W3	W6-W7	3.25 Hz	1.99 Hz	18	15	***	<0.001
			W2-W3	W8-W9	3.25 Hz	2.28 Hz	18	16	***	<0.001
			W4-W5	W6-W7	2.34 Hz	1.99 Hz	14	15	ns	0.290
			W4-W5	W8-W9	2.34 Hz	2.28 Hz	14	16	ns	0.990

			W6-W7	W8-W9	1.99 Hz	2.28 Hz	15	16	ns	0.423
Fig. Supp7 (middle)	IN	SHAM	W2-W3	W4-W5	28.58 Hz	22.26 Hz	10	11	ns	0.582
			W2-W3	W6-W7	28.58 Hz	12.35 Hz	10	5	*	0.047
			W2-W3	W8-W9	28.58 Hz	27.84 Hz	10	9	ns	0.999
			W4-W5	W6-W7	22.26 Hz	12.35 Hz	11	5	ns	0.104
			W4-W5	W8-W9	22.26 Hz	27.84 Hz	11	9	ns	0.725
			W6-W7	W8-W9	12.35 Hz	27.84 Hz	5	9	ns	0.087
Fig. Supp7 (middle)	IN	SHAM CORR	W2-W3	W4-W5	38.92 Hz	14.03 Hz	7	9	***	<0.001
			W2-W3	W6-W7	38.92 Hz	24.58 Hz	7	9	**	0.008
			W2-W3	W8-W9	38.92 Hz	26.18 Hz	7	12	*	0.013
			W4-W5	W6-W7	14.03 Hz	24.58 Hz	9	9	*	0.048
			W4-W5	W8-W9	14.03 Hz	26.18 Hz	9	12	*	0.010
			W6-W7	W8-W9	24.58 Hz	26.18 Hz	9	12	ns	0.970
Fig. Supp7 (middle)	IN	SHAM PREV	W2-W3	W4-W5	28.28 Hz	18.96 Hz	18	23	**	0.001
			W2-W3	W6-W7	28.28 Hz	19.39 Hz	18	19	**	0.004
			W2-W3	W8-W9	28.28 Hz	21.53 Hz	18	16	ns	0.060
			W4-W5	W6-W7	18.96 Hz	19.39 Hz	23	19	ns	0.998
			W4-W5	W8-W9	18.96 Hz	21.53 Hz	23	16	ns	0.735
			W6-W7	W8-W9	19.39 Hz	21.53 Hz	19	16	ns	0.846
Fig. Supp7 (middle)	DN	SHAM	W2-W3	W4-W5	29.96 Hz	22.64 Hz	28	30	ns	0.191
			W2-W3	W6-W7	29.96 Hz	19.02 Hz	28	5	ns	0.369
			W2-W3	W8-W9	29.96 Hz	26.47 Hz	28	28	ns	0.782
			W4-W5	W6-W7	22.64 Hz	19.02 Hz	30	5	ns	0.949

			W4-W5	W8-W9	22.64 Hz	26.47 Hz	30	28	ns	0.718
			W6-W7	W8-W9	19.02 Hz	26.47 Hz	5	28	ns	0.685
Fig. Supp7 (middle)	DN	SHAM PREV	W2-W3	W4-W5	29.52 Hz	18.95 Hz	10	12	**	0.006
			W2-W3	W6-W7	29.52 Hz	21.48 Hz	10	11	ns	0.060
			W2-W3	W8-W9	29.52 Hz	19.48 Hz	10	13	**	0.008
			W4-W5	W6-W7	18.95 Hz	21.48 Hz	12	11	ns	0.828
			W4-W5	W8-W9	18.95 Hz	19.48 Hz	12	13	ns	0.997
			W6-W7	W8-W9	21.48 Hz	19.48 Hz	11	13	ns	0.902
Fig. Supp7 (middle)	FN	SHAM	W2-W3	W4-W5	24.46 Hz	25.18 Hz	7	8	ns	0.988
			W2-W3	W8-W9	24.46 Hz	19.50 Hz	7	3	ns	0.737
			W4-W5	W8-W9	25.18 Hz	19.50 Hz	8	3	ns	0.662
Fig. Supp7 (middle)	FN	SHAM PREV	W2-W3	W4-W5	34.79 Hz	15.57 Hz	18	14	***	<0.001
			W2-W3	W6-W7	34.79 Hz	12.11 Hz	18	15	***	<0.001
			W2-W3	W8-W9	34.79 Hz	18.13 Hz	18	16	***	<0.001
			W4-W5	W6-W7	15.57 Hz	12.11 Hz	14	15	ns	0.774
			W4-W5	W8-W9	15.57 Hz	18.13 Hz	14	16	ns	0.888
			W6-W7	W8-W9	12.11 Hz	18.13 Hz	15	16	ns	0.320
Fig. Supp7 (lower)	IN	SHAM	W2-W3	W4-W5	18.12 Hz	13.31 Hz	10	11	ns	0.749
			W2-W3	W6-W7	18.12 Hz	7.41 Hz	10	5	ns	0.303
			W2-W3	W8-W9	18.12 Hz	18.49 Hz	10	9	ns	1
			W4-W5	W6-W7	13.31 Hz	7.41 Hz	11	5	ns	0.754
			W4-W5	W8-W9	13.31 Hz	18.49 Hz	11	9	ns	0.723
			W6-W7	W8-W9	7.41 Hz	18.49 Hz	5	9	ns	0.290

Fig. Supp7 (lower)	IN	SHAM CORR	W2-W3	W4-W5	11.99 Hz	10.13 Hz	12	9	ns	0.561
			W2-W3	W6-W7	11.99 Hz	6.01 Hz	12	9	***	< 0.001
			W2-W3	W8-W9	11.99 Hz	10.57 Hz	12	12	ns	0.703
			W4-W5	W6-W7	10.13 Hz	6.01 Hz	9	9	*	0.047
			W4-W5	W8-W9	10.13 Hz	10.57 Hz	9	12	ns	0.989
			W6-W7	W8-W9	6.01 Hz	10.57 Hz	9	12	*	0.013
Fig. Supp7 (lower)	IN	SHAM PREV	W2-W3	W4-W5	15.70 Hz	6.49 Hz	18	23	***	<0.001
			W2-W3	W6-W7	15.70 Hz	8.38 Hz	18	19	**	0.002
			W2-W3	W8-W9	15.70 Hz	10.02 Hz	18	16	*	0.036
			W4-W5	W6-W7	6.49 Hz	8.38 Hz	23	19	ns	0.307
			W4-W5	W8-W9	6.49 Hz	10.02 Hz	23	16	ns	0.074
			W6-W7	W8-W9	8.38 Hz	10.02 Hz	19	16	ns	0.703
Fig. Supp7 (lower)	DN	SHAM	W2-W3	W4-W5	15.57 Hz	15.49 Hz	28	30	ns	1
			W2-W3	W6-W7	15.57 Hz	14.47 Hz	28	19	ns	0.980
			W2-W3	W8-W9	15.57 Hz	15.62 Hz	28	28	ns	1
			W4-W5	W6-W7	15.49 Hz	14.47 Hz	30	19	ns	0.984
			W4-W5	W8-W9	15.49 Hz	15.62 Hz	30	28	ns	1
			W6-W7	W8-W9	14.47 Hz	15.62 Hz	19	28	ns	0.977
Fig. Supp7 (lower)	DN	SHAM PREV	W2-W3	W4-W5	25.75 Hz	8.78 Hz	10	12	***	<0.001
			W2-W3	W6-W7	25.75 Hz	8.23 Hz	10	11	***	<0.001
			W2-W3	W8-W9	25.75 Hz	12.22 Hz	10	13	***	<0.001
			W4-W5	W6-W7	8.78 Hz	8.23 Hz	12	11	ns	0.997
			W4-W5	W8-W9	8.78 Hz	12.22 Hz	12	13	ns	0.570

			W6-W7	W8-W9	8.23 Hz	12.22 Hz	11	13	ns	0.464
Fig. Supp7 (lower)	FN	SHAM	W2-W3	W4-W5	15.59 Hz	15.16 Hz	7	8	ns	0.994
			W2-W3	W8-W9	15.59 Hz	10.37 Hz	7	3	ns	0.623
			W4-W5	W8-W9	15.16 Hz	10.37 Hz	8	3	ns	0.660
Fig. Supp7 (lower)	FN	SHAM PREV	W2-W3	W4-W5	26.22 Hz	11.01 Hz	18	14	***	<0.001
			W2-W3	W6-W7	26.22 Hz	7.32 Hz	18	15	***	<0.001
			W2-W3	W8-W9	26.22 Hz	11.81 Hz	18	16	***	<0.001
			W4-W5	W6-W7	11.01 Hz	7.32 Hz	14	15	ns	0.714
			W4-W5	W8-W9	11.01 Hz	11.81 Hz	14	16	ns	0.995
			W6-W7	W8-W9	7.32 Hz	11.81 Hz	15	16	ns	0.545

Table S10: Precision measures, exact p-values, and replicate date relevant to Supplementary Figure8a

Fig	Reg	Group	Weeks1	Weeks2	Mean1	Mean2	n1	n2	Sum	Adjusted p Value
Fig. Supp8a	IN	SHAM	W2-W3	W4-W5	1.78 Hz	2.25 Hz	10	11	ns	0.768
			W2-W3	W6-W7	1.78 Hz	0.30 Hz	10	5	ns	0.091
			W2-W3	W8-W9	1.78 Hz	2.20 Hz	10	9	ns	0.839
			W4-W5	W6-W7	2.25 Hz	0.30 Hz	11	5	*	0.014
			W4-W5	W8-W9	2.25 Hz	2.20 Hz	11	9	ns	1
			W6-W7	W8-W9	0.30 Hz	2.20 Hz	5	9	*	0.021
Fig. Supp8a	IN	LID	W2-W3	W4-W5	1.25 Hz	0.26 Hz	25	8	*	0.011
			W2-W3	W6-W7	1.25 Hz	0.12 Hz	25	9	**	0.002

			W2-W3	W8-W9	1.25 Hz	0.22 Hz	25	13	**	0.006
			W4-W5	W6-W7	0.26 Hz	0.12 Hz	8	9	ns	0.400
			W4-W5	W8-W9	0.26 Hz	0.22 Hz	8	13	ns	0.949
			W6-W7	W8-W9	0.12 Hz	0.22 Hz	9	13	ns	0.053
Fig. Supp8a	IN	LID CORR	W2-W3	W4-W5	0.70 Hz	2.70 Hz	19	24	ns	0.193
			W2-W3	W6-W7	0.70 Hz	0.94 Hz	19	12	ns	0.997
			W2-W3	W8-W9	0.70 Hz	2.10 Hz	19	11	ns	0.664
			W4-W5	W6-W7	2.70 Hz	0.94 Hz	24	12	ns	0.418
			W4-W5	W8-W9	2.70 Hz	2.10 Hz	24	11	ns	0.956
			W6-W7	W8-W9	0.94 Hz	2.10 Hz	12	11	ns	0.825
Fig. Supp8a	IN	LID PREV	W2-W3	W4-W5	0.94 Hz	1.03 Hz	31	32	ns	0.979
			W2-W3	W6-W7	0.94 Hz	1.34 Hz	31	26	ns	0.407
			W2-W3	W8-W9	0.94 Hz	1.31 Hz	31	27	ns	0.477
			W4-W5	W6-W7	1.03 Hz	1.34 Hz	32	26	ns	0.633
			W4-W5	W8-W9	1.03 Hz	1.31 Hz	32	27	ns	0.708
			W6-W7	W8-W9	1.34 Hz	1.31 Hz	26	27	ns	0.999
Fig. Supp8a	DN	SHAM	W2-W3	W4-W5	1.21 Hz	1.52 Hz	28	30	ns	0.853
			W2-W3	W6-W7	1.21 Hz	0.60 Hz	28	5	ns	0.825
			W2-W3	W8-W9	1.21 Hz	1.74 Hz	28	28	ns	0.538
			W4-W5	W6-W7	1.52 Hz	0.60 Hz	30	5	ns	0.564
			W4-W5	W8-W9	1.52 Hz	1.74 Hz	30	28	ns	0.942
			W6-W7	W8-W9	0.60 Hz	1.74 Hz	5	28	ns	0.383
Fig.	DN	LID	W2-W3	W4-W5	1.27 Hz	0.25 Hz	41	33	***	<0.001

Supp8a			W2-W3	W6-W7	1.27 Hz	0.40 Hz	41	17	**	0.002
			W2-W3	W8-W9	1.27 Hz	0.28 Hz	41	27	***	<0.001
			W4-W5	W6-W7	0.25 Hz	0.40 Hz	33	17	ns	0.447
			W4-W5	W8-W9	0.25 Hz	0.28 Hz	33	27	ns	0.984
			W6-W7	W8-W9	0.40 Hz	0.28 Hz	17	27	ns	0.702
Fig. Supp8a	DN	LID CORR	W2-W3	W4-W5	1.56 Hz	0.27 Hz	12	17	ns	0.083
			W2-W3	W6-W7	1.56 Hz	0.36 Hz	12	10	ns	0.115
			W2-W3	W8-W9	1.56 Hz	0.38 Hz	12	12	ns	0.122
			W4-W5	W6-W7	0.27 Hz	0.36 Hz	17	10	ns	0.814
			W4-W5	W8-W9	0.27 Hz	0.38 Hz	17	12	ns	0.641
			W6-W7	W8-W9	0.36 Hz	0.38 Hz	10	12	ns	0.998
Fig. Supp8a	DN	LID PREV	W2-W3	W4-W5	1.77 Hz	1.11 Hz	34	26	ns	0.339
			W2-W3	W6-W7	1.77 Hz	0.52 Hz	34	25	*	0.010
			W2-W3	W8-W9	1.77 Hz	1.04 Hz	34	16	ns	0.372
			W4-W5	W6-W7	1.11 Hz	0.52 Hz	26	25	ns	0.481
			W4-W5	W8-W9	1.11 Hz	1.04 Hz	26	16	ns	0.998
			W6-W7	W8-W9	0.52 Hz	1.04 Hz	25	16	ns	0.698
Fig. Supp8a	FN	SHAM	W2-W3	W4-W5	1.56 Hz	2.71 Hz	7	8	ns	0.175
			W2-W3	W8-W9	1.56 Hz	2.01 Hz	7	3	ns	0.845
			W4-W5	W8-W9	2.71 Hz	2.01 Hz	8	3	ns	0.661
Fig. Supp8a	FN	LID	W2-W3	W4-W5	0.92 Hz	0.65 Hz	41	42	ns	0.592
			W2-W3	W6-W7	0.92 Hz	0.32 Hz	41	49	*	0.015
			W2-W3	W8-W9	0.92 Hz	0.44 Hz	41	27	ns	0.080

			W4-W5	W6-W7	0.65 Hz	0.32 Hz	42	49	*	0.025
			W4-W5	W8-W9	0.65 Hz	0.44 Hz	42	27	ns	0.310
			W6-W7	W8-W9	0.32 Hz	0.44 Hz	49	27	ns	0.188
Fig. Supp8a	FN	LID CORR	W2-W3	W4-W5	1.22 Hz	0.95 Hz	15	22	ns	0.940
			W2-W3	W6-W7	1.22 Hz	0.56 Hz	15	20	ns	0.505
			W2-W3	W8-W9	1.22 Hz	1.20 Hz	15	17	ns	1
			W4-W5	W6-W7	0.95 Hz	0.56 Hz	22	20	ns	0.791
			W4-W5	W8-W9	0.95 Hz	1.20 Hz	22	17	ns	0.943
			W6-W7	W8-W9	0.56 Hz	1.20 Hz	20	17	ns	0.494
Fig. Supp8a	FN	LID PREV	W2-W3	W4-W5	2.27 Hz	1.09 Hz	31	32	ns	0.120
			W2-W3	W6-W7	2.27 Hz	0.68 Hz	31	32	**	0.001
			W2-W3	W8-W9	2.27 Hz	0.86 Hz	31	29	*	0.031
			W4-W5	W6-W7	1.09 Hz	0.68 Hz	32	32	ns	0.341
			W4-W5	W8-W9	1.09 Hz	0.86 Hz	32	29	ns	0.833
			W6-W7	W8-W9	0.68 Hz	0.86 Hz	32	29	ns	0.751

Table S11: Precision measures, exact p-values, and replicate date relevant to Supplementary Figure8b

Fig	Reg	Group	Weeks1	Weeks2	Mean1	Mean2	n1	n2	Sum	Adjusted p Value

Fig. Supp8b	IN	SHAM	W2-W3	W4-W5	1.19 Hz	0.58 Hz	10	11	ns	0.504
			W2-W3	W6-W7	1.19 Hz	0.19 Hz	10	5	ns	0.141
			W2-W3	W8-W9	1.19 Hz	0.30 Hz	10	9	ns	0.211
			W4-W5	W6-W7	0.58 Hz	0.19 Hz	11	5	**	0.005
			W4-W5	W8-W9	0.58 Hz	0.30 Hz	11	9	ns	0.050
			W6-W7	W8-W9	0.19 Hz	0.30 Hz	5	9	ns	0.173
Fig. Supp8b	IN	LID	W2-W3	W4-W5	0.77 Hz	1.39 Hz	25	8	ns	0.773
			W2-W3	W6-W7	0.77 Hz	1.01 Hz	25	9	ns	0.981
			W2-W3	W8-W9	0.77 Hz	1.53 Hz	25	13	ns	0.507
			W4-W5	W6-W7	1.39 Hz	1.01 Hz	8	9	ns	0.960
			W4-W5	W8-W9	1.39 Hz	1.53 Hz	8	13	ns	0.997
			W6-W7	W8-W9	1.01 Hz	1.53 Hz	9	13	ns	0.873
Fig. Supp8b	IN	LID CORR	W2-W3	W4-W5	0.49 Hz	0.56 Hz	19	24	ns	0.974
			W2-W3	W6-W7	0.49 Hz	1.10 Hz	19	12	**	0.005
			W2-W3	W8-W9	0.49 Hz	0.60 Hz	19	11	ns	0.926
			W4-W5	W6-W7	0.56 Hz	1.10 Hz	24	12	**	0.009
			W4-W5	W8-W9	0.56 Hz	0.60 Hz	24	11	ns	0.992
			W6-W7	W8-W9	1.10 Hz	0.60 Hz	12	11	ns	0.067
Fig. Supp8b	IN	LID PREV	W2-W3	W4-W5	0.78 Hz	0.94 Hz	31	32	ns	0.641
			W2-W3	W6-W7	0.78 Hz	1.05 Hz	31	26	ns	0.126
			W2-W3	W8-W9	0.78 Hz	0.73 Hz	31	27	ns	0.976
			W4-W5	W6-W7	0.94 Hz	1.05 Hz	32	26	ns	0.871
			W4-W5	W8-W9	0.94 Hz	0.73 Hz	32	27	ns	0.421

			W6-W7	W8-W9	1.05 Hz	0.73 Hz	26	27	ns	0.051
Fig. Supp8b	DN	SHAM	W2-W3	W4-W5	0.46 Hz	0.39 Hz	28	30	ns	0.884
			W2-W3	W6-W7	0.46 Hz	0.31 Hz	28	5	ns	0.862
			W2-W3	W8-W9	0.46 Hz	0.48 Hz	28	28	ns	0.996
			W4-W5	W6-W7	0.39 Hz	0.31 Hz	30	5	ns	0.980
			W4-W5	W8-W9	0.39 Hz	0.48 Hz	30	28	ns	0.778
			W6-W7	W8-W9	0.31 Hz	0.48 Hz	5	28	ns	0.805
Fig. Supp8b	DN	LID	W2-W3	W4-W5	0.61 Hz	1.19 Hz	41	33	***	<0.001
			W2-W3	W6-W7	0.61 Hz	2.47 Hz	41	17	ns	0.299
			W2-W3	W8-W9	0.61 Hz	3.10 Hz	41	27	***	<0.001
			W4-W5	W6-W7	1.19 Hz	2.47 Hz	33	17	ns	0.609
			W4-W5	W8-W9	1.19 Hz	3.10 Hz	33	27	**	0.006
			W6-W7	W8-W9	2.47 Hz	3.10 Hz	17	27	ns	0.943
Fig. Supp8b	DN	LID CORR	W2-W3	W4-W5	0.42 Hz	0.66 Hz	12	17	ns	0.371
			W2-W3	W6-W7	0.42 Hz	0.44 Hz	12	10	ns	0.999
			W2-W3	W8-W9	0.42 Hz	0.42 Hz	12	12	ns	1
			W4-W5	W6-W7	0.66 Hz	0.44 Hz	17	10	ns	0.495
			W4-W5	W8-W9	0.66 Hz	0.42 Hz	17	12	ns	0.363
			W6-W7	W8-W9	0.44 Hz	0.42 Hz	10	12	ns	0.999
Fig. Supp8b	DN	LID PREV	W2-W3	W4-W5	0.47 Hz	0.86 Hz	34	26	**	0.009
			W2-W3	W6-W7	0.47 Hz	1.52 Hz	34	25	***	<0.001
			W2-W3	W8-W9	0.47 Hz	0.60 Hz	34	16	ns	0.324
			W4-W5	W6-W7	0.86 Hz	1.52 Hz	26	25	ns	0.061

			W4-W5	W8-W9	0.86 Hz	0.60 Hz	26	16	ns	0.192
			W6-W7	W8-W9	1.52 Hz	0.60 Hz	25	16	**	0.004
Fig. Supp8b	FN	SHAM	W2-W3	W4-W5	0.85 Hz	0.58 Hz	7	8	ns	0.383
			W2-W3	W8-W9	0.85 Hz	0.25 Hz	7	3	ns	0.083
			W4-W5	W8-W9	0.58 Hz	0.25 Hz	8	3	ns	0.403
Fig. Supp8b	FN	LID	W2-W3	W4-W5	0.64 Hz	1.00 Hz	41	42	ns	0.435
			W2-W3	W6-W7	0.64 Hz	2.91 Hz	41	49	**	0.006
			W2-W3	W8-W9	0.64 Hz	1.27 Hz	41	27	ns	0.191
			W4-W5	W6-W7	1.00 Hz	2.91 Hz	42	49	*	0.019
			W4-W5	W8-W9	1.00 Hz	1.27 Hz	42	27	ns	0.670
			W6-W7	W8-W9	2.91 Hz	1.27 Hz	49	27	ns	0.073
Fig. Supp8b	FN	LID CORR	W2-W3	W4-W5	1.65 Hz	0.73 Hz	15	22	ns	0.500
			W2-W3	W6-W7	1.65 Hz	0.79 Hz	15	20	ns	0.559
			W2-W3	W8-W9	1.65 Hz	0.66 Hz	15	17	ns	0.448
			W4-W5	W6-W7	0.73 Hz	0.79 Hz	22	20	ns	0.932
			W4-W5	W8-W9	0.73 Hz	0.66 Hz	22	17	ns	0.948
			W6-W7	W8-W9	0.79 Hz	0.66 Hz	20	17	ns	0.685
Fig. Supp8b	FN	LID PREV	W2-W3	W4-W5	0.71 Hz	0.99 Hz	31	32	ns	0.072
			W2-W3	W6-W7	0.71 Hz	0.73 Hz	31	32	ns	0.993
			W2-W3	W8-W9	0.71 Hz	0.54 Hz	31	29	ns	0.136
			W4-W5	W6-W7	0.99 Hz	0.73 Hz	32	32	ns	0.134
			W4-W5	W8-W9	0.99 Hz	0.54 Hz	32	29	***	<0.001
			W6-W7	W8-W9	0.73 Hz	0.54 Hz	32	29	ns	0.105

Table S12: STDP in $D2^-$ and $D2^+$ MSN from SHAM, SHAM_PREV, LID and LID_PREV mice. Related to Figure 6.

Group	$D2^-$ MSN	$D2^+$ MSN
SHAM (N=5)	149 ± 2, p<0.0001 (n=11)	142 ± 4, p<0.0001 (n=10)
SHAM_PREV (N=5)	123 ± 1, p<0.0001 (n=10)	127 ± 1, p<0.0001 (n=10)
LID (N=7)	172 ± 1, p<0.0001 (n=12)	132 ± 3, p<0.0001 (n=9)
LID_PREV (N=5)	65 ± 1, p<0.0001 (n=9)	142 ± 6, p=0.0029 (n=10)